UNIVERSITY OF CALIFORNIA
RIVERSIDE

Development of Methods for the Total Analysis and Serum Profiling of MicroRNA Biomarkers

A Dissertation submitted in partial satisfaction
of the requirements for the degree of

Doctor of Philosophy

in

Chemistry

by

Kenneth Patrick Flack

December 2015

Dissertation Committee:
Dr. Wenwan Zhong, Chairperson
Dr. Quan 'Jason' Cheng
Dr. Ryan Julian

The Dissertation of Kenneth Patrick Flack is approved:

_____

_____

_____

Committee Chairperson

University of California, Riverside

Acknowledgements

Firstly and most importantly, I would like to acknowledge my PhD advisor Dr. Wenwan Zhong for all of her guidance, inspiration, mentorship and support. I would also like to acknowledge and thank the other members of my dissertation committee, Dr. Jason Cheng and Dr. Ryan Julian, for their time, guidance, and the motivation I needed over the years and for all they have taught me. I would also like to acknowledge the chemistry department and faculty at UCR for their support.

The material in Chapter 2 was previously published, reprinted with permission from 'Distribution Profiling of Circulating MicroRNAs in Serum', Jonathan Ashby, Kenneth Flack, Luis A. Jimenez, Yaokai Duan, Abdel-Kareem Khatib, George Somlo, Shizhen Emily Wang, Xinping Cui, and Wenwan Zhong Analytical Chemistry 2014 86 (18), 9343-9349, 2014 American Chemical Society. The material in Chapter 3 has been filed for patent, Patent Application No. 62/045,503 and was supported by a NIH grant #R01CA188991-01. A portion of material in Chapter 4 used previously published material, adapted from 'Tagging the rolling circle products with nanocrystal clusters for cascade signal increase in the detection of miRNA', J. Yao, K. Flack, L. Ding and W. Zhong, Analyst, 2013, 138, 3121 with permission from The Royal Society of Chemistry. Lastly, I would like to acknowledge the contribution of all coauthors in the above work and also acknowledge my colleagues Luis Jimenez and Marissa Gionet-Gonzales for their contributed work on the material in the latter part of Chapter 5.

Dedication

First I would like to dedicate this to my wonderful wife, Kelley, for her love and supporting me during these years of graduate school and for believing in me even when I had doubt. Without her love and support I would have been lost. Kelley, you are a true blessing, thank you for everything and for always being by my side. Also a dedication to my two beautiful children, and to my family and friends for their love and support.

Secondly, I want to make a special dedication to my parents, Michael and Ramona Flack. They were my first teachers and mentors in life, raising me to be the person I have become. It is their support and belief in my talents and abilities that encouraged me to always pursue higher education.

Lastly, I want to make a special dedication of this dissertation and my research in the memory of my mother, Ramona Marie McConnell Flack (October 20, 1958 – July 9 2015). Her strength and willpower has and will continue to be an inspiration in all that I do. It is my mother that drove me to strive for my best, and attempt new challenges in life.

ABSTRACT OF THE DISSERTATION

Development of Methods for the Total Analysis and Serum Profiling of MicroRNA Biomarkers

by

Kenneth Patrick Flack

Doctor of Philosophy, Graduate Program in Chemistry
University of California, Riverside, December 2015
Dr. Wenwan Zhong, Chairperson

MicroRNA (miRNA) are short 20 to 25 nucleotide, non-coding RNA strands that bind to messenger RNAs (mRNAs) to inhibit translation through post-transcriptional modifications and induced mRNA degradation. The dysregulation of the expression of various miRNA could be the result of abnormal states; such as cancers, coronary artery disease, diabetes, Alzheimer's disease, etc. MiRNAs have been found to be more closely related to disease stages and more tissue specific than the widely used mRNA disease markers. As a result, being able to quantitate miRNA levels is essential to early-stage disease detection and prognosis. MiRNAs can be released into the circulatory system and present at stable levels detectable by sensitive techniques. However, the perceived ranges of healthy miRNA levels can span several orders of magnitude and the overall serum content may differ very little in diseased states, making early stage detection difficult.

Quantifying the levels of miRNA bound to a particular carrier can make it possible to identify miRNA biomarkers, and allow for earlier and more accurate diagnosis of disease.

Asymmetrical flow field-flow fractionation (AF4) is an open channel separation method which offers an alternative to conventional packed column techniques. AF4 is a size-based separation technique capable of separating the variety of serum components while maintaining native interactions. Correlation of miRNA content associated to different fractions of miRNA carriers reveals highly specific association and larger differences between diseased and healthy states than total serum content.

Microfluidic technology allows for increased rate of sample processing and analysis, and reduced sample consumption. A simple microfluidic technique was developed for the rapid and selective isolation of miRNA bound to three fractions of miRNA carriers; proteins, lipoprotein complexes, and exosomes. Application to the analysis of case and control sera shows differentiation between disease state and cancer stages.

The development of highly sensitive isothermal miRNA detection platforms offers an alternative to conventional RT-qPCR analysis techniques. These novel detection techniques are more clinically relevant and offer simpler detection which is competitive with the sensitivity of qPCR. Finally, solid-phase extraction techniques for isolation and enrichment of miRNA have been pursued and optimized to yield high recovery from complex media.

Table of Contents

List of Figures

List of Tables

Chapter 1: Introduction

1.1: General Introduction

The keys to eradicating diseases such as cancer are in the development of better treatments and foremost the development of better detection techniques leading to earlier diagnosis of the disease. Detection of cancers at the earlier stages results in higher survival rates between 90 to 100 percent, owing to the fact that the disease is both easier to treat and the treatments are less harmful to the patient's general health.[1–3] Along with this, better long term prognosis for the patient with less chance for recurrence is expected. The discovery, detection, and analysis of better biomarkers are essential in improving our ability to diagnose cancers at an early stage.[4,5] However there is a necessity for the technique to be both highly sensitive and selective to avoid the rate of false negative or false positive diagnosis at these early disease stages.[3] The cost and simplicity of the technique also has to be considered for widespread use in discovery and diagnosis. Therefore, both the choice of analyte and the technique, and detection platform need to be carefully selected.

1.2: Biomarkers

Biomarkers are simple molecules of biological origin which can be used to indicate or monitor a variety of biological processes, diseases, immune-response, drug metabolism or effectiveness, or any distress on bodily organs.[4–6] Biomarkers can range in size from small molecular species such as ions or metabolites to large proteins or long DNA and RNA species. Currently the most commonly used biomarkers in the detection and monitoring of cancer are proteins such as prostate-specific antigen (prostate cancer),[7]

cancer antigens 15-3 and 27-29 (breast cancer),[8,9] along with many others. Biomarkers are extremely valuable in the detection and monitoring of cancer, especially at early stages of cancer or during remission when tumors are either too small for conventional imaging techniques or not clearly distinguishable from healthy tissue even during invasive surgery. Using biomarkers with high sensitivity, cancers can possibly be discovered and monitored during the precancerous stage (carcinoma in situ) when tumors may not exist and instead consist of a relatively small group of abnormal cells. The existence of cancer specific biomarkers combined with selective and sensitive detection techniques are vital for the monitoring of the effectiveness of cancer treatments and during cancer remission to identify reduction or growth of the cancer and detect possible metastasis of cancers. DNA and RNA biomarkers have potential for detection of genetically associated cancers and detection of cancerous mutations within abnormal cells and tissue. BRCA 1 and 2 are examples of gene biomarkers which can be used to identify the genetic risk of developing breast cancer in some patients along with the correlated proteins that are expressed.[10,11] Messenger RNAs (mRNAs) are potentially powerful biomarkers as they contain the genetic information for the expression of specific genes and the translation to the corresponding peptides and proteins.[12,13] If the expressed peptides or proteins have correlation to tumor specific species then the detection of the parent mRNA can be used for sensitive detection of abnormalities or synthetic regulation of these mRNA can be employed for genetic therapy. However invasive biopsy or tissue excision are commonly needed for detection of these DNA and RNA species as they are either absent in bodily fluids or are in too low of concentrations

to be detected in reasonably small sample volumes. However, small RNA species have been found in a variety of bodily fluids at detectable levels. One of these small RNA species with high potential as a group of cancer biomarkers are single stranded microRNA (miRNA).[14–20]

1.3: MicroRNA Structure, Biogenesis, and Function

MicroRNA are small, non-coding, 20-25 nucleotide long single stranded RNA species responsible for regulating gene expression through the post-transcriptional modification of mRNA, RNA silencing, and inhibition of protein synthesis.[21–23] MicroRNAs are encoded in the DNA genome and the human genome is suspected to encode well over 1000 unique mature miRNA sequences.[24] The biogenesis of miRNA is illustrated in Figure 1.01. The encoded miRNA within the DNA genome are transcribed by RNA polymerase II as a miRNA precursor that may be several hundred nucleotides in length with a polyadenylated 5' end and stem loop structures known as primary miRNA (pri-miRNA). Pri-miRNA undergoes nuclear processing via RNA-binding DGCR8 protein and the Drosha RNAse enzyme to produce a shortened stem-loop RNA molecule which is about 70-80 nucleotides in length, known as precursor miRNA (pre-miRNA), containing a single mature miRNA in its sequence. This pre-miRNA is then exported from the nucleus to the cytoplasm of the cell via Exportin-5 mediated transport.[25] Within the cytoplasm the Dicer RNAse enzyme then cleaves the pre-miRNA to produce a miRNA duplex, of which one strand typically becomes the mature miRNA while the other strand undergoes degradation. In a few cases the second strand of the miRNA duplex can also have function as a mature miRNA, although this is less common. The

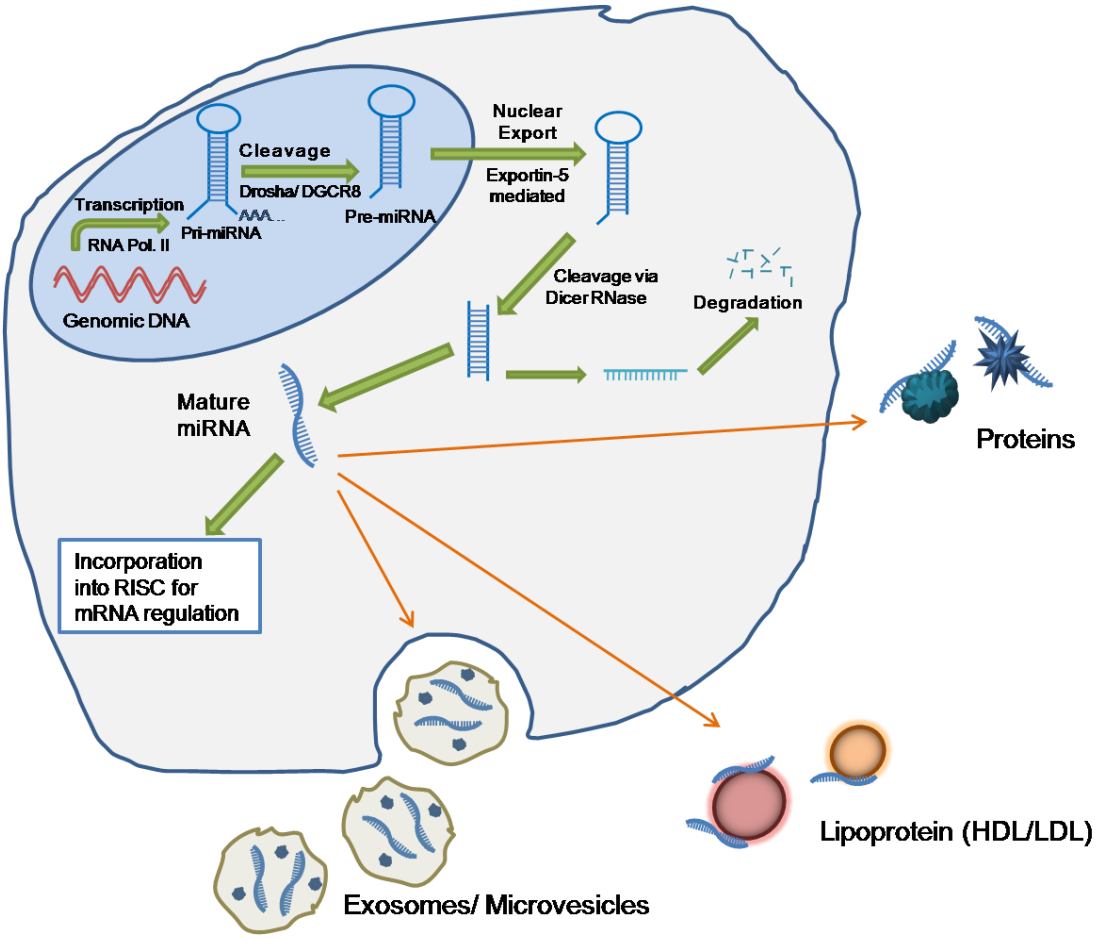

Figure 1.01. Illustration of mammalian microRNA biogenesis, intracellular transport, processing, and release from cells.

mature miRNA sequence in complementary to a portion of a specific mRNA sequence that is regulated. The RNA-induced silencing complex (RISC) incorporates mature miRNA and becomes active in mRNA binding, modification, inhibition of protein translation, and even cleavage of mRNA leading to degradation of the mRNA.[23,26,27] RISC is a multi-protein complex containing several proteins essential to incorporation of miRNA and the binding to mRNA along with its regulation of mRNA translation. Of these proteins, argonaute 2 (Ago2) may be the most important component for the incorporation and stabilization of miRNA as well as silencing and cleavage of mRNA.[28]

In their involvement in cancer, miRNAs can be divided into two subclasses, oncogenic miRNA and tumor-suppressive miRNA which regulate mRNA corresponding to tumor-suppressive and oncogenic genes respectively.[15,16,29] Therefore in cancerous cells oncogenic miRNA production will be increased, and these oncogenic miRNA will then down-regulate the expression of tumor-suppressive genes. Likewise tumor-suppressive miRNA production will decline and oncogenic gene expression will be up-regulated. It has also been observed that different miRNA will be under or over expressed at different stages of cancer progression including some miRNA which may be essential in tumor growth and metastasis of cancer.

1.4: Circulating MicroRNA as a Biomarker in Disease

MicroRNA can be exported from cells in a variety of forms and become known as extracellular miRNA or circulating miRNA.[30,31] Cells can expel small microvesicles known as exosomes which can contain a variety of cellular components found in the cytoplasm.[32,33] Normal cells release these exosomes regularly, and it has been found that

diseased cancer cells can release an increased quantity of these vesicles or produce exosomes of abnormal size or shape.[33] Exosomes are believed to be integral in cell-cell communication and play a major role in the spread of cancer through tumor growth and metastasis. MiRNA are one species found in exosomes which may be responsible for this, and the study of exosomal miRNA composition between healthy and cancerous cells is of great interest.[34–36] Additionally other species capable of transporting and harboring miRNA outside of cells include a variety of cellular proteins, especially Ago2 and other RISC species,[37] and both high and low density lipoprotein complexes.[38–40] Once within the blood, miRNA can transiently exchange from one carrier to another, perhaps due to stronger miRNA interactions with these species. All of these extracellular miRNA carriers are found within the circulatory system after release, with the concentration of miRNA within the circulatory system being correlated with cellular concentrations and impacted by diseases such as cancer. There is uncertainty of the significance of different miRNA carriers in serum to the spread and growth of cancer. However the correlation of exosomal miRNA and cancer has been more heavily investigated recently especially concerned with metastasis. Investigation which is more inclusive of other significant miRNA carriers is not as heavily studied, with exception perhaps of HDL bound miRNAs.

1.5: Amplification and Detection of Nucleic Acids

Nucleic acids such as deoxyribonucleic acids (DNA) and ribonucleic acids (RNA) are optimal biomarkers due to the plethora of techniques accessible to amplify the nucleic acids through a variety of enzymatic reactions available to replicate, elongate, fragment,

or otherwise modify the molecules for detection of minute quantities in minimal sample volume. Some of these techniques for amplification are well developed, while others are quite novel and on the forefront of developing better techniques for nucleic acid detection.

The traditional technique which laid the foundation for nucleic acid research is polymerase chain reaction (PCR).[41] PCR takes advantage of the natural process of DNA polymerization using either natural or modified polymerase enzymes. DNA polymerases have the ability to add nucleotides in the 5'-3' direction onto a DNA fragment (referred to as a primer) hybridized with a nucleic acid template, reading the template in the 3'-5' direction. The addition of nucleotides to the primer results from base pair matching to the template, yielding a strand complimentary to the original template. A primer specific to the 3' end of the complimentary strand can be used to create its compliment which is identical to the original template sequence. In this manner PCR allows for amplification of both a single stranded template sequence and its complimentary sequence through the use of two primers (known as forward and reverse primers). PCR utilizes the artificial replication in cycles allowing for one replication per template in each cycle. As the polymerization is symmetrical, 2 strands will become 4 after 1 cycle, and then become 8 after the next cycle, and then 16 in the following cycle, continuing in this fashion yielding exponential amplification of a few copies to thousands, millions, or billions of amplicons reliant on the number of cycles.

There are numerous variants of traditional PCR with the most notable for quantitative analysis being real-time or quantitative PCR (usually abbreviated as

qPCR).[42] Through the monitoring of DNA amplicon concentration at the end of each cycle, the amplification can be detected as a function of cycle number. The amplification of DNA in qPCR is usually detected by the use of either double strand DNA intercalating dyes (such as SYBR fluorescent dyes) or fluorescent DNA probes (such as Taqman probes). Intercalating nucleic acid dyes such as SYBR green dye have a high sensitivity for double stranded DNA and can therefore generate fluorescence of the double stranded PCR products at the end of each cycle. As these dyes have poor sensitivity for single stranded nucleic acids, yet become highly fluorescent upon binding to double stranded DNA, there is little background due to excess primers. Intercalating dyes give no sequence specificity and therefore can only be used for a single template reaction. Taqman probes consist of a short oligonucleotide labeled with a fluorophore and quencher on opposite ends with a sequence complimentary to the template. The probe is non-fluorescent due to the close proximity of the fluorophore and quencher, after hybridization to the template and upon polymerization the Taq polymerase enzyme degrades the Taq probe releasing the fluorophore which can then reach a distance from the quencher molecule to avoid quenching and fluorescence can then be measured. These probes offer greater sensitivity and low detection limits due to the absence of background signal and high specificity for the target sequence. Multiplexed qPCR is possible as different fluorophores of varied excitation/ emission wavelengths can be employed depending on the capability of the qPCR instrument. As the amount of DNA increases exponentially with the number of cycles in qPCR, the theoretical detection limit of qPCR

is a single copy of the target. The best experimental limits of detection are realized with highly optimized specific primer sets and the use of specific probe based detection.

An additional variation of PCR with high significance is reverse transcription PCR (RT-PCR).[43] Reverse transcription reaction allows for the application of PCR to RNA species through reverse transcription of RNA into complementary DNA (cDNA) which can then be amplified efficiently by DNA polymerases which typically have poor reverse transcription ability. In addition to the poor reverse transcription ability of many DNA polymerases, RNA itself is prone to hydrolysis and degradation which is more likely to occur at the temperatures utilized in PCR. Reverse transcriptase enzymes derived from retroviruses are employed, most commonly Moloney murine leukemia virus (M-MLV) and avian myeloblastosis virus (AMV). Reverse transcriptase enzymes are RNA-dependent DNA polymerases which read RNA templates in the 3' to 5' direction and synthesize complementary DNA in the 5' to 3' direction, building on the 3' end of a DNA primer. Advantages of the reverse transcription applied to PCR include synthesis of stable cDNA to avoid degradation of RNA samples and the possibility to create elongated cDNA which is especially useful in the detection of short RNA targets and increase both specificity and sensitivity in the PCR.

Methods for isothermal amplification of nucleic acids have been developed towards the development of effective target amplification without the need for thermocycling.[44–48] Development of these techniques have grown to yield isothermal amplification reactions which can be more rapid than traditional PCR for detection and have been developed to occur at lower temperatures rather than the more extreme

temperatures of PCR. DNA polymerases such as Phi29, Klenow Fragment, and T7 DNA polymerases have optimal activity between 30 to 37 degrees Celsius and can exhibit adequate amplification at room temperature. A variety of isothermal reactions employing other enzymes like helicase enzymes in helicase-dependent amplification (HDA) and those using endonuclease or exonuclease enzymes have been developed. Also some reactions not requiring enzymes have been developed, such as hybridization chain reaction (HCR)[49] which only requires stem-loop hairpin nucleic acid primers and an initiator sequence which can be the target or another strand such as an extended primer or an aptamer. Aptamers are RNA, LNA, or most commonly DNA sequences with strong and specific binding to molecules or proteins of biological interest, which are designed and selected through specialized techniques.

1.6: Biosensing and MicroRNA Detection

Biosensors are defined by the use of a biological component for the recognition of the analyte of interest and the use of electrochemical or optical sensors to determine concentration of the analyte.[50] Biosensors are of great interest for microfluidic technologies and in routine medical diagnostics for the development of all-in-one device for the detection of analytes of biological significance. The bio-recognition element can be a variety of biological molecules including polypeptides, enzymes, antibodies, and nucleic acids giving capability to detect essentially any analyte with high selectivity and sensitivity in combination with a sensing element. Common sensing elements for biosensors are electrode based detection of electrochemically active species or optical detectors for measuring fluorescence, luminescence, or colorimetric changes. An example

of a common biosensor is blood glucose sensors which typically use glucose oxidase to produce electrochemically active species which can be oxidized via electrodes for determination of glucose concentration.[51] For recognition and sensing of miRNA, biosensors can be developed using nucleic acids with complementary sequences to a portion or the entire sequence of the miRNA combined with amplification strategies for selective and sensitive detection.[52–54]

1.7: Methods of Nucleic Acid Extraction

Traditionally organic solvent based techniques have been employed in the lysis or disruption of biological samples for precipitation based isolation of nucleic acids. The most common chemical separation is phenol-chloroform extraction of nucleic acids.[55] The phenol-chloroform extraction is traditionally used for DNA species, in an optimized form which uses a phenol solution containing guanidine isothiocyanate high quality RNA can be isolated.[56] The method uses phenol-guanidine isothiocyanate solution for lysis and disruption of the sample with the addition of chloroform for isolation. After incubation and centrifugation the solution will form two distinct layers, upper aqueous phase and lower organic phase, with a possible interphase between them. The upper aqueous layer exclusively contains RNA which is precipitated with isopropanol and washed with ethanol to remove contaminants such as guanidine isothiocyanate. DNA is exclusively isolated in the bottom organic layer while proteins and lipids are in both the lower phase and interphase. DNA and proteins and be sequentially isolated via ethanol and isopropanol precipitation of each respectively. The main advantages of the guanidine isothiocyanate-phenol-chloroform extraction are the sequential purification of RNA,

DNA, and protein with practically no contamination of the three species with each other as well as rapid isolation in about an hour. However, the method suffers from selective isolation of larger RNA species and yields very poor extraction efficiencies when isolating small RNAs including miRNA, due to the difficulty of precipitation of these more soluble species. Efficiency of small RNA extraction can be improved through addition of glycogen as a co-precipitant, elongated precipitation times at -20 degrees Celsius, and increased centrifugation speeds.

Solid phase extraction techniques have also been developed and are commercially produced for the extraction of DNA, RNA, and miRNA from a variety of sample types. Silica can be used as a solid phase material for the binding of nucleic acids in high salt or low pH solutions through interactions through the silanol groups on silica surfaces and the phosphate groups on the nucleic acid backbone.[57] In high salt solutions this will primarily occur as a result of salt cation bridging of negatively charged deprotonated silanol to the negatively charged phosphate group of DNA and RNA. In low pH solutions when the silanol groups of silica are protonated, hydrogen bonding between the silanol group and negatively charged phosphate group will cause binding of nucleic acids. The commercial methods use a centrifugal filter design utilizing a porous silica membrane and optimized lysis/binding and wash solutions to yield high quality and pure nucleic acid in a short period of time. However these methods can suffer from poor extraction efficiency of miRNA from complex sample matrices. Non-specific adsorption of other biological species and lower binding strength of miRNA to silica surfaces can cause reduction in extraction efficiency. Importance can be placed on available silica surface

area as well as effective suspension and incubation with the silica and sample for improvement of extraction efficiency. Improvements on solid phase extraction of nucleic acids have been focused on improving the solid phase material. In addition to porous silica membranes, monolithic silica surfaces, silica microparticles, silica nanomaterials, and silicon carbide materials have been investigated to yield better extraction results. Since the adsorption of nucleic acids on silica is based on binding to the phosphate groups on the nucleic acid backbone, other metal oxides with favorable binding can be investigate such as titanium dioxide and zirconium dioxide which have been shown to adsorb DNA and phosphorylated proteins.[58,59]

1.8: Asymmetrical Flow Field-Flow Fractionation

Separation of miRNA carriers is important in better biomarker discovery. Asymmetrical Flow Field-Flow Fractionation, or AF4, is an open channel separation technique based on the theory of Field-Flow Fractionation, or FFF, introduced in 1987 by Wahlund and Giddings.[60] AF4 and FFF are gentle separation techniques due to the open channel design and relatively low flow rates and therefore do stress or denature analytes and native binding of molecules or particles is retained. For these reasons AF4 can offer many advantages over other techniques such as high performance liquid chromatography (HPLC), size exclusion chromatography (SEC), and fast protein liquid chromatography (FPLC). These chromatography techniques are traditionally used in the separation of mixtures of biological analytes and proteins, however they are harsher separation techniques that used higher pressure and packed columns to achieve separation. These techniques may disrupt native structure and native binding such as that between proteins

and miRNA. Also the size ranges for separation in these chromatography techniques is typically more limited than FFF. Field-Flow Fractionation methods allow for separation of analytes over the size range of one nanometer to several microns.[61] AF4 is differentiated from FFF by an asymmetrical cross flow induced through the pulling of carrier solvent through a porous bottom channel versus the symmetrical cross flow in FFF which results from the flow of solvent through two permeable walls of the channel. As a result of this difference, the set-up of the instrument is less complicated and the channel is simpler in design. Since in AF4 the carrier fluid exits the bottom permeable wall without being replenished, the channel in AF4 is tapered from the injection side to the detector exit side in order to reduce the effect of the fluid loss on the flow rate over the distance of the channel. The equation defining the separation in AF4 is shown below in equation 1.1 where; t_r is the retention time, η is the fluid viscosity, w is the channel thickness, d is the analyte hydrodynamic diameter, V_c is the cross flow velocity, k is the Boltzmann constant, T is channel temperature, and V° is the channel flow velocity.[62] The retention time is directly proportional to the hydrodynamic diameter of the analyte. Keeping separation temperature and solvent viscosity constant the retention time for an analyte is affected by the ratio of the cross flow to the channel flow, which can be adjusted for resolution of analytes.

$$t_r = \frac{\pi \eta w^2 d V_c}{2kTV^\circ} \qquad \text{Equation 1.1}$$

A porous membrane of a chosen molecular weight cutoff is used to select the minimal size of molecules or particles retained in the channel. Spacers are used to determine the channel thickness (typically 100-300 μm) between the membrane located

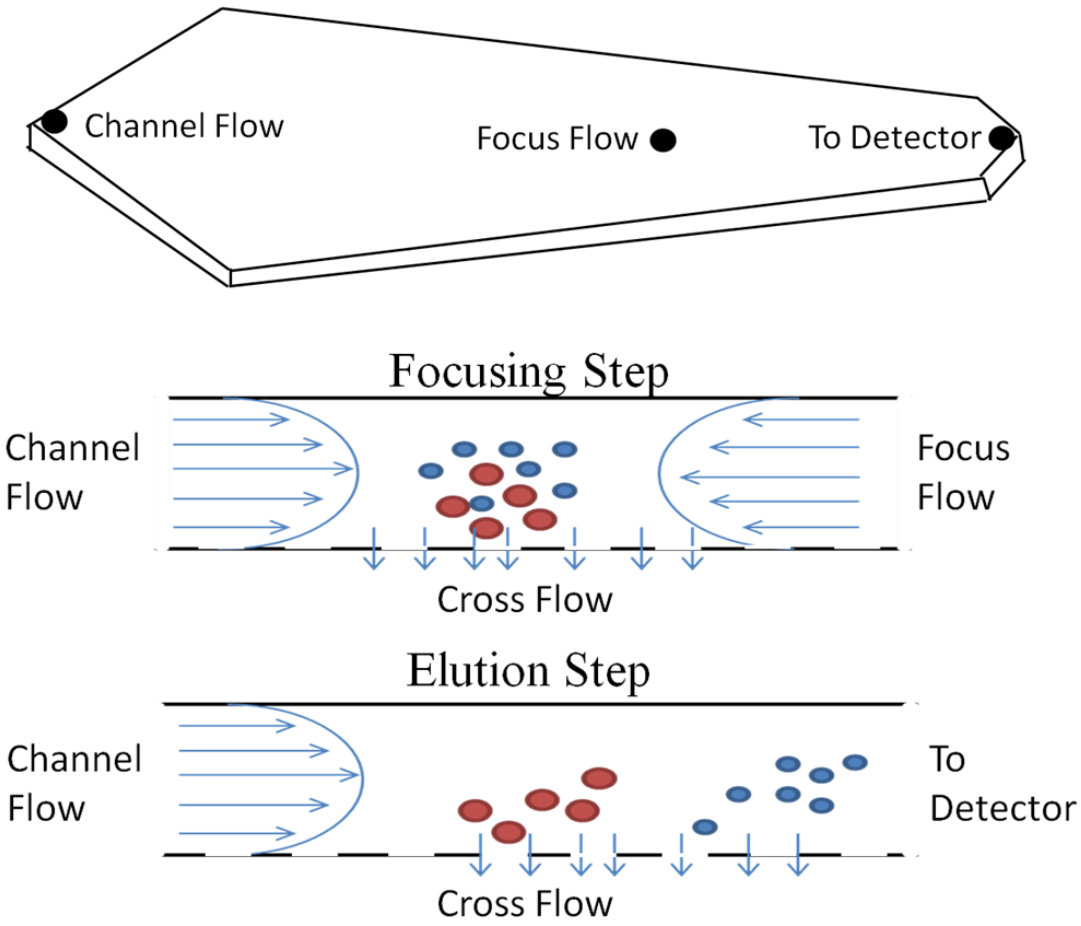

Figure 1.02. Illustration of AF4 channel and separation dynamics.

on the permeable wall and the top of the channel. Figure 1.02 illustrates the design of the AF4 channel and the focusing and elution conditions in the separation method. After injection of a sample into the channel, the sample is focused as a narrow band at the top of the channel and pulled against the porous membrane via a focus flow and the cross flow. After the sample is focused the sample is eluted from the channel via the axial channel flow. Separation of analytes results from the perpendicular cross flow rate and the diffusion of analytes towards the center of the channel. Smaller species diffuse further towards the center of the channel then larger species and therefore elute faster due to the parabolic flow profile in the channel. In order to achieve resolution of analytes with small size differences larger cross flow rates can be used. Also gradient elution over a large size range can be achieved through gradual decrease of the cross flow. AF4 has been used in the separation and analysis of nanoparticles, proteins, polymers, and nucleic acids and in studying the interactions between them. This separation ability can be used in the separation of serum components. Human serum is a complex mixture containing small molecules, proteins, lipoproteins, and microvesicles. These species can range in size from small ions to exosomes and very low density lipoproteins (30nm to over 100nm). AF4 can eliminate small species under the size cutoff of the membrane and reduce the complexity of the serum to potential miRNA carriers and the separation conditions can be tailored to achieve isolation of all components.

1.9: Microfluidic Technology

High-throughput analysis is a necessity for discovery of selective and accurate biomarkers. Microfluidic systems enable miniaturization of analytical laboratory

techniques on a single device small enough to fit in the palm of a hand. Integration of techniques for the processing and separation of samples reduces the issues with traditional bench top techniques such as large sample sizes, more reagent waste, samples loss, and contamination.[63,64] In addition, microfluidic technology often time consumption and can produce a simpler technique which is less labor intensive and can be high-throughput. These devices can be made by a variety of processes and out of a variety of materials, some devices being rather complex while others are very simple. Photolithography is the fabrication method of choice as it is relatively simple and can be done outside of a clean-room environment with more accessible equipment. Of the materials typically employed in microfluidic technology, glass/silica and polydimethylsiloxane (PDMS) are the choice materials due to their desirable properties.[65,66] PDMS can be easily molded to conform to any shape or design and cured at relatively low temperatures, and can easily be cut or have holes punched post-cure. PDMS is flexible and durable, biocompatible, and optically transparent. In addition, PDMS can be chemically modified if necessary through oxidation of the PDMS along with silanization techniques. Separation and purification techniques such as electrophoresis, size-exclusion filtration/ chromatography (SEC), solid phase extraction (SPE), and affinity capture have been successfully employed on microfluidic devices.[67–69] Furthermore, it is possibly to integrate amplification and detection techniques on devices to develop a total analysis system; decreasing the time required for analysis, cost of analysis, and sample loss due to solution transfer.

References:

(1) Welch H; Schwartz LM; Woloshin S. ARe Increasing 5-Year Survival Rates Evidence of Success against Cancer? *JAMA* **2000**, *283* (22), 2975–2978.

(2) Etzioni, R.; Urban, N.; Ramsey, S.; McIntosh, M.; Schwartz, S.; Reid, B.; Radich, J.; Anderson, G.; Hartwell, L. The Case for Early Detection. *Nat. Rev. Cancer* **2003**, *3* (4), 243–252.

(3) Smith, R. A.; Cokkinides, V.; von Eschenbach, A. C.; Levin, B.; Cohen, C.; Runowicz, C. D.; Sener, S.; Saslow, D.; Eyre, H. J. American Cancer Society Guidelines for the Early Detection of Cancer. *CA. Cancer J. Clin.* **2002**, *52* (1), 8–22.

(4) Ludwig, J. A.; Weinstein, J. N. Biomarkers in Cancer Staging, Prognosis and Treatment Selection. *Nat. Rev. Cancer* **2005**, *5* (11), 845–856.

(5) Mayeux, R. Biomarkers: Potential Uses and Limitations. *NeuroRx* **2004**, *1* (2), 182–188.

(6) Alvarez, M. L.; Khosroheidari, M.; Kanchi Ravi, R.; DiStefano, J. K. Comparison of Protein, microRNA, and mRNA Yields Using Different Methods of Urinary Exosome Isolation for the Discovery of Kidney Disease Biomarkers. *Kidney Int.* **2012**, *82* (9), 1024–1032.

(7) Catalona, W. J.; Richie, J. P.; Ahmann, F. R.; Hudson, M. A.; Scardino, P. T.; Flanigan, R. C.; deKernion, J. B.; Ratliff, T. L.; Kavoussi, L. R.; Dalkin, B. L. Comparison of Digital Rectal Examination and Serum Prostate Specific Antigen in the Early Detection of Prostate Cancer: Results of a Multicenter Clinical Trial of 6,630 Men. *J. Urol.* **1994**, *151* (5), 1283–1290.

(8) S, L.; L, T.; F, B.; G, L.; E, B.; A, G.; Mg, R.; A, V. Comparison of CEA, MCA, CA 15-3 and CA 27-29 in Follow-up and Monitoring Therapeutic Response in Breast Cancer Patients. *Anticancer Res.* **1998**, *19* (4C), 3511–3515.

(9) Frenette, P. S.; Thirlwell, M. P.; Trudeau, M.; Thomson, D. M. P.; Joseph, L.; Shuster, J. S. The Diagnostic Value of CA 27-29, CA 15-3, Mucin-Like Carcinoma Antigen, Carcinoembryonic Antigen and CA 19-9 in Breast and Gastrointestinal Malignancies. *Tumor Biol.* **1994**, *15* (5), 247–254.

(10) Futreal, P. A.; Liu, Q.; Shattuck-Eidens, D.; Cochran, C.; Harshman, K.; Tavtigian, S.; Bennett, L. M.; Haugen-Strano, A.; Swensen, J.; Miki, Y.; Et, A. BRCA1 Mutations in Primary Breast and Ovarian Carcinomas. *Science* **1994**, *266* (5182), 120–122.

(11) Veronesi, A.; Giacomi, C. de; Magri, M. D.; Lombardi, D.; Zanetti, M.; Scuderi, C.; Dolcetti, R.; Viel, A.; Crivellari, D.; Bidoli, E.; Boiocchi, M. Familial Breast Cancer: Characteristics and Outcome of BRCA 1–2 Positive and Negative Cases. *BMC Cancer* **2005**, *5* (1), 70.

(12) Ariazi, E. A.; Clark, G. M.; Mertz, J. E. Estrogen-Related Receptor α and Estrogen-Related Receptor γ Associate with Unfavorable and Favorable Biomarkers, Respectively, in Human Breast Cancer. *Cancer Res.* **2002**, *62* (22), 6510–6518.

(13) Ross, J. S.; Fletcher, J. A.; Linette, G. P.; Stec, J.; Clark, E.; Ayers, M.; Symmans, W. F.; Pusztai, L.; Bloom, K. J. The HER-2/neu Gene and Protein in Breast Cancer 2003: Biomarker and Target of Therapy. *The Oncologist* **2003**, *8* (4), 307–325.

(14) Cho, W. C. S. MicroRNAs: Potential Biomarkers for Cancer Diagnosis, Prognosis and Targets for Therapy. *Int. J. Biochem. Cell Biol.* **2010**, *42* (8), 1273–1281.

(15) Calin, G. A.; Croce, C. M. MicroRNA-Cancer Connection: The Beginning of a New Tale. *Cancer Res.* **2006**, *66* (15), 7390–7394.

(16) Garzon, R.; Calin, G. A.; Croce, C. M. MicroRNAs in Cancer. *Annu. Rev. Med.* **2009**, *60* (1), 167–179.

(17) Yanaihara, N.; Caplen, N.; Bowman, E.; Seike, M.; Kumamoto, K.; Yi, M.; Stephens, R. M.; Okamoto, A.; Yokota, J.; Tanaka, T.; Calin, G. A.; Liu, C.-G.; Croce, C. M.; Harris, C. C. Unique microRNA Molecular Profiles in Lung Cancer Diagnosis and Prognosis. *Cancer Cell* **2006**, *9* (3), 189–198.

(18) Slack, F. J.; Weidhaas, J. B. MicroRNA in Cancer Prognosis. *N. Engl. J. Med.* **2008**, *359* (25), 2720–2722.

(19) Lu, J.; Getz, G.; Miska, E. A.; Alvarez-Saavedra, E.; Lamb, J.; Peck, D.; Sweet-Cordero, A.; Ebert, B. L.; Mak, R. H.; Ferrando, A. A.; Downing, J. R.; Jacks, T.; Horvitz, H. R.; Golub, T. R. MicroRNA Expression Profiles Classify Human Cancers. *Nature* **2005**, *435* (7043), 834–838.

(20) Schetter AJ; Leung S; Sohn JJ; et al. MIcrorna Expression Profiles Associated with Prognosis and Therapeutic Outcome in Colon Adenocarcinoma. *JAMA* **2008**, *299* (4), 425–436.

(21) Winter, J.; Jung, S.; Keller, S.; Gregory, R. I.; Diederichs, S. Many Roads to Maturity: microRNA Biogenesis Pathways and Their Regulation. *Nat. Cell Biol.* **2009**, *11* (3), 228–234.

(22) Kim, V. N. MicroRNA Biogenesis: Coordinated Cropping and Dicing. *Nat. Rev. Mol. Cell Biol.* **2005**, *6* (5), 376–385.

(23) Gregory, R. I.; Chendrimada, T. P.; Cooch, N.; Shiekhattar, R. Human RISC Couples MicroRNA Biogenesis and Posttranscriptional Gene Silencing. *Cell* **2005**, *123* (4), 631–640.

(24) Griffiths-Jones, S.; Grocock, R. J.; Dongen, S. van; Bateman, A.; Enright, A. J. miRBase: microRNA Sequences, Targets and Gene Nomenclature. *Nucleic Acids Res.* **2006**, *34* (suppl 1), D140–D144.

(25) Lund, E.; Güttinger, S.; Calado, A.; Dahlberg, J. E.; Kutay, U. Nuclear Export of MicroRNA Precursors. *Science* **2004**, *303* (5654), 95–98.

(26) Pratt, A. J.; MacRae, I. J. The RNA-Induced Silencing Complex: A Versatile Gene-Silencing Machine. *J. Biol. Chem.* **2009**, *284* (27), 17897–17901.

(27) Engels, B. M.; Hutvagner, G. Principles and Effects of microRNA-Mediated Post-Transcriptional Gene Regulation. *Oncogene* **2006**, *25* (46), 6163–6169.

(28) Rand, T. A.; Ginalski, K.; Grishin, N. V.; Wang, X. Biochemical Identification of Argonaute 2 as the Sole Protein Required for RNA-Induced Silencing Complex Activity. *Proc. Natl. Acad. Sci. U. S. A.* **2004**, *101* (40), 14385–14389.

(29) Shenouda, S. K.; Alahari, S. K. MicroRNA Function in Cancer: Oncogene or a Tumor Suppressor? *Cancer Metastasis Rev.* **2009**, *28* (3-4), 369–378.

(30) Kosaka, N.; Iguchi, H.; Ochiya, T. Circulating microRNA in Body Fluid: A New Potential Biomarker for Cancer Diagnosis and Prognosis. *Cancer Sci.* **2010**, *101* (10), 2087–2092.

(31) Chen, X.; Ba, Y.; Ma, L.; Cai, X.; Yin, Y.; Wang, K.; Guo, J.; Zhang, Y.; Chen, J.; Guo, X.; Li, Q.; Li, X.; Wang, W.; Zhang, Y.; Wang, J.; Jiang, X.; Xiang, Y.; Xu, C.; Zheng, P.; Zhang, J.; Li, R.; Zhang, H.; Shang, X.; Gong, T.; Ning, G.; Wang, J.; Zen, K.; Zhang, J.; Zhang, C.-Y. Characterization of microRNAs in Serum: A Novel Class of Biomarkers for Diagnosis of Cancer and Other Diseases. *Cell Res.* **2008**, *18* (10), 997–1006.

(32) Théry, C.; Zitvogel, L.; Amigorena, S. Exosomes: Composition, Biogenesis and Function. *Nat. Rev. Immunol.* **2002**, *2* (8), 569–579.

(33) Pant, S.; Hilton, H.; Burczynski, M. E. The Multifaceted Exosome: Biogenesis, Role in Normal and Aberrant Cellular Function, and Frontiers for Pharmacological and Biomarker Opportunities. *Biochem. Pharmacol.* **2012**, *83* (11), 1484–1494.

(34) Valadi, H.; Ekström, K.; Bossios, A.; Sjöstrand, M.; Lee, J. J.; Lötvall, J. O. Exosome-Mediated Transfer of mRNAs and microRNAs Is a Novel Mechanism of Genetic Exchange between Cells. *Nat. Cell Biol.* **2007**, *9* (6), 654–659.

(35) Fong, M. Y.; Zhou, W.; Liu, L.; Alontaga, A. Y.; Chandra, M.; Ashby, J.; Chow, A.; O'Connor, S. T. F.; Li, S.; Chin, A. R.; Somlo, G.; Palomares, M.; Li, Z.; Tremblay, J. R.; Tsuyada, A.; Sun, G.; Reid, M. A.; Wu, X.; Swiderski, P.; Ren, X.; Shi, Y.; Kong, M.; Zhong, W.; Chen, Y.; Wang, S. E. Breast-Cancer-Secreted miR-122 Reprograms Glucose Metabolism in Premetastatic Niche to Promote Metastasis. *Nat. Cell Biol.* **2015**, *17* (2), 183–194.

(36) Zhou, W.; Fong, M. Y.; Min, Y.; Somlo, G.; Liu, L.; Palomares, M. R.; Yu, Y.; Chow, A.; O'Connor, S. T. F.; Chin, A. R.; Yen, Y.; Wang, Y.; Marcusson, E. G.; Chu, P.; Wu, J.; Wu, X.; Li, A. X.; Li, Z.; Gao, H.; Ren, X.; Boldin, M. P.; Lin, P. C.; Wang, S. E. Cancer-Secreted miR-105 Destroys Vascular Endothelial Barriers to Promote Metastasis. *Cancer Cell* **2014**, *25* (4), 501–515.

(37) Arroyo, J. D.; Chevillet, J. R.; Kroh, E. M.; Ruf, I. K.; Pritchard, C. C.; Gibson, D. F.; Mitchell, P. S.; Bennett, C. F.; Pogosova-Agadjanyan, E. L.; Stirewalt, D. L.; Tait, J. F.; Tewari, M. Argonaute2 Complexes Carry a Population of Circulating microRNAs Independent of Vesicles in Human Plasma. *Proc. Natl. Acad. Sci. U. S. A.* **2011**, *108* (12), 5003–5008.

(38) Vickers, K. C.; Palmisano, B. T.; Shoucri, B. M.; Shamburek, R. D.; Remaley, A. T. MicroRNAs Are Transported in Plasma and Delivered to Recipient Cells by High-Density Lipoproteins. *Nat. Cell Biol.* **2011**, *13* (4), 423–433.

(39) Vickers, K. C.; Remaley, A. T. Lipid-Based Carriers of microRNAs and Intercellular Communication: *Curr. Opin. Lipidol.* **2012**, *23* (2), 91–97.

(40) Wagner, J.; Riwanto, M.; Besler, C.; Knau, A.; Fichtlscherer, S.; Röxe, T.; Zeiher, A. M.; Landmesser, U.; Dimmeler, S. Characterization of Levels and Cellular Transfer of Circulating Lipoprotein-Bound MicroRNAs. *Arterioscler. Thromb. Vasc. Biol.* **2013**, *33* (6), 1392–1400.

(41) Erlich, H. A. Polymerase Chain Reaction. *J. Clin. Immunol.* **1989**, *9* (6), 437–447.

(42) Heid, C. A.; Stevens, J.; Livak, K. J.; Williams, P. M. Real Time Quantitative PCR. *Genome Res.* **1996**, *6* (10), 986–994.

(43) Chen, C.; Ridzon, D. A.; Broomer, A. J.; Zhou, Z.; Lee, D. H.; Nguyen, J. T.; Barbisin, M.; Xu, N. L.; Mahuvakar, V. R.; Andersen, M. R.; Lao, K. Q.; Livak, K. J.; Guegler, K. J. Real-Time Quantification of microRNAs by Stem–loop RT–PCR. *Nucleic Acids Res.* **2005**, *33* (20), e179–e179.

(44) Gill, P.; Ghaemi, A. Nucleic Acid Isothermal Amplification Technologies—A Review. *Nucleosides Nucleotides Nucleic Acids* **2008**, *27* (3), 224–243.

(45) Kim, J.; Easley, C. J. Isothermal DNA Amplification in Bioanalysis: Strategies and Applications. *Bioanalysis* **2011**, *3* (2), 227–239.

(46) Demidov, V. V. Rolling-Circle Amplification in DNA Diagnostics: The Power of Simplicity. *Expert Rev. Mol. Diagn.* **2002**, *2* (6), 542–548.

(47) Vincent, M.; Xu, Y.; Kong, H. Helicase-Dependent Isothermal DNA Amplification. *EMBO Rep.* **2004**, *5* (8), 795–800.

(48) Jia, H.; Li, Z.; Liu, C.; Cheng, Y. Ultrasensitive Detection of microRNAs by Exponential Isothermal Amplification. *Angew. Chem. Int. Ed.* **2010**, *49* (32), 5498–5501.

(49) Dirks, R. M.; Pierce, N. A. Triggered Amplification by Hybridization Chain Reaction. *Proc. Natl. Acad. Sci. U. S. A.* **2004**, *101* (43), 15275–15278.

(50) Lowe, C. R. An Introduction to the Concepts and Technology of Biosensors. *Biosensors* **1985**, *1* (1), 3–16.

(51) Wang, J. Electrochemical Glucose Biosensors. *Chem. Rev.* **2008**, *108* (2), 814–825.

(52) Johnson, B. N.; Mutharasan, R. Biosensor-Based microRNA Detection: Techniques, Design, Performance, and Challenges. *The Analyst* **2014**, *139* (7), 1576.

(53) Catuogno, S.; Esposito, C. L.; Quintavalle, C.; Cerchia, L.; Condorelli, G.; De Franciscis, V. Recent Advance in Biosensors for microRNAs Detection in Cancer. *Cancers* **2011**, *3* (2), 1877–1898.

(54) Hamidi-Asl, E.; Palchetti, I.; Hasheminejad, E.; Mascini, M. A Review on the Electrochemical Biosensors for Determination of microRNAs. *Talanta* **2013**, *115*, 74–83.

(55) Sambrook, J.; Russell, D. W. Purification of Nucleic Acids by Extraction with Phenol:Chloroform. *Cold Spring Harb. Protoc.* **2006**, *2006* (1), pdb.prot4455.

(56) Chomczynski, P.; Sacchi, N. The Single-Step Method of RNA Isolation by Acid Guanidinium Thiocyanate–phenol–chloroform Extraction: Twenty-Something Years on. *Nat. Protoc.* **2006**, *1* (2), 581–585.

(57) Boom, R.; Sol, C. J.; Salimans, M. M.; Jansen, C. L.; Dillen, P. M. W.; Noordaa, J. van der. Rapid and Simple Method for Purification of Nucleic Acids. *J. Clin. Microbiol.* **1990**, *28* (3), 495–503.

(58) Zhang, X.; Wang, F.; Liu, B.; Kelly, E. Y.; Servos, M. R.; Liu, J. Adsorption of DNA Oligonucleotides by Titanium Dioxide Nanoparticles. *Langmuir* **2014**, *30* (3), 839–845.

(59) Liu, S.-Q.; Xu, J.-J.; Chen, H.-Y. A Reversible Adsorption–desorption Interface of DNA Based on Nano-Sized Zirconia and Its Application. *Colloids Surf. B Biointerfaces* **2004**, *36* (3–4), 155–159.

(60) Wahlund, K. G.; Giddings, J. C. Properties of an Asymmetrical Flow Field-Flow Fractionation Channel Having One Permeable Wall. *Anal. Chem.* **1987**, *59* (9), 1332–1339.

(61) Giddings, J. C. Field-Flow Fractionation: Analysis of Macromolecular, Colloidal, and Particulate Materials. *Science* **1993**, *260* (5113), 1456–1465.

(62) Schimpf, M. E.; Caldwell, K.; Giddings, J. C. *Field-Flow Fractionation Handbook*; John Wiley & Sons, 2000.

(63) Gravesen, P.; Branebjerg, J.; Jensen, O. S. Microfluidics-a Review. *J. Micromechanics Microengineering* **1993**, *3* (4), 168.

(64) Whitesides, G. M. The Origins and the Future of Microfluidics. *Nature* **2006**, *442* (7101), 368–373.

(65) Kartalov, E. P.; Anderson, W. F.; Scherer, A. The Analytical Approach to Polydimethylsiloxane Microfluidic Technology and Its Biological Applications. *J. Nanosci. Nanotechnol.* **2006**, *6* (8), 2265–2277.

(66) McDonald, J. C.; Duffy, D. C.; Anderson, J. R.; Chiu, D. T.; Wu, H.; Schueller, O. J.; Whitesides, G. M. Fabrication of Microfluidic Systems in Poly(dimethylsiloxane). *Electrophoresis* **2000**, *21* (1), 27–40.

(67) Wu, D.; Qin, J.; Lin, B. Electrophoretic Separations on Microfluidic Chips. *J. Chromatogr. A* **2008**, *1184* (1–2), 542–559.

(68) Chirica, G.; Lachmann, J.; Chan, J. Size Exclusion Chromatography of Microliter Volumes for On-Line Use in Low-Pressure Microfluidic Systems. *Anal. Chem.* **2006**, *78* (15), 5362–5368.

(69) Giordano, B. C.; Burgi, D. S.; Hart, S. J.; Terray, A. On-Line Sample Pre-Concentration in Microfluidic Devices: A Review. *Anal. Chim. Acta* **2012**, *718*, 11–24.

Chapter 2: Asymmetrical Flow Field Flow Fractionation of Serum Components for Carrier Based Quantification of MicroRNA in Serum

2.1: Introduction

Early detection of cancer can enhance the survival rate of patients, but the success relies on the availability of specific and sensitive biomarkers. One class of promising biomarkers for cancer diagnosis is microRNAs (miRNAs). They bind to target mRNAs and inhibit translation or induce degradation of target transcripts.[1,2] Over-expression of miRNAs that inhibit the tumor suppressor genes can interfere with the anti-oncogenic pathway, whereas reduction of miRNAs that target oncogenes can increase oncogenic potency.[3–6] It is also recognized that miRNA profiles more accurately reflect the developmental lineage and tissue origin of human cancers than the mRNA profiles.[7–9] Compared to proteins, miRNAs have a simpler structure and less complex post-synthesis processing, and can be detected by highly sensitive qPCR methods. More appealing, miRNAs can be released into the circulation system and are present at stable levels that are detectable by sensitive and selective techniques like RT-qPCR.[10–13] Accumulating evidence shows that circulating miRNAs exhibit varied patterns between cancer patients and healthy controls, with the patterns of some secretory miRNAs altered in the early stage on cancer initiation.[14–16] Because sampling from bodily fluids such as blood, urine, saliva, etcetera is considered to be convenient and noninvasive compared to other biopsy methods, more and more research efforts have been devoted to obtaining the comprehensive profiles of circulating miRNAs, and validate their utility ad biomarkers as compared to tissue biopsy miRNA profiles.[17,18]

Still, it is a long route from proof-of-principle to creation of reliable and reproducible miRNA clinical tests. One obstacle is that not all circulating miRNAs are related to cancer development. The abundance of cancer-irrelevant miRNAs can be secreted by blood cells, secreted normally from healthy cells, or shed upon cell death. They could then contribute to large variances in miRNA abundances between individuals and add to signals from the cancer relevant miRNAs during quantification. It has been known that the cell-free miRNAs are protected from ribonucleases present in extracellular environments and bodily fluids by various types of carrier species. The carriers can be proteins like argonaute 2 (Ago2) or GW182[19,20] that belong to the RNA-induced silencing complex (RISC), high density lipoprotein (HDL) particles that could mediate cellular communication,[21,22] or micro vesicles such as exosomes[23–25] which could be one of the main exportation routes for miRNAs from malignant cells.[26] The active miRNA secretion by malignant cells could be the consequence of dysregulation of cellular pathways. The purposeful exportation and uptake could be related to tumor progression and metastasis.[27–29] Therefore, to better eliminate the cancer irrelevant miRNAs and reveal the more specific miRNA markers, isolation of miRNAs from carriers that are specifically secreted by cancer cells could be a solution. Thus, HDL and exosomes have recently been the focus in studies of circulating miRNAs.

Purified HDL and exosomes are often obtained by ultracentrifugation[20,21,26,30–32] and immunoaffinity capture.[33,34] Ultracentrifugation can provide good size and density resolution, but it requires large sample volumes, is very tedious and time consuming, and typically yields low recovery. Immunoaffinity capture is easy to perform and provides

high specificity, targeting one specific type of carriers at a time.[35,36] In the pioneering study of miRNA carriers by Arroyo et al,[19] serum was fractionated with size exclusion chromatography (SEC) to reveal the existence of the exosomal and exosome-free circulating miRNAs. Vickers et al also applied SEC to further characterize the HDL isolated by ultracentrifugation.[21] However, in SEC good separation resolution can only be achieved within a small size range, interaction of biomolecules with the column materials is problematic, and integrity of complexes or vesicles after passing through packed columns is of concern.

There exists no conclusive evidence about which miRNA carriers are more important in cancer diagnosis. The study of miRNA distribution across all types of carriers in serum is necessary to draw specific conclusions on the importance of specific carriers with different miRNA targets. Compared to SEC and ultracentrifugation, asymmetrical flow field flow fractionation (AF4) is a gentler separation technique for better preservation of native biomolecule and bioparticle structure and their binding to miRNAs.[37] As AF4 is an open channel separation technique with no interactive stationary phase, AF4 can isolate intact macromolecular complexes such as nucleic acid-protein, antibody-antigen, and protein-drug interactions.[38–40] In addition, AF4 has previously been used for separation and analysis of exosomes in serum.[41–43] Therefore, AF4 is the method of choice for separation of different miRNA carriers based on their range of hydrodynamic sizes, enabling screening of miRNA distribution among all potential carriers. Comparing the distribution profiles obtained from cancer patients to healthy individuals may indicate which types of carriers are more relevant to cancer

development, enhancing the sensitivity and specificity when using carrier specific miRNA in cancer diagnosis.

Herein this chapter, we employed AF4 to fractionate whole serum, and six discrete elution fractions were collected. Carrier species in each fraction were identified through the extraction of proteins and mass spectrometry (MS) analysis as well as direct detection using enzyme-linked immunosorbent assay (ELISA). Total RNA was extracted from each of the fractions, and the amounts of eight selected miRNA targets were quantified via RT-qPCR. The aim of the analysis was to investigate the usefulness of miRNA quantities associated with particular carrier species in differentiating breast cancer patients from healthy individuals versus total serum concentrations of the miRNAs.

2.2: Materials and Methods

2.2.1: Chemicals and Biomaterials

All chemicals used to prepare the AF4 running buffer of 1× PBS (10 mM phosphate at pH 7.4, 137 mM NaCl, 2.7 mM KCl, and 1.0mM MgCl2), ethylene glycol, dimethyl sulfoxide, guanidine hydrochloride, RNA-grade glycogen, 2-propanol, and chloroform were purchased from Thermo Fisher (Pittsburgh, PA). All single proteins used as AF4 standards were purchased from Sigma-Aldrich (St. Luis, MO). Taq 5× master mix was purchased from New England Biolabs. High- and low- density lipoproteins were purchased from CalBioChem (EMD Millipore, Billerica, MA). TRIzol LS, 3,3’-dioctadecyloxacarbocyanine perchlorate (DiO), Total Exosome Isolation kit, and TaqMan MicroRNA Assays specific for each target were purchased from Life

Technologies (Carlsbad, CA). Synthesized MicroRNA standards and exogenous control were purchased from Integrated DNA Technologies (Coralville, IA). The serum sample used for exosome extraction and separation method optimization was pooled healthy male AB serum from Sigma Aldrich. The serum samples used in the distribution profile study were provided by our collaborators at the City of Hope Medical Center (Duarte, CA). The samples were obtained from voluntarily consenting female patients under institutional review board-approved protocols. The two breast cancer patients had infiltrating ductal carcinoma and were ER/PR/HER2 positive (ER-estrogen receptor; PR-progesterone receptor; HER2-human epidermal growth factor receptor).

2.2.2: Serum Fractionation by AF4

An AF200 system manufactured by Postnova Analytics (Salt Lake City, UT) was used in this study. The trapezoidal separation channel was 0.350 mm thick (spacer thickness) and its tip-to-tip length was 275 mm, with an inlet triangle width of 20 mm and an outlet width of 5 mm. The injection loop volume was 20 µL. The surface area of the accumulation wall was 3160 mm^2, which was composed of a regenerated cellulose ultrafiltration membrane (Postnova Analytics) with a molecular weight cutoff value of 10 kDa. The eluate exiting AF4 passed through a SPD-20A absorbance detector (Shimadzu) followed by a fraction collector (Bio-Rad). The running buffer used in all separations was 1× PBS (10 mM phosphate at pH 7.4, 137 mM NaCl, and 2.7 mM KCl). During serum fractionation, an initial focusing step of 8 min was used, with the cross-flow (the flow exiting the channel through the porous membrane wall) at 3.00 mL/min, tip flow (the channel inlet flow) at 0.30 mL/min, and the focus flow (a flow entering at a position

further down from the inlet to focus the analyte into a narrow sample zone) at 3.00 mL/min. After the focusing period, there was a 1 minute transition period where the tip flow was increased to 3.30 mL/min and the focus flow was reduced to zero. Afterward, the tip flow was kept at 3.30 mL/min for 5 min and then reduced to 0.30 mL/min over the course of 15 min. In each case, the cross flow was reduced to keep the detector flow (the channel outlet flow) at 0.30 mL/min. A fraction collector was used to perform stepwise collections in 1 minute intervals. These 1 minute collections for each sample were combined into six fractions, with fraction 1 (F1) collected from 6 to 9 min, F2 from 9 to 13 min, F3 from 13 to 16 min, F4 from 16 to 19 min, F5 from 19 to 23 min, and F6 from 23 to 28 min.

2.2.3: RNA and Protein Extraction from Collected Fractions

Each fraction was spiked with 0.31 fmol of exogenous *Caenorhabditis elegans* miRNA, *cel-miR*-67, and subjected to guanidine isothiocyanate-phenol-chloroform extraction using TRIzol LS reagent. For extraction each fraction was split into several ~450 µL aliquots. Each aliquot was homogenized with 1 mL of TRIzol LS reagent and incubated briefly, followed with the addition of 300 µL of chloroform and thorough mixing. After brief incubation and centrifugation, the aqueous phase exclusively containing RNA was isolated and RNA-grade glycogen was added. The RNAs were precipitated by the addition of 1 mL of 100% isopropanol. The RNA pellet was washed once by 80% ethanol, dried, and then all pellets for the same fraction were combined before going through an additional round of isopropanol precipitation and 100% ethanol

wash. The fractions were then dried and stored at -20 °C until RT-qPCR analysis. The protein-containing organic fraction was precipitated using the suggested protocol.

2.2.4: MicroRNA Analysis

To acquire sufficient miRNA input for accurate RT-qPCR analysis, two collections were carried out for each replicate of each serum sample. One collection was used to quantify *hsa-miR*-16, *miR*-17, *miR*-155, *miR*-191, *Let*-7a, and *miR*-375, for which the RNA pellets were reconstituted in 31 µL of RNase-free water. The other collection was used to quantify *miR*-21, *miR*-105 (dropped from analysis due to very low presence in serum), and *miR*-122 for which the RNA pellets were reconstituted in 16 µL. The exogenous *cel-miR*-67 spiked in each fraction prior to extraction of total RNA was used as an internal standard to account for miRNA loss during the extraction and for elution volume variability. Absolute quantification and normalization of miRNA quantity in each fraction of each sample was obtained using an external standard calibration curve prepared from synthetic miRNA standards for each target in addition to the exogenous control which was ran in addition to samples on every qPCR plate.

An optimized RT-qPCR protocol was used for analysis employing the individual TaqMan MicroRNA Assay kits (Applied Biosystems). In each RT reaction, 5 µL of sample extract (1 µL for endogenous control) was mixed with 3 µL of a reverse transcription master mix and 2 µL of a corresponding stem-loop RT primer for each miRNA target strand. The RT master mix consisted of 1.1 µL nuclease-free water, 1 µL of a 10× RT buffer, 0.13 µL of RNAse inhibitor, 0.1 µL of a dNTP mix, and 0.67 µL reverse transcriptase (all components were provided in a TaqMan reverse transcription

kit). After mixing and brief centrifugation, 5 μL of silicone oil was layered on top of the RT mixture, and reverse transcription conducted on a Perkin-Elmer 2400 GeneAmp PCR Thermocycler. The RT reaction consisted of a 30-minute annealing step at 16°C, a 32-minute reverse transcription step at 42°C, and a 5-minute denaturing step at 85°C. After RT, the samples underwent quantitative PCR (qPCR). On the qPCR plate, 1 μL of the RT product was mixed with 9 μL of qPCR master mix for a final volume of 10μL. As an overlay, 5 μL of silicone oil was added to the top of each sample to limit evaporation. The PCR master mix consisted of 4.9 μL of nuclease-free water, 1 μL of ethylene glycol, 0.1 μL of DMSO, 0.5 μL of 25 mM magnesium chloride, 2 μL of Taq 5× master mix, and 0.5 μL of 20× qPCR primer mix (specific forward and reverse PCR primers, and specific TaqMan fluorescent probe). Each sample RT product was plated in triplicate, and standards corresponding to the samples analyzed (high- versus low-abundance) were plated in singlet. The qPCR analysis was conducted on a Bio-Rad CFX real-time instrument, with an initial activation step at 95 °C for 90s followed by an initial annealing step at 59°C for 50s, followed by a 40-cycle PCR with 30s denaturation at 95 °C and 70s annealing/extension at 53 °C in each cycle.

2.3: Results and Discussion

2.3.1: AF4 Separation of miRNA Carriers

Due to the large differences in the hydrodynamic diameters between proteins and exosomes, the AF4 separation conditions need to be optimized for elution of all miRNA carriers in a reasonable period of time while maintaining modest resolution between different species. In particular, elution of large particles like LDL and exosomes could

take a very long time because they diffuse more slowly. Under a constant channel/cross-flow condition, the exosomes prepared by the Total Exosome Isolation kit were injected but not eluted within 30 min, unless the cross-flow was reduced gradually to zero. It turned out that better resolution between exosomes and smaller serum components, as well as quick elution of the exosomes could be achieved if the cross flow was gradually decreased to zero between 5 to 20 minutes in the separation period. Using this separation flow program, protein standards with various hydrodynamic diameters (d_h) including; albumin (67 kDa, d_h~4 nm), IgG (150 kDa, d_h~8 nm), and thyroglobulin (660 kDa, d_h~16 nm) were eluted at different times with adequate resolution from polystyrene particle standard (d_h=50 ±7 nm). In addition HDL (d_h~7-10 nm), LDL (d_h~21-28 nm), and exosomes (d_h~30-120 nm) could be effectively separated, although there can be overlap between very-low-density lipoprotein (VLDL, d_h~30-80 nm) and exosomes. The results support the major serum carriers could be eluted in the order of single protein < HDL < LDL < exosomes (ranking by elution time). Determination of elution windows for collected fractions and identity of carriers in fractions was determined through the separation of standards, ELISA, and MS analysis. For the determination of HDL and LDL windows in serum fractionation, pure HDL and LDL were spiked into whole human serum purchased from Sigma Aldrich. The absorbance fractograms for serum compared with the HDL or LDL spiked sera indicate approximate elution windows for the majority of HDL within 10-15 min and LDL within 17-23 min (Figure 2.01a). The fluorescence fractograms, employing DiO lipophilic dye for HDL, LDL, and exosome fluorescence, were used to indicate exosome elution using the Total Exosome Isolation kit extract and

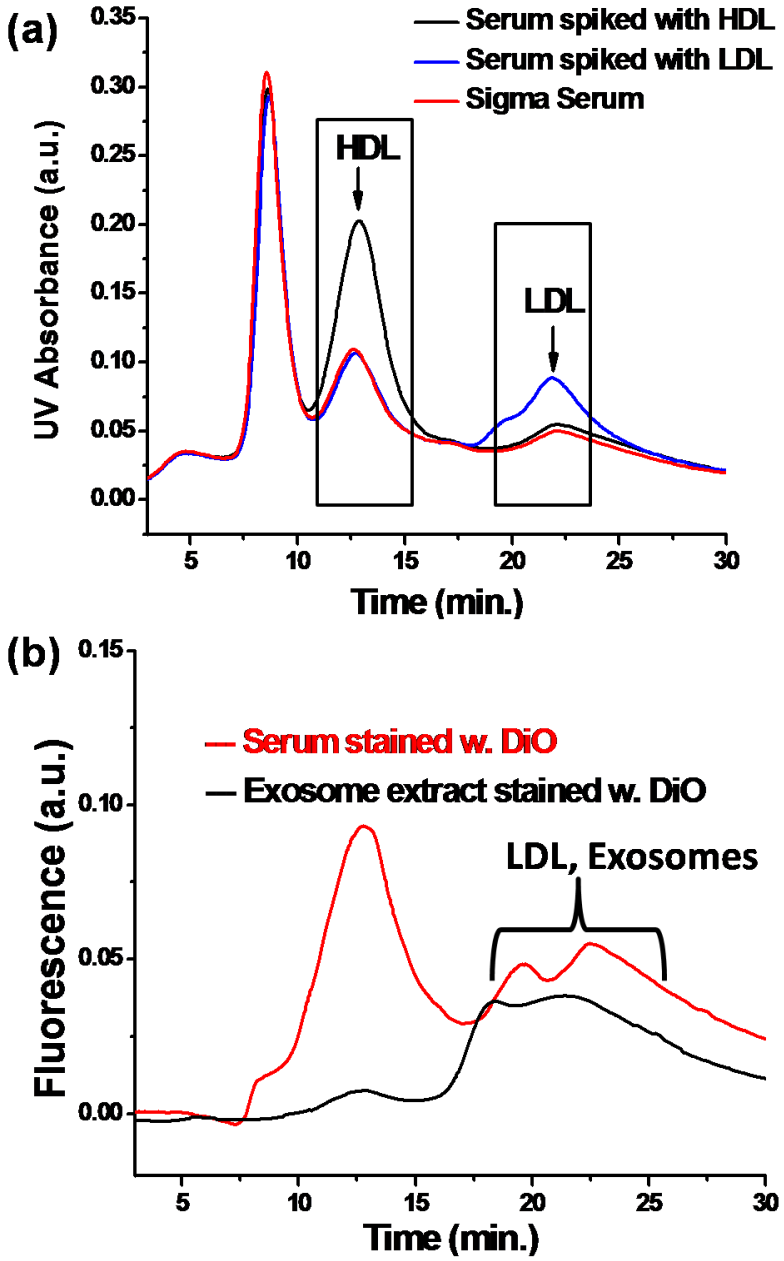

Figure 2.01. (a) Fractograms (UV absorption at 280 nm) for serum before and after spiking with HDL or LDL. (b) Comparison of fractograms (detected by fluorescence with 480 nm excitation/510 nm emission) of serum and exosome extract after DiO staining.

illustrate moderate resolution of HDL, LDL, and exosome in DiO stained whole serum (Figure 2.01b).

2.3.2: Fractionation of Patient Serum and Confirmation of Eluted Carriers

Once the approximate windows for elution of the miRNA carriers were known, we fractionated sera samples collected from two healthy females (Control #1 and #2) and two breast cancer (BC) patients (Case #1 and #2) (Figure 2.02). Six fractions were collected to increase the purity of miRNA carriers isolated in each fraction. The collection window for each fraction was determined by the relative elution times of HDL, LDL, and exosomes from the above study (inset table in Figure 2.02). Separation was highly reproducible: relative standard deviation (RSD) of the elution time of the peak within each fraction was <8% using all eight fractograms compared (four serum samples, each with two repeats). We also performed DiO staining for the four serum samples tested and confirmed the reproducible elution of the carriers with rich lipid structures, such as HDL, LDL, and exosomes. The highly reproducible separation profiles obtained by both UV absorption and DiO staining coupled with fluorescence detection helped to confirm the similarity in regular protein (represented by the peak intensity of serum albumin and IgG) and lipid (represented by the two major peaks detected by DiO staining) contents among these samples. This can ensure that the difference detected in miRNA distribution profiles was originated from the presence of BC but not from normal differences in carrier abundance. Moreover, the high reproducibility of elution greatly simplified the after-column collection: a fraction collector was programmed to collect the

Fraction #	F1	F2	F3	F4	F5	F6
Fraction time range	6-9 min	9-13 min	13-16 min	16-19 min	19-23 min	23-28 min
RSD of peak elution time	8.0%	7.0%	N/A	4.4%	0.77%	N/A
Carrier (known or potential) enrichment	Single proteins, mainly albumin	HDL	HDL	HDL	LDL	Exosomes

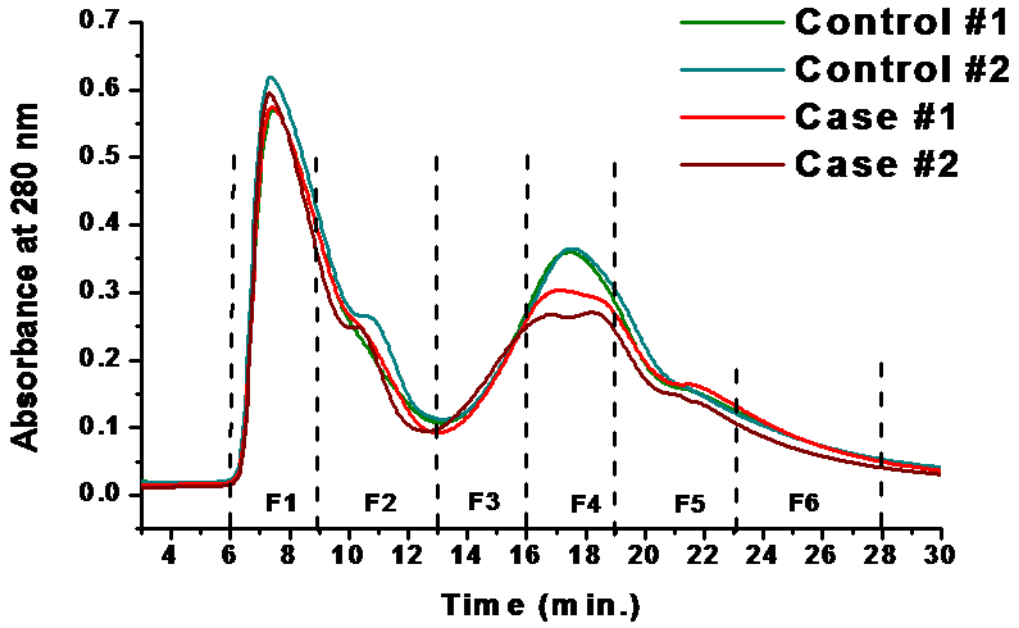

Figure 2.02. Fractograms for serum samples from healthy individuals (controls) and breast cancer patients (cases) with indication of each fraction. The table shows the time range of each collected fraction, and the RSD values of the peak elution time for each fraction. N/A means that there is no distinct peak in the fraction for calculation.

eluent every 1 min, and the eluent fractions within the desired time windows were combined for subsequent miRNA and protein extraction.

To confirm the identities of carriers enriched in each fraction, proteins eluted in F1-F6 were collected, digested by trypsin, and analyzed by LC-MS/MS. The relative abundance of the eluted proteins was evaluated by spectral counting,[44–46] which counts the number of mass spectra collected for a specific protein. The percentage of the spectra number for a particular protein among all spectra identified in one sample should be semi-quantitatively proportional to its relative abundance in the mixture.[47] Apolipoproteins belonging to various lipoprotein complexes, such as apolipoprotein A-I (ApoA1), A-II (ApoA2) and B-100 (ApoB), were found in multiple fractions (Figure 2.03a). ApoA1, as a marker for HDL and LDL, was found in F2-F6 correlating with the possible elution of HDL in F2-F4 and LDL in F4-F6. ApoA2, as a specific marker for HDL, was present in F2-F4, and most enriched in F3. Considering the size range of HDL reported in literature, 7-10 nm,[48] we concluded the heterogeneous high-density lipoprotein (HDL) particles were eluted in F2, F3, and F4. ApoB is the marker protein for LDL as well as VLDL,[49] and was found to be present in F4, F5, and F6, with ApoB most enriched in F5, matching with the elution window of pure LDL as shown in Figure 1a.

LC-MS/MS did not identify any marker proteins for exosomes, probably due to the signal suppression resulted from the highly abundant serum proteins like immunoglobulin G (IgG) and serum albumin. Instead we tested the major marker protein for serum exosomes, CD-63, in each fraction by ELISA (Figure 2.03b). About 20 ng of the protein extracted from each fraction (determined through the bicinchoninic acid assay

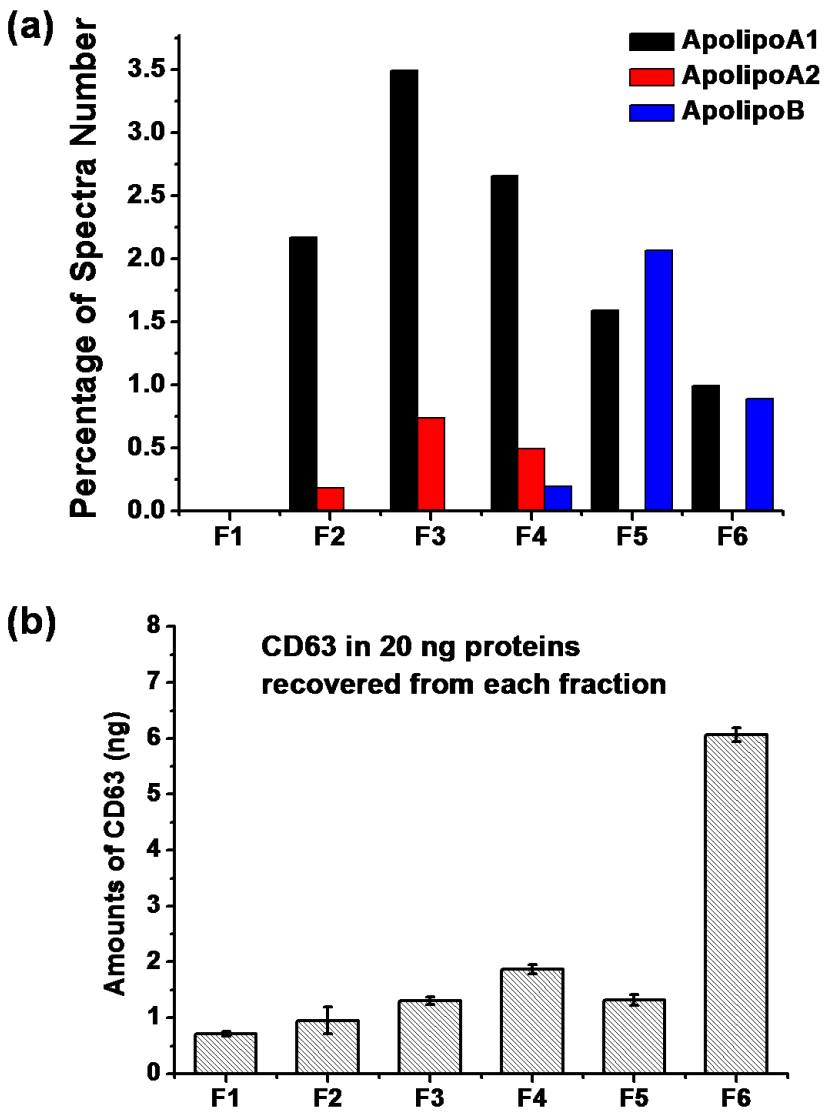

Figure 2.03. (a) Spectral counting results for selected lipoproteins in the AF4 fractions. (b) ELISA detection of CD-63 protein in the collected fractions.

, BCA assay) was adsorbed to the bottom of the wells on a microtiter plate. CD-63 was targeted by anti-CD63 antibody and the HRP-labeled secondary antibody. A substantial amount of CD-63 (~6 ng/20 ng) was only detected in F6. As was concluded from the standards analysis, F6 was where exosomes are primarily located.

Overall, the above results point out that F1 contained mainly albumin and single proteins with MW < 100 kDa. HDL and LDL should be enriched in F3 and F5 respectively, and exosomes mainly eluted in F6, but could also be in F5 at low abundance. VLDL was co-eluted with exosomes in F6. Although co-elution of multiple carriers was seen using the current separation method, such as the overlap of HDL and LDL in F4, and the co-elution of exosomes and VLDL in F6, enriching specific carriers in particular fractions should already allow us to look at the general distribution of miRNAs among the carriers. Higher resolution will indeed enhance the accuracy in distribution profiling, and can be achieved by injecting lower amounts of serum in each round of the separation, but multiple collections will definitely be needed, increasing the overall labor in the analysis, which is not a favorable choice. Increasing the separation force by using a higher cross-flow may also be beneficial to separation resolution, but we take the risk of losing more miRNAs due to membrane adsorption of carriers. Thus, we used the current fractionation conditions for the present work. Our results, as would be seen in the following discussion, showed that the coarse distribution profiles were adequate in differentiating the cancer patients from healthy controls, as well as in revealing miRNA targets and particular carriers that were important to the differentiation.

Strand	Sequence (5'-3')	Rational to be included in our study
cel-miR-67	cgcucauucugccgguuguuaug	Exogenous control used as a standard for correction of extraction efficiency
hsa-let-7a	ugagguaguagguuguauaguu	Reported as potential BC marker, upregulated in references (Arroyo, 2011)
hsa-miR-16	uagcagcacguaaauauuggcg	Reported in miRNAdola as circulating miRNA; reported as potential BC marker, protein-bound miRNA (Arroyo, 2011)
hsa-miR-191	caacggaaucccaaaagcagcug	Reported in miRNAdola as a circulating, exosomal miRNA; potential BC marker (Elyakin, 2010)
hsa-miR-17	caaagugcuuacagugcagguag	Reported in miRNAdola as circulating in BC; HDL-bound miRNA (Vickers, 2011)
hsa-miR-155	uuaaugcuaaucgugauaggggu	Reported in miRNAdola as an exosomal miRNA; potential BC marker
hsa-miR-375	uuuguucguucggcucgcguga	Reported by our collaborator, Dr. Emily Wang, as a potential marker for prediction of clinical outcome of BC patients (Ref. 18); in miRNAdola as exosomal miRNA; HDL-bound miRNA (Vickers, 2011)
hsa-miR-21	uagcuuaucagacugauguuga	Reportedas potential BC marker, upregulated in references; in miRNAdola as a circulating miRNA; protein-bound miRNA (Arroyo, 2011)
hsa-miR-122	uggagugugacaaugguguuug	Discovered by our collaborator as a potential BC marker located mainly in exosomes

Table 2.1. Targets included in our study.

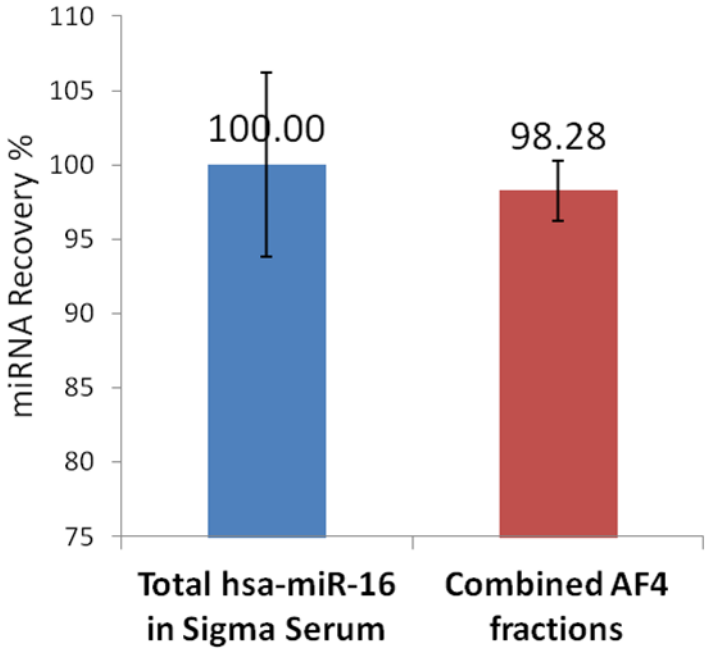

Figure 2.04. Recovery of hsa-miR-16 from AF4 fractions compared to the total miR-16 recovered from whole serum.

2.3.3: Distribution of miRNAs in Serum

The total RNA chemically extracted using TRIzol LS reagent were precipitated, dried, and reconstituted in water for quantification by RT-PCR. As stated above, sera from two groups of donors (all females) were tested. The sera from healthy individuals (Control #1 and #2) and those from breast cancer patients (Case #1 and #2) were analyzed, each with two repeated measurements. Eight miRNAs were quantified by RT-qPCR. Their sequences are listed in Table 2.1, together with the rationale of their inclusion in our study.

Recovery of miRNAs in our method was evaluated by quantification of *miR*-16 in the Sigma serum. The total content of *miR*-16 directly extracted from the 20 μL of whole serum by the TRIzol LS reagent was compared with the sum *miR*-16 quantity recovered from all AF4 fractions obtained with the injection of the same serum volume. A recovery as high as 98% was achieved for *miR*-16 (Figure 2.04), indicating no significant loss of miRNAs due to membrane adsorption inside the AF4 channel. The resulted copy number of each miRNA tested in 20 μL of whole serum normally ranged from 10^4 to 10^{10}. MiRNAs *miR*-375 and *miR*-122 were present at much lower abundances than other strands or even not detected in some of the fractions.

The high reproducibility in the separation step and careful processing in miRNA extraction and quantification ensured high analytical reproducibility: the RSD for the Log value of the total miRNA content in the two repeated measurements was < 5% for most of the strands, except for *miR*-375, *miR*-21, and *miR*-122 which could vary by up to 15%. In agreement with previous reports large variations in the detected microRNA quantities

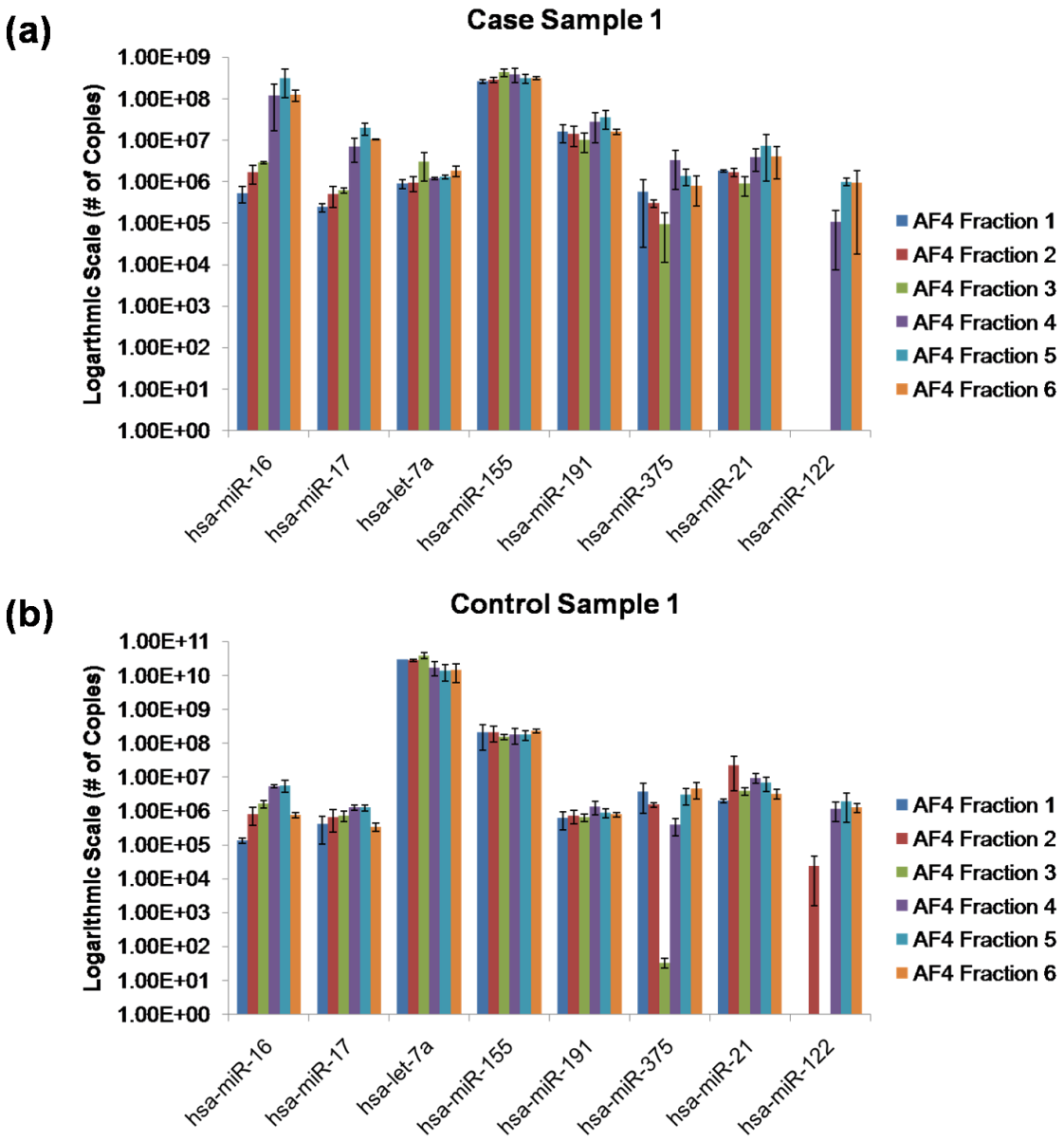

Figure 2.05. Distribution profiles of the eight tested miRNAs in the serum from one breast cancer patient (Case #1)(a) and one healthy donor (Control #1)(b).

were observed among individuals, even between the two samples within the same health group: the controls or the BC cases. Evaluation of the RSD of the total miRNA amount in all serum samples points out that *miR*-16 and *miR*-17 had relatively more stable expression among individuals than other miRNA species. Their RSD was below 15%. However, this RSD already corresponds to about 10-fold alteration in the miRNA copy numbers if the base value is around 10^6. For *miR*-122, RSD values close to 120% were observed between the two samples within the same group.

Because each fraction enriched a particular type of miRNA carrier, the copy number found in each fraction corresponded to the miRNA level bound with that particular carrier. Different miRNAs showed distinct distribution patterns among the carriers, as demonstrated by the distribution profile of Case #1 and Control #1 (Figure 2.05). In this sample, higher amounts of *miR*-16, *miR*-17, and *miR*-122 were found in F4-F6. There was even no detectible *miR*-122 in F1-F3. Thus, these three miRNAs should mainly locate in lipoprotein complexes and exosomes in this serum sample. On the contrary, *Let*-7a, *miR*-155, and *miR*-191 had quite flat distribution profiles among all fractions. The main type of carriers for each miRNA could be related to the major pathway it takes when exiting the cells, and be possibly linked to their biological functions. By fractionating the carriers prior to miRNA quantification, our method provides rich information about how the miRNAs are present in serum, which can be further explored to solve the fundamentals of miRNA secretion and transportation.

We compared the miRNA copy number found in each fraction between the control and case (BC) samples. Figure 2.06a shows the Log ratio of the averaged miRNA

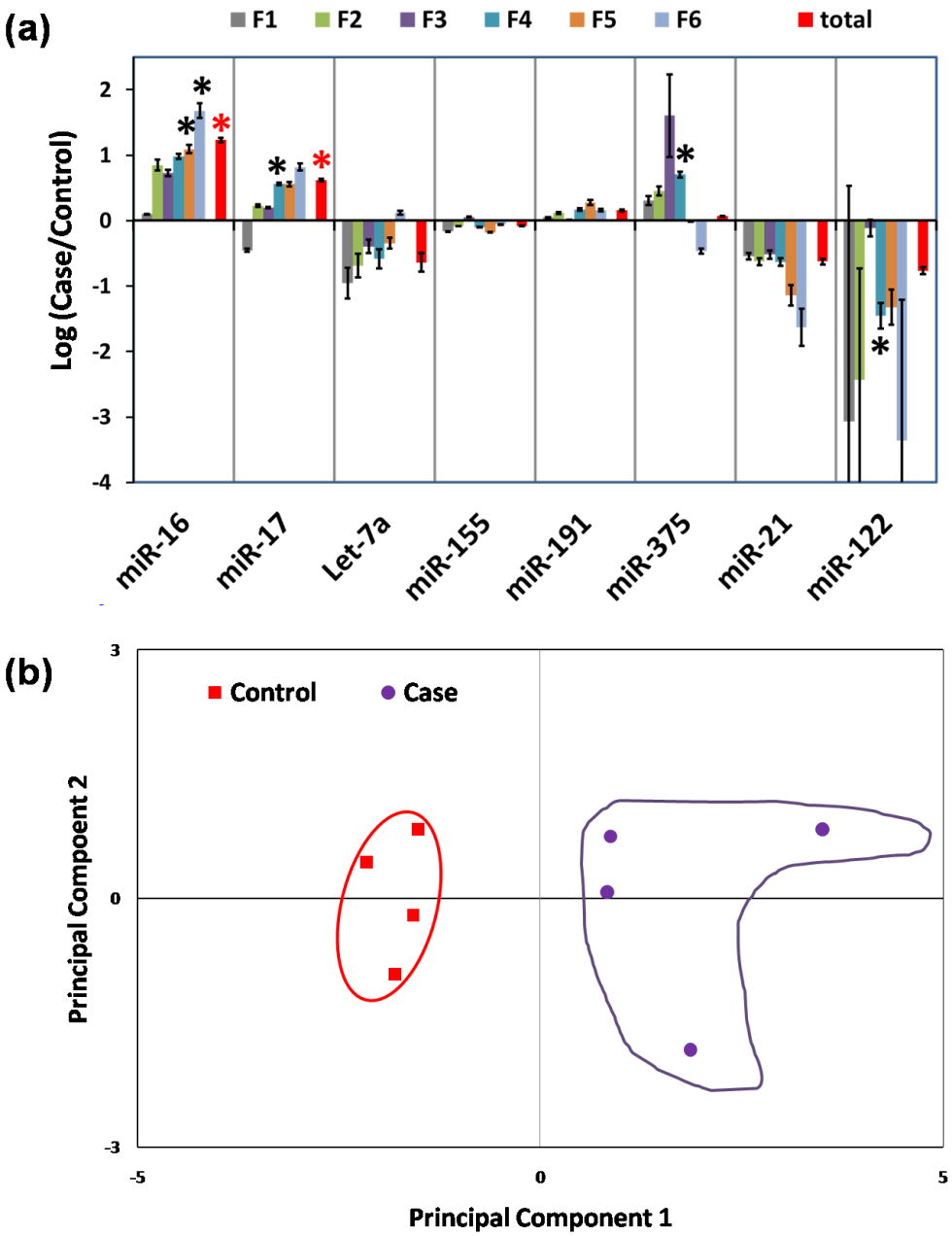

Figure 2.06. (a) Change in the averaged log value of miRNA copies (counting all four tests, two samples with two repeats in each group) between the controls and cases. An asterisk marks those showing significant difference between BC patients (cases) and healthy donors (controls) with $p < 0.05$. (b) Score plot of principal component 1 versus principal component 2 obtained by PCA on the miRNA quantity of miR-16, -17, -375, -122 in certain fractions as indicated. The arbitrary circles illustrate the separation between case and control groups.

copy number in the BC samples over that in the control samples; i.e. Log(Case/Control), for each miRNA. If the average miRNA level was lower in the BC cases than in the controls, a negative Log(ratio) value would be obtained, and vice versa. Larger absolute values of Log(Case/Control) would indicate a more obvious difference between these two groups. We also included the Log(Case/Control) obtained using the summed total miRNA quantity from all fractions (displayed as red bars). The sum was to represent the result attainable with the standard approaches in miRNA study, in which the overall expression level of each miRNA is quantified in serum quantity. Figure 4b clearly showed that larger differences between the BC and control samples was observed in some particular fractions than in the sum value for all miRNAs tested, except for *miR*-155 and *miR*-191. This result hints that the miRNA quantity change in some of the carriers could be more sensitive in differentiating the cancer patients from healthy controls than the overall quantity in the whole serum. This speculation was actually supported by the following statistical analysis of the distribution profiles.

2.3.4: Statistical Analysis of the miRNA Distribution Profiles

To see whether the distribution profile could tell the difference between healthy donors and breast cancer patients, and whether more reliable miRNA biomarkers can be found using these profiles, for the eight miRNAs listed in Table 2.1, we fitted their quantities in each fraction in the linear mixed effects model shown in Equation 2.1, using R 3.0.2. For a miRNA in a given fraction, Y is the log value of the observed miRNA copy number. For example, for *miR*-16 in F1, Y_{111} is the log value of the miRNA copy number from one of the two repeats of Control #1. This linear mixed effects model

allows us to account for sample to sample variation σ^2_b, as well as within sample variation σ^2, when comparing healthy donors to breast cancer patients, i.e., testing the hypothesis H_0: $b_1 = b_2 = 0$. We tested this hypothesis for each fraction of each one of the eight miRNAs using likelihood ratio test. To compare with standard approach, the same test was also performed on the sum of all fractions for each miRNA. More miRNA strands (*miR*-16, *miR*-17, *miR*-375, and *miR*-122) in particular fractions (*miR*-16 in F5 & F6, *miR*-17 in F4, *miR*-375 in F4, and *miR*-122 in F4) yielded significant difference between healthy donors and breast cancer patients at the level of 0.05, as marked by the asterisk sign in Figure 4b; whereas only *miR*-16 and *miR*-17 showed significant difference if the sum value was used in the analysis.

$$Y_{ijk} = \mu + b_i + b_{j(i)} + \varepsilon_{ijk}\ , \qquad \textbf{Equation 2.1}$$

i= 1,2(# of patient group), j=1,2(sample# in each group), k=1,2(replicate#)

b_i: effect on ith group (fixed, 1 for the control group, 2 for the case group)

$b_{j(i)}$: effect of jth sample in group i(variable x(y);x=replicate#;y control=1,case=2)

$b_{j(i)} \sim N(0,\sigma_b^2)$, $\varepsilon_{ijk} \sim N(0,\sigma^2)$, $b_{j(i)}$ and ε_{ijk} are independent

It is interesting to see that miRNA quantity in F4 or F6 seems to matter the most in differentiating cases from controls. Although F6 mainly contained exosomes, F4 enriched HDL and LDL. Then it is possible that, while all four markers may be valuable in diagnosis of breast cancer, they may be released by cancer cells via different pathways. For instance, *miR*-16 could be secreted in exosomes; but *miR*-17, *miR*-375, and *miR*-122 in the lipoprotein complexes could be more relevant to the development breast cancer than the exosomal fraction. This highlights the necessity of testing the miRNA quantities within multiple carriers, instead of those only associated to one specific carrier.

To visualize the effectiveness of the quantity of *miR*-16 in F5 and F6; *miR*-17 in F4; *miR*-375 in F4, and *miR*-122 in F4, in discriminating healthy donors and breast cancer patients, we performed principal component analysis (PCA) using XLSTAT 2014 (Addinsoft). The contents of each miRNA in individual fractions were considered as the variables. For example, the *miR*-16 content in F6 is one variable and named as *miR*-16-F6. A total of eight observations were made in our study (two repeats for each sample) were counted as two independent observations. PCA suggests that the first principal component with loadings -0.436, -0.598,-0.167,-0.258, and +0.599 on *miR*-16-F5, *miR*-16-F6, *miR*-17-F4, *miR*-375-F4, and *miR*-122-F4, respectively, can potentially separate healthy donors from breast cancer patients, as shown in the scores plot in Figure 2.06b. In fact, the first principal component already accounts for 87.1% total variation. Certainly, a sample set containing a much larger number of both healthy controls and cancer patients should be analyzed to draw affirmative conclusion about the capability of these potential markers in cancer diagnosis.

2.4: Conclusion

In this research, AF4 was used to rapidly and reproducibly separate serum into fractions, thereby enriching various types of miRNA carriers. Accurate quantification of the miRNA in each fraction yielded the distribution profile. Applying our method to study the miRNA distribution profiles in number of clinical samples, we found that the quantity of some miRNAs in particular fractions exhibited more distinct differences between healthy individuals and breast cancer patients than either the overall quantity or the quantity associated with only one carrier. Our results indicate that such miRNAs,

when associated with some type of carriers, could be more specific and sensitive biomarkers for cancer diagnosis. The knowledge of the carrier then could help to improve our understanding on the fundamentals behind differential secretion of the miRNA markers by cancer cells and their transportation pathways in the circulation system. Such information can help to interpret their functions and help with discovery of more effective therapeutic approaches.

References:

(1) Chowdhury, D.; Choi, Y. E.; Brault, M. E. Charity Begins at Home: Non-Coding RNA Functions in DNA Repair. *Nat. Rev. Mol. Cell Biol.* **2013**, *14* (3), 181–189.

(2) Wahlestedt, C. Targeting Long Non-Coding RNA to Therapeutically Upregulate Gene Expression. *Nat. Rev. Drug Discov.* **2013**, *12* (6), 433–446.

(3) Hagen, J. W.; Lai, E. C. microRNA Control of Cell-Cell Signaling during Development and Disease. *Cell Cycle Georget. Tex* **2008**, *7* (15), 2327–2332.

(4) Nicoloso, M. S.; Spizzo, R.; Shimizu, M.; Rossi, S.; Calin, G. A. MicroRNAs--the Micro Steering Wheel of Tumour Metastases. *Nat. Rev. Cancer* **2009**, *9* (4), 293–302.

(5) Shi, M.; Liu, D.; Duan, H.; Shen, B.; Guo, N. Metastasis-Related miRNAs, Active Players in Breast Cancer Invasion, and Metastasis. *Cancer Metastasis Rev.* **2010**, *29* (4), 785–799.

(6) Volinia, S.; Galasso, M.; Costinean, S.; Tagliavini, L.; Gamberoni, G.; Drusco, A.; Marchesini, J.; Mascellani, N.; Sana, M. E.; Abu Jarour, R.; Desponts, C.; Teitell, M.; Baffa, R.; Aqeilan, R.; Iorio, M. V.; Taccioli, C.; Garzon, R.; Di Leva, G.; Fabbri, M.; Catozzi, M.; Previati, M.; Ambs, S.; Palumbo, T.; Garofalo, M.; Veronese, A.; Bottoni, A.; Gasparini, P.; Harris, C. C.; Visone, R.; Pekarsky, Y.; de la Chapelle, A.; Bloomston, M.; Dillhoff, M.; Rassenti, L. Z.; Kipps, T. J.; Huebner, K.; Pichiorri, F.; Lenze, D.; Cairo, S.; Buendia, M.-A.; Pineau, P.; Dejean, A.; Zanesi, N.; Rossi, S.; Calin, G. A.; Liu, C.-G.; Palatini, J.; Negrini, M.; Vecchione, A.; Rosenberg, A.; Croce, C. M. Reprogramming of miRNA Networks in Cancer and Leukemia. *Genome Res.* **2010**, *20* (5), 589–599.

(7) Dontu, G.; Rinaldis, E. de. MicroRNAs: Shortcuts in Dealing with Molecular Complexity? *Breast Cancer Res.* **2010**, *12* (1), 301.

(8) Ma, L.; Weinberg, R. A. Micromanagers of Malignancy: Role of microRNAs in Regulating Metastasis. *Trends Genet. TIG* **2008**, *24* (9), 448–456.

(9) Ventura, A.; Jacks, T. MicroRNAs and Cancer: Short RNAs Go a Long Way. *Cell* **2009**, *136* (4), 586–591.

(10) Creemers, E. E.; Tijsen, A. J.; Pinto, Y. M. Circulating microRNAs: Novel Biomarkers and Extracellular Communicators in Cardiovascular Disease? *Circ. Res.* **2012**, *110* (3), 483–495.

(11) Laganà, A.; Russo, F.; Veneziano, D.; Bella, S. D.; Giugno, R.; Pulvirenti, A.; Croce, C. M.; Ferro, A. Extracellular Circulating Viral microRNAs: Current Knowledge and Perspectives. *Front. Genet.* **2013**, *4*.

(12) Olivieri, F.; Rippo, M. R.; Procopio, A. D.; Fazioli, F. Circulating Inflamma-miRs in Aging and Age-Related Diseases. *Front. Genet.* **2013**, *4*, 121.

(13) Rykova, E. Y.; Laktionov, P. P.; Vlassov, V. V. Circulating Nucleic Acids in Health and Disease. In *Extracellular Nucleic Acids*; Kikuchi, Y., Rykova, E. Y., Eds.; Nucleic Acids and Molecular Biology; Springer Berlin Heidelberg, 2010; pp 93–128.

(14) Williams, Z.; Ben-Dov, I. Z.; Elias, R.; Mihailovic, A.; Brown, M.; Rosenwaks, Z.; Tuschl, T. Comprehensive Profiling of Circulating microRNA via Small RNA Sequencing of cDNA Libraries Reveals Biomarker Potential and Limitations. *Proc. Natl. Acad. Sci.* **2013**, *110* (11), 4255–4260.

(15) Mitchell, P. S.; Parkin, R. K.; Kroh, E. M.; Fritz, B. R.; Wyman, S. K.; Pogosova-Agadjanyan, E. L.; Peterson, A.; Noteboom, J.; O'Briant, K. C.; Allen, A.; Lin, D. W.; Urban, N.; Drescher, C. W.; Knudsen, B. S.; Stirewalt, D. L.; Gentleman, R.; Vessella, R. L.; Nelson, P. S.; Martin, D. B.; Tewari, M. Circulating microRNAs as Stable Blood-Based Markers for Cancer Detection. *Proc. Natl. Acad. Sci.* **2008**, *105* (30), 10513–10518.

(16) Russo, F.; Di Bella, S.; Nigita, G.; Macca, V.; Laganà, A.; Giugno, R.; Pulvirenti, A.; Ferro, A. miRandola: Extracellular Circulating MicroRNAs Database. *PLoS ONE* **2012**, *7* (10), e47786.

(17) Wu, X.; Somlo, G.; Yu, Y.; Palomares, M. R.; Li, A. X.; Zhou, W.; Chow, A.; Yen, Y.; Rossi, J. J.; Gao, H.; Wang, J.; Yuan, Y.-C.; Frankel, P.; Li, S.; Ashing-Giwa, K. T.; Sun, G.; Wang, Y.; Smith, R.; Robinson, K.; Ren, X.; Wang, S. E. De Novo Sequencing of Circulating miRNAs Identifies Novel Markers Predicting Clinical Outcome of Locally Advanced Breast Cancer. *J. Transl. Med.* **2012**, *10* (1), 42.

(18) Samantarrai, D.; Dash, S.; Chhetri, B.; Mallick, B. Genomic and Epigenomic Cross-Talks in the Regulatory Landscape of miRNAs in Breast Cancer. *Mol. Cancer Res.* **2013**, *11* (4), 315–328.

(19) Arroyo, J. D.; Chevillet, J. R.; Kroh, E. M.; Ruf, I. K.; Pritchard, C. C.; Gibson, D. F.; Mitchell, P. S.; Bennett, C. F.; Pogosova-Agadjanyan, E. L.; Stirewalt, D. L.; Tait, J. F.; Tewari, M. Argonaute2 Complexes Carry a Population of Circulating microRNAs Independent of Vesicles in Human Plasma. *Proc. Natl. Acad. Sci.* **2011**, *108* (12), 5003–5008.

(20) Li, L.; Zhu, D.; Huang, L.; Zhang, J.; Bian, Z.; Chen, X.; Liu, Y.; Zhang, C.-Y.; Zen, K. Argonaute 2 Complexes Selectively Protect the Circulating MicroRNAs in Cell-Secreted Microvesicles. *PLoS ONE* **2012**, *7* (10), e46957.

(21) Vickers, K. C.; Palmisano, B. T.; Shoucri, B. M.; Shamburek, R. D.; Remaley, A. T. MicroRNAs Are Transported in Plasma and Delivered to Recipient Cells by High-Density Lipoproteins. *Nat. Cell Biol.* **2011**, *13* (4), 423–433.

(22) Vickers, K. C.; Remaley, A. T. Lipid-Based Carriers of microRNAs and Intercellular Communication: *Curr. Opin. Lipidol.* **2012**, *23* (2), 91–97.

(23) Diehl, P.; Fricke, A.; Sander, L.; Stamm, J.; Bassler, N.; Htun, N.; Ziemann, M.; Helbing, T.; El-Osta, A.; Jowett, J. B. M.; Peter, K. Microparticles: Major Transport Vehicles for Distinct microRNAs in Circulation. *Cardiovasc. Res.* **2012**, *93* (4), 633–644.

(24) Xu, J.; Chen, Q.; Zen, K.; Zhang, C.; Zhang, Q. Synaptosomes Secrete and Uptake Functionally Active microRNAs via Exocytosis and Endocytosis Pathways. *J. Neurochem.* **2013**, *124* (1), 15–25.

(25) Yang, M.; Chen, J.; Su, F.; Yu, B.; Su, F.; Lin, L.; Liu, Y.; Huang, J.-D.; Song, E. Microvesicles Secreted by Macrophages Shuttle Invasion-Potentiating microRNAs into Breast Cancer Cells. *Mol. Cancer* **2011**, *10*, 117.

(26) Palma, J.; Yaddanapudi, S. C.; Pigati, L.; Havens, M. A.; Jeong, S.; Weiner, G. A.; Weimer, K. M. E.; Stern, B.; Hastings, M. L.; Duelli, D. M. MicroRNAs Are Exported from Malignant Cells in Customized Particles. *Nucleic Acids Res.* **2012**, *40* (18), 9125–9138.

(27) Kosaka, N.; Iguchi, H.; Yoshioka, Y.; Takeshita, F.; Matsuki, Y.; Ochiya, T. Secretory Mechanisms and Intercellular Transfer of MicroRNAs in Living Cells. *J. Biol. Chem.* **2010**, *285* (23), 17442–17452.

(28) Kosaka, N.; Iguchi, H.; Yoshioka, Y.; Hagiwara, K.; Takeshita, F.; Ochiya, T. Competitive Interactions of Cancer Cells and Normal Cells via Secretory MicroRNAs. *J. Biol. Chem.* **2012**, *287* (2), 1397–1405.

(29) Umezu, T.; Ohyashiki, K.; Kuroda, M.; Ohyashiki, J. H. Leukemia Cell to Endothelial Cell Communication via Exosomal miRNAs. *Oncogene* **2013**, *32* (22), 2747–2755.

(30) Gallo, A.; Tandon, M.; Alevizos, I.; Illei, G. G. The Majority of MicroRNAs Detectable in Serum and Saliva Is Concentrated in Exosomes. *PLoS ONE* **2012**, *7* (3), e30679.

(31) Turchinovich, A.; Weiz, L.; Langheinz, A.; Burwinkel, B. Characterization of Extracellular Circulating microRNA. *Nucleic Acids Res.* **2011**, *39* (16), 7223–7233.

(32) Zhou, W.; Fong, M. Y.; Min, Y.; Somlo, G.; Liu, L.; Palomares, M. R.; Yu, Y.; Chow, A.; O'Connor, S. T. F.; Chin, A. R.; Yen, Y.; Wang, Y.; Marcusson, E. G.; Chu, P.; Wu, J.; Wu, X.; Li, A. X.; Li, Z.; Gao, H.; Ren, X.; Boldin, M. P.; Lin, P. C.; Wang, S. E. Cancer-Secreted miR-105 Destroys Vascular Endothelial Barriers to Promote Metastasis. *Cancer Cell* **2014**, *25* (4), 501–515.

(33) Yoo, C. E.; Kim, G.; Kim, M.; Park, D.; Kang, H. J.; Lee, M.; Huh, N. A Direct Extraction Method for microRNAs from Exosomes Captured by Immunoaffinity Beads. *Anal. Biochem.* **2012**, *431* (2), 96–98.

(34) Mathivanan, S.; Lim, J. W. E.; Tauro, B. J.; Ji, H.; Moritz, R. L.; Simpson, R. J. Proteomics Analysis of A33 Immunoaffinity-Purified Exosomes Released from the Human Colon Tumor Cell Line LIM1215 Reveals a Tissue-Specific Protein Signature. *Mol. Cell. Proteomics* **2010**, *9* (2), 197–208.

(35) Tauro, B. J.; Greening, D. W.; Mathias, R. A.; Ji, H.; Mathivanan, S.; Scott, A. M.; Simpson, R. J. Comparison of Ultracentrifugation, Density Gradient Separation, and Immunoaffinity Capture Methods for Isolating Human Colon Cancer Cell Line LIM1863-Derived Exosomes. *Methods* **2012**, *56* (2), 293–304.

(36) Yamada, T.; Inoshima, Y.; Matsuda, T.; Ishiguro, N. Comparison of Methods for Isolating Exosomes from Bovine Milk. *J. Vet. Med. Sci. Jpn. Soc. Vet. Sci.* **2012**, *74* (11), 1523–1525.

(37) Wahlund, K. G.; Giddings, J. C. Properties of an Asymmetrical Flow Field-Flow Fractionation Channel Having One Permeable Wall. *Anal. Chem.* **1987**, *59* (9), 1332–1339.

(38) Madörin, M.; van Hoogevest, P.; Hilfiker, R.; Langwost, B.; Kresbach, G. M.; Ehrat, M.; Leuenberger, H. Analysis of Drug/plasma Protein Interactions by Means of Asymmetrical Flow Field-Flow Fractionation. *Pharm. Res.* **1997**, *14* (12), 1706–1712.

(39) Pollastrini, J.; Dillon, T. M.; Bondarenko, P.; Chou, R. Y.-T. Field Flow Fractionation for Assessing Neonatal Fc Receptor and Fcγ Receptor Binding to Monoclonal Antibodies in Solution. *Anal. Biochem.* **2011**, *414* (1), 88–98.

(40) Schachermeyer, S.; Ashby, J.; Zhong, W. Aptamer-Protein Binding Detected by Asymmetric Flow Field Flow Fractionation. *J. Chromatogr. A* **2013**, *1295*, 107–113.

(41) Kim, K. H.; Moon, M. H. Chip-Type Asymmetrical Flow Field-Flow Fractionation Channel Coupled with Mass Spectrometry for Top-Down Protein Identification. *Anal. Chem.* **2011**, *83* (22), 8652–8658.

(42) Oh, S.; Kang, D.; Ahn, S.-M.; Simpson, R. J.; Lee, B.-H.; Moon, M. H. Miniaturized Asymmetrical Flow Field-Flow Fractionation: Application to Biological Vesicles. *J. Sep. Sci.* **2007**, *30* (7), 1082–1087.

(43) Yang, I.; Kim, K. H.; Lee, J. Y.; Moon, M. H. On-Line Miniaturized Asymmetrical Flow Field-Flow Fractionation-Electrospray Ionization-Tandem Mass Spectrometry with Selected Reaction Monitoring for Quantitative Analysis of Phospholipids in Plasma Lipoproteins. *J. Chromatogr. A* **2014**, *1324*, 224–230.

(44) Chien, K.; Goshe, M. Advances in Quantitative Mass Spectrometry Analysis: Weighing in on Isotope Coding and Label-Free Approaches for Expression and Functional Proteomics. *Curr. Anal. Chem.* **2009**, *5* (2), 166–185.

(45) Neilson, K. A.; Ali, N. A.; Muralidharan, S.; Mirzaei, M.; Mariani, M.; Assadourian, G.; Lee, A.; van Sluyter, S. C.; Haynes, P. A. Less Label, More Free: Approaches in Label-Free Quantitative Mass Spectrometry. *Proteomics* **2011**, *11* (4), 535–553.

(46) Zhu, W.; Smith, J. W.; Huang, C.-M. Mass Spectrometry-Based Label-Free Quantitative Proteomics. *J. Biomed. Biotechnol.* **2010**, *2010*, 840518.

(47) Zhou, W.; Liotta, L. A.; Petricoin, E. F. The Spectra Count Label-Free Quantitation in Cancer Proteomics. *Cancer Genomics Proteomics* **2012**, *9* (3), 135–142.

(48) Camont, L.; Chapman, M. J.; Kontush, A. Biological Activities of HDL Subpopulations and Their Relevance to Cardiovascular Disease. *Trends Mol. Med.* **2011**, *17* (10), 594–603.

(49) Kim, K. H.; Lee, J. Y.; Lim, S.; Moon, M. H. Top-down Lipidomic Analysis of Human Lipoproteins by Chip-Type Asymmetrical Flow Field-Flow Fractionation-Electrospray Ionization-Tandem Mass Spectrometry. *J. Chromatogr. A* **2013**, *1280*, 92–97.

Chapter 3: Microfluidic Based Isolation and Extraction for Distribution Profiling of Circulating MicroRNAs in Serum for Potential in Cancer Diagnosis

3.1: Introduction

Accurate detection of cancer, at its earliest stages of development, can enhance the quality of life and survival rate of patients by enabling timely therapeutic intervention before the growth and spread of the disease. The success of the accuracy of early detection strongly relies on highly specific and sensitive biomarkers. Commonly used biomarkers in cancer detection are gene marker proteins and Messenger RNA (mRNA). As relatively non-invasive biomarkers are preferred both for screening and reoccurring testing, circulating biomarkers found in bodily fluid are optimal and can often negate the need for tissue biopsy. Messenger RNA are not typically present at high enough concentrations in serum samples to be used and gene marker proteins can have relatively high false positive and negative rates in diagnostics as they are downstream products of the complex situation within cells. One class of very promising potential biomarkers are microRNAs (miRNAs) for diagnosis and monitoring of not only cancer but many other diseases including diabetes, drug resistant epilepsy, liver disease, coronary artery disease, and Alzheimer disease among others. MicroRNAs are short 20-25 nucleotide non-coding RNAs which regulate gene expression. MicroRNAs are responsible for post-transcriptional regulation of mRNA translation through action of the RNA-induced silencing complex (RISC) in inhibiting mRNA translation or induce mRNA cleavage and degradation.[1,2] Compared to more widely used nucleic acid-based disease markers (mRNAs), miRNAs have been found to be more closely related to disease stages and sub-

type and are tissue specific.[3–6] In addition, they have simpler structure and less complex post-synthesis processing than other biomarkers such as proteins. Moreover, miRNAs can be released into the circulation system and are stably present at levels detectible by sensitive techniques like RT-qPCR.[7–10] Sampling blood for analysis of circulating miRNAs is also simpler and much less invasive for the patient compared to conventional tissue biopsies used in cancer diagnosis. Owing to their appealing features, circulating miRNAs have attracted great research efforts to study their expression profiles, as well as discovery and validation of their relationship with diseases.[11–13]

The application of miRNAs in cancer diagnosis is exciting and of high importance due to the disruption of normal levels of miRNA early on in cancer development. Over-expression of oncogenic miRNAs that inhibit the tumor suppressor genes can interfere with the anti-oncogenic pathway, while deletion or epigenetic silencing of tumor-suppressive miRNAs that can target oncogenes can increase oncogenic potency.[14–17] Therefore the levels of oncogenic and tumor-suppressive miRNAs are found to be increased and decreased respectively in cancerous tissues versus healthy tissues. Accumulating evidence shows that circulating miRNAs exhibit varied patterns between cancer patients and healthy controls, caused by the corresponding changes in the miRNA levels in the cancerous versus healthy tissues.[18–20] Most previous studies on the relationship between circulating miRNAs and cancer development rely solely on the extraction and quantification of the total quantities of miRNAs from plasma or serum. Potential markers are identified via comparing the total miRNA quantities obtained from cancer patients to those from healthy controls. However not all circulating miRNAs are

relevant to the development of cancer, such as the miRNAs that are normally secreted by tissue and blood cells or release upon death or rupture of cells. These add significantly to the concentration of miRNAs in blood, plasma, and serum increasing the variances in miRNA abundance between individuals within the same health group. This background diminishes the relevance of total miRNA levels in plasma and serum and yield inconsistency in identification of relevant miRNA markers. Another difficulty in the discovery and application of circulating miRNA cancer biomarkers is the presence of several pre-analytical variables; these include changes induced by sample collection methods, storage, and handling prior to and during miRNA extractions. Among studies that found potential miRNA markers for breast cancer, there was large variability and few miRNAs were repeatedly identified and some were found with opposing trends.[21–35] The variable data highlight the complexity in the study of the expression of circulating miRNAs.[36] Even highly similar datasets with identical sample size, substrate, and profiling platform could have substantial discrepancy.[37] To overcome these barriers, more effective methods for screening and of the circulating miRNAs than the current approaches is necessary for the application on miRNA as more specific cancer biomarkers.

Cell-free miRNAs found in the extracellular environment of circulatory fluids are protected from the abundant ribonucleases in that environment by various types of carriers.[38,39] These carriers can be the vehicle, by which the miRNA is secreted from cells which can indicate their origin, how they are secreted and transported to other cells for cell-cell communication.[40] Many extracellular miRNAs can be found bound to RISC

associated proteins such as Argonaute 2 (AGO2) or GW182.[41–45] Additionally, miRNAs have been found associated with high-density lipoprotein (HDL) as a significant carrier[46,47] and may mediate intracellular communication.[44,46] HDL-associated miRNA are of additional interest as they have been recently found to traverse the blood-brain barrier.[48] MiRNA may also associate with low-density lipoproteins (LDL)[49] and free apo-lipoproteins (ApoA-I, ApoA-II, ApoB) which are major components of HDL and LDL and as such may have RNA binding ability. Alternatively, miRNAs can be secreted by small cellular vesicles known as exosomes[44,45,50–52] which have been studied as one of the exportation routes of malignant cells.[53] Exosomes also may be involved in metastasis of cancer as they can be transfer from malignant cells to normal cells, function as silencers of target mRNA after their uptake,[54–57] and therefore are potential markers for both early and latter stages of cancer. While miRNA secretion by malignant cells could be the consequence of dysregulation of cellular pathways related to the development of the cancer, intentional exportation and resulting uptake could be related to metastasis and the progression of the cancer.[42,52,54,56,58] Therefore, it is more informative to present the relative levels of miRNAs with correlation to their extracellular carriers providing linkage to their secretion pathways in comparison to simply quantifying their overall quantities in the extracellular fluid as a whole.

We hypothesize that changes in miRNA quantity within particular types of carriers and the relative miRNA abundance among different carriers, are more relevant to cancer initiation and development than the overall expression. To study this hypothesis we aim to obtain distribution profiles of circulating miRNAs in serum that describe their

presence in three dimensions; carrier species, absolute quantity, and target miRNA sequence. This simultaneous profiling of miRNAs associated within all carriers can help to obtain a more comprehensive view of the relationship between cancer and miRNA distribution amongst various carriers. Through the comparison of the distribution profiles of miRNAs in sera samples collected from breast cancer patients and healthy controls, we hope to reveal more specific and sensitive miRNA biomarkers identified by their particular serum carriers. The information gained from the distribution profiling both aid in biomarker discovery while also simplifying the design on miRNA-based point-of-care clinical tests for cancer diagnosis.

In our previous work, we employed asymmetrical flow-field flow (AF4) fractionation of serum components for distribution profiling of miRNAs associated to differently sized carriers in serum.[59] We optimized the separation profile to effectively isolate 4 major carriers within 6 fractions; these include small protein (<100 kDa), HDL, LDL, and exosomes. As proof of principle we investigated the distribution profiles of 8 miRNA targets (selected based on their reported relevance to breast cancer) amongst two breast cancer patients (cases) and two healthy controls for comparison. Larger differences between cases and controls were observed in miRNA recovered in our individual fractions using our distribution profiling method then by analyzing total miRNA quantities. Using our method four out of the eight targets showed significant differences for cases versus controls whereas the total quantities only showed two miRNAs with significant differences. Although our AF4-based method provides comprehensive distribution profiling by separating carriers into six fractions, the method still has some

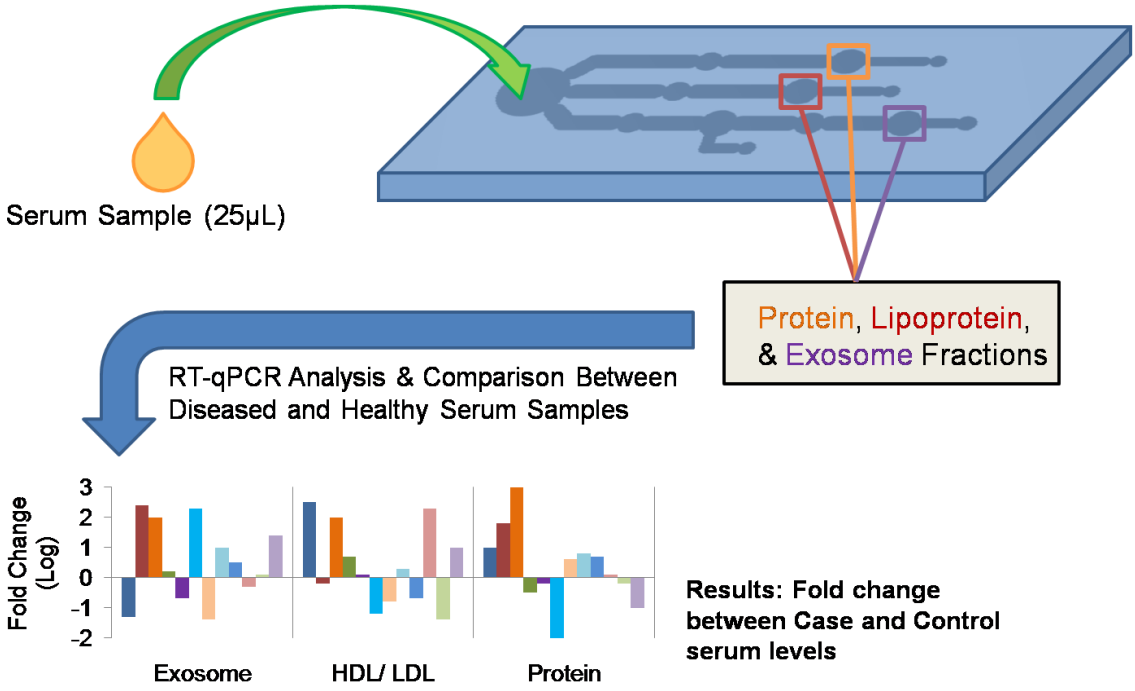

Figure 3.01. Scheme illustrating the experimental design. From 25 µL of serum on the device, the technique is able to isolate miRNA from 3 distinct fractions for downstream analysis.

inadequacies. The recovery of miRNAs from the large elution volumes of the AF4 is difficult and irreproducible, labor intensive, and time consuming. Additionally, due to AF4 separating species solely on size and the resolution limits of separating species over such a large size range from an adequate serum volume, the resolution of different carriers may not be satisfactory. Large proteins (>100 kDa), such as IgG, co-elute with HDL while massive proteins and multi-protein complexes co-elute with LDL. Also co-elution between VLDL and exosomes was obvious. To further improve upon our previous work in terms of carrier isolation, miRNA recovery, and work/time efficiency, we continued to develop a microfluidic based distribution profiling technique (Figure 3.01) which could be more clinically relevant and provide a more efficient method of biomarker discovery.

Microfluidic technology is a currently investigated field for improving sample work-flow, increasing the rate of sample processing and analysis, and reducing sample consumption. Microfluidics allows for greater sample manipulation without possible contamination or sample loss associated with bench top techniques. Microfluidic technology towards distribution profiling of serum miRNA carriers also provides the foundation of point-of-care devices with integrated detection. The currently developed technique allows for the isolation of 3 discrete sub-fractions of miRNA carriers with minimal cross-contamination between carriers; these carrier fractions are proteins, lipoprotein complexes (HDL/LDL), and exosomes.

3.2: Materials and Methods

3.2.1: Chemicals and Biomaterials

All chemicals used to prepare 1× PBS (10 mM phosphate at pH 7.4, 137 mM NaCl, 2.7 mM KCl, and 1.0mM MgCl2), ethylene glycol, dimethyl sulfoxide, guanidine hydrochloride, guanidine isothiocyanate, potassium chloride, ethanol, silicone oil, sulfo-N-hydroxysuccinimide (sulfo-NHS), Pierce ECL Substrate, and NeutrAvidin were purchased from Thermo Fisher (Pittsburgh, PA). Carboxyl magnetic polystyrene particles (2.5% w/v) with a nominal diameter of 350 nm were acquired from Spherotech Inc. (Lake Forest, IL). Superparamagnetic silica particles with a nominal diameter of 1.0 μm were purchased from Bioclone Inc. (San Diego, CA). 1-(3-dimethylaminopropyl)-3-ethylcarbodiimide hydrochloride (EDC), and 1,7-dichloro-octamethyltetrasiloxane were purchased from Acros Organics (Pittsburgh, PA). Bovine serum albumin (BSA), and Tween-20 were obtained from Sigma Aldrich (St. Louis, MO). Goat anti-Mouse IgG and biotinylated chicken anti-Human HDL and LDL antibodies were purchased from Abcam (Cambridge, UK). Mouse anti-human CD63 antibodies were purchased from Novus Biologicals (San Diego, CA). Polydimethyl siloxane (PDMS) was purchased from Dow Corning (Midland, MI). Taq 5× master mix was purchased from New England Biolabs. TaqMan MicroRNA Assays specific for each target were purchased from Life Technologies (Carlsbad, CA). Synthesized MicroRNA standards and exogenous control were purchased from Integrated DNA Technologies (Coralville, IA) according to the mature 5’ sequences from miRBase.

Case Sera Samples				
Sample	**Stage**	**Diagnosed disease type**	**Age**	**Race/ethnicity**
COH-01	IV	Infiltrating ductal carcinoma	48	Blk-African American/not Hispanic
COH-02	IV	Infiltrating ductal carcinoma	52	UNK/ Hispanic
COH-03	III	Infiltrating ductal carcinoma	50	WHT/Not Hispanic
COH-04	III	Infiltrating ductal carcinoma	53	Asian/Not hispanic
COH-05	III	Infiltrating ductal carcinoma	51	WHT/not Hispanic
COH-06	IV	Infiltrating ductal carcinoma	33	WHT/not Hispanic
COH-07	IV	Infiltrating ductal carcinoma	48	Race not reported/Hispanic
COH-08	III	Infiltrating ductal carcinoma	57	WHT/Not Hispanic
COH-09	III	Infiltrating ductal carcinoma	47	UNK/ Hispanic
COH-10	II	Infiltrating ductal carcinoma	49	WHT/Hispanic
COH-11	III	Infiltrating ductal carcinoma	41	WHT/Hispanic
COH-12	IV	Inflammmatory ductal carcinoma	32	WHT/Hispanic

Table 3.1. Sera samples from breast cancer patients used in this study.

Control Sera Samples		
Sample	**Age**	**Race**
HFS-01	32	White
HFS-02	47	White
HFS-03	49	White
HFS-04	51	Hispanic
HFS-05	53	Hispanic
HFS-06	48	White
HFS-07	33	White

Table 3.2. Healthy sera samples used in study.

The twelve breast cancer patient serum samples (cases) used in the microfluidic distribution profile study were obtained from our collaborators at the City of Hope Medical Center (Duarte, CA). The samples were obtained from voluntarily consenting female patients under institutional review board-approved protocols. The donor's age and race, along with the cancer stage and types are shown in Table 3.1. Eleven of the patients have infiltrating ductal carcinoma while one patient has the rarer inflammatory ductal carcinoma with their stages ranging from II to IV. A total of seven single donor healthy female serum samples were purchased from Innovative Research Incorporated (Novi, MI), considering the age and race of the donors to roughly match that of the breast cancer patients for use as controls (Table 3.2).

3.2.2: Microfluidic Chip Fabrication

The chip fabrication method is similar to that published in our previous work.[60] The final microfluidic device was made by bonding a 75 mm × 25 mm glass microscope slide (0.5 mm thick) as a substrate and a cured PDMS layer containing the features of the channels and wells. In order to mold and cure the PDMS with the desired features (channels and wells), a total of three chip masters were prepared (ChipMs-1, ChipMs-2, and ChipMs-3). PDMS was prepared with the Sylgard 184 Silicone Elastomer kit (Dow Corning, MI) using a 10:1 mass ratio of the monomer base to the reactive curing agent. Firstly ChipMs-1, which contained only the channel features, was fabricated from the thiolene-based UV curable optical adhesive, NOA81 (Norland Products, NJ), by an open faced method. NOA81 exhibits rapid curing and strong glass-bonding upon UV irradiation and is able to sufficiently produce cured structures with dimensions from

about one hundred microns to several millimeters. However, NOA81 demonstrates poor adhesion to PDMS due to both the hydrophobicity of the methylated surface and oxygen dissolved in the PDMS interfering with adhesive curing in the monolayer in contact with the PDMS, thus allowing for removal of the master from the stage. In this method, NOA81 was pre-cured onto a glass slide (air plasma treated) and a PDMS coated working stage by 5-second irradiation using a collimated UV light source (365 nm, ~8.3 mW/ cm^2) to produce the channel features with dimensions defined by a printed photomask. The stage consists of a glass substrate with a thin PDMS coating to prevent adhesion of NOA81 to the platform. The thickness of ChipMs-1 was determined by the use of spacers (~400 µm) placed between the stage and the glass slide. After the short UV exposure, the glass slide was slowly removed from the PDMS stage, with the pre-cured NOA81 attached to the glass surface. The excess uncured adhesive was removed and the slide was rinsed by syringe with ethanol, then 1:1 ethanol:acetone, then again with ethanol and air dried. The ChipMs-1 was then exposed to UV light for 345 seconds, a post-cure step to fully cure NOA81 and unsure adhesion to the glass. A subsequent ~12 hour thermal cure at 50 °C was carried out to extend the structure's lifetime. Thereafter, ChipMs-1 was treated by 1,7-dichloro-octamethyltetrasiloxane (vapor deposition) to produce a non-stick surface on the master and utilized to mold the PDMS substrate for making ChipMs-2. The PDMS substrate was degassed and was cured at 60 °C for 4 hours and then peeled off the ChipMs-1. Appropriately sized holes were punched in the location of the open wells to form ChipMs-2. After temporarily attaching ChipMs-2 to a plasma-treated glass slide, NOA81 was injected into the channels and wells without trapping air bubbles,

cured under UV for 1300 seconds, and thermally aged at 50 °C for ~12 hours. By carefully removing the PDMS-ChipMs-2, ChipMs-3 was accomplished containing both the low channel features and the tall pillar/well structures on the surface. After treatment with 1,7-dichloro-octamethyltetrasiloxane (vapor deposition), ChipMs-3 could then be used for replication of the PDMS substrate for the manufacture of microchips used for miRNA extractions. The microchips were finally manufactured by covalent bonding of the final formed PDMS substrate on a glass microscope slide through plasma oxidation of both surfaces followed by immediate attachment. The channels of the device are then methylated by washing and incubating with 1M sodium hydroxide for 10 minutes, washing with water, ethanol, then drying with air, followed by incubation of the 1,7-dichloro-octamethyltetrasiloxane reagent (10% v/v in ethanol). The chip is then rinsed with ethanol and thoroughly dried, then either immediately used or stored in a desiccator until use.

3.2.3: Preparation of Microparticles

Magnetic silica microbeads were washed three times with nuclease-free ultrapure water and concentrated up to 100 µg/µL before use in extractions. For the immuno-based isolation of lipoproteins, 350 nm carboxyl magnetic polystyrene particles were conjugated to NeutrAvidin using traditional carbodiimide cross-linking followed by incubation with either anti-HDL or anti-LDL chicken IgG. For the preparation of anti-CD63 microbeads, 350 nm carboxyl magnetic polystyrene particles were conjugated to goat anti-Mouse IgG using carbodiimide cross-linking. The carbodiimide cross-linking protocol is as follows; A mixture of 10 mg 1-Ethyl-3-(3-dimethylaminopropyl)-

carbodiimide (EDC) and N-hydroxysulfosuccinimide (sulfo-NHS) was added to 1 mg (20 mg/mL) microparticles suspended in 50 mM MES activation buffer (pH~5.5). After 30 min incubation, the activation buffer was removed and the particles were washed two times with the coupling buffer (1× PBS, pH~7.2). Then the appropriate amount of protein (NeutrAvidin or anti-mouse IgG), saturate the particle surface, was added to the particles which are resuspended in the coupling buffer at a final concentration of 10 mg/ml. The mixture was then incubated with mixing overnight at 4 °C. The beads were then washed twice with the coupling buffer and then resuspended in 25 mM glycine quenching buffer (pH~7.2), and incubated for 30 minutes at RT to block any residual reactive sites. After two washes with 1× PBS containing 1% BSA, the beads were dispersed in storage buffer (1× PBS with 0.01% BSA) to the desired particle concentration of 25 mg/mL. Before usage, the microparticles would be mixed with the respective antibody (either biotinylated anti-human HDL/LDL or mouse anti-human CD63) at a final bead concentration of 10 mg/mL in 1×PBS, followed with overnight incubation with mixing at 4 °C. After protein binding, the beads were then washed three times with 1× PBS and stored in the storage buffer.

3.2.4: Pooled RT-qPCR

An optimized pooled RT-qPCR protocol was used for analysis of 9 human miRNA targets and two exogenous controls from *Caenorhabditis elegans* (*C. elegans*) employing the individual TaqMan MicroRNA Assay kits (Applied Biosystems) diluted and pooled together for simultaneous reverse transcription of all targeted miRNAs in the serum extracts, followed by simultaneous pre-amplification those targets prior to splitting

(a)

Component	Volume per Reaction
RT Primer Pool (0.1x)	3.00 µL
dNTPs(100mM)	0.31 µL
MultiScribe Reverse Transcriptase (50 U/µL)	2.00 µL
10x RT Buffer	1.50 µL
RNase Inhibitor (20 U/µL)	0.19 µL
Nuclease Free Water	0.50 µL
Total	7.50 µL

Thermocycling; 16°C for 32min → 42°C for 32min → 85°C for 5min

(b)

Component	Volume per Reaction
RT Product	1.6 µL
SsoAdvanced PreAmp Supermix (2x)	8 µL
PreAmp Primer Pool (0.2x)	2.56 µL
Nuclease Free Water	3.84 µL
Total	**16 µL**

Thermocycling; 95°C for 3min → 58°C for 2min → 72°C for 2min →
[95°C for 15sec→58°C for 4min]$_{12\ Cycles}$ → 100°C for 5min → Held at 4°C

(c)

Component	Volume per Well
(1:9) Diluted PreAmp Product	1 µL
20x TaqMan MicroRNA Assays	0.5 µL
TaqMan 5x Master Mix	2 µL
DMSO	0.1 µL
Ethylene Glycol	1 µL
Magnesium Chloride	0.5 µL
Nuclease Free Water	4.9 µL
Total	**10 µL**

Thermocycling; 95°C for 5min → 59°C for 50sec →
[95°C for 35sec→53°C for 70sec→Plate Read]$_{45\ Cycles}$ → 16°C for 2.5min

Figure 3.02. Reaction mixtures and thermocycling conditions for (a) reverse transcription, (b) pre-amplification, and (c) quantitative PCR.

into separate qPCR reactions on the PCR plate. For absolute quantification of the miRNA targets, synthetic miRNA standards were prepared and amplified via the same pooled RT-qPCR method. Reverse transcription conducted on a Perkin-Elmer 2400 GeneAmp PCR Thermocycler. The qPCR analysis was conducted on a Bio-Rad CFX real-time instrument with all targets for each fraction of the sample plated in technical duplicates for qPCR analysis and standards plated in singlet at three different RT-qPCR input amounts. For statistically significant analysis, triplicate microfluidic extractions were conducted for triplicate RT-qPCR results. The details for the pooled reverse transcription, pooled pre-amplification, and quantitative polymerase chain reactions can be seen in Figure 3.02.

3.2.5: Serum Fractionation by AF4

Fractionation of serum by AF4 was performed as we previously published.[59] An AF200 system manufactured by Postnova Analytics (Salt Lake City, UT) was used, with separation channel thickness of 0.350 mm and injection loop volume of 20 µL, and membrane cutoff of 10 kDa (regenerated cellulose, Postnova Analytics). The running buffer used in all separations was 1× PBS (10 mM phosphate at pH 7.4, 137 mM NaCl, and 2.7 mM KCl). During serum fractionation, an initial focusing step of 8 min was used, with the cross-flow at 3.00 mL/min, tip flow at 0.30 mL/min, and the focus flow at 3.00 mL/min. After the focusing period, there was a 1 minute transition period where the tip flow was increased to 3.30 mL/min and the focus flow was reduced to zero. Afterward, the tip flow was kept at 3.30 mL/min for 5 min and then reduced to 0.30 mL/min over 15 min along with equal reduction of crossflow (maintaining outlet flow of 0.30 mL/min).

Fractions were collected in 1 minute intervals by automatic fraction collector (Bio-rad) and combined to provide 8 fractions containing all significant serum components. Fraction 1 (F1) collected from 6 to 9 min, F2 from 9 to 13 min, F3 from 13 to 16 min, F4 from 16 to 19 min, F5 from 19 to 23 min, F6 from 23 to 28 min, F7 from 28 to 32 min, and F8 from 32-36 min.

3.2.6: ELISA; CD-63 Plate Assays for Exosome Determination

For each of the eight fractions collected from the AF4, 50 µL of the fractions were added to the wells of a 96-well high binding fluorescence/ luminescence microtiter plate (Thermo Fisher) for the adsorption of the isolated serum components. The ELISA plate was incubated overnight at 4 °C to let all the proteins/ carrier species be adsorbed onto the bottom of each well. Then, the supernatant solution was discarded, and the plate was washed two times with 200 µL 1×PBS (all washing buffers used in our assay were 1×PBS), before 200 µL of the blocking buffer containing 5% non-fat milk in 1×PBS was added for each well. The plate was then incubated overnight at 4 °C with gentle shaking to efficiently block the exposed surface of each well. Then the blocking buffer was discarded and the wells were washed twice with washing buffer. Next, 100 µL of the primary antibody (mouse anti-human CD63, Catalog #ab8219, Abcam, Cambridge, MA) in 1 : 5000 dilution with 1× PBS was added to the wells, followed with a 2-hr incubation at room temperature. After removal of the supernatant and the following four washes, 100 µL of the secondary antibody, horseradish peroxidase (HRP) conjugated rabbit anti-mouse IgG (Catalog # ab97046, Abcam) in a 1 : 25000 dilution in 1× PBS was added and incubated for 1 hour at room temperature with gentle shaking. The supernatant was again

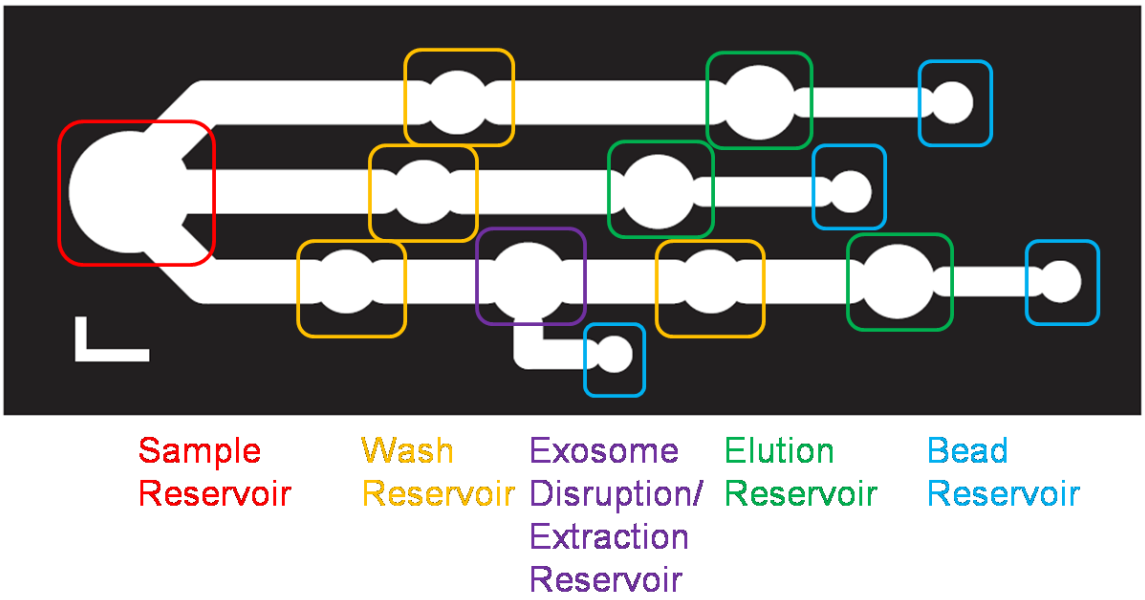

Figure 3.03. Illustration of microfluidic device design. The device has open wells and closed channels, with all channel and well feature in the PDMS layer. The glass bottom is functionalized with methyl groups to reduce adsorption of particles or biomolecules. All wells for washing, exosome disruption, and elution are prefilled with the appropriate reagents and separated by the silicone oil which fills the channels, bead reservoir, and initially the sample reservoir. The scale bars 3 × 5 mm.

discarded and the plate was washed four times with wash buffer. Next 50 μL of the Pierce enhanced chemiluminescence (ECL) substrate (Thermo Fisher) was added, and incubated for 5 minutes. The resulting chemiluminescence was immediately detected. Three replicates were measured on the same plate for each of the eight AF4 fractions and samples. For the standard curve, two replicates of pure human CD63 (Sino Biology) with serial-diluted concentrations in the relevant concentration range were added in the same plate. The blank contained only 1×PBS in the adsorption step but was treated equally in all other steps.

3.2.7: Microfluidic Extraction of MiRNAs

The layout of the microfluidic chip is illustrated in Figure 3.03. The device has three channels for the extraction of miRNAs in one particular serum carrier type per channel. Each channel is connected to the main sample reservoir and contains silicone oil, linking several wells and reservoirs while maintaining isolation of those wells. The device channels are filled with silicone oil and the wells and reservoirs other than the main sample reservoir are pre-loaded with the appropriate reagents or aqueous solutions, forming condense droplets in those wells. Channels 1 and 2 contain wash, elution, and bead collection reservoirs for the extraction and isolation of protein- and lipoprotein-bound miRNAs. Channel 3 is designed specifically for the isolation of exosomes and extraction of exosomal miRNA. Channel 3 contains the regular was, elution, and bead collection reservoirs seen in channels 1 and 2, but in addition contains additional wells before those regular ones. These wells are for the washing of beads in exosome purification followed by a well for the disruption of exosomes and sequential extraction

of the miRNA, along with an additional bead reservoir for containment of the used polystyrene beads after exosome disruption.

The microfluidic extraction begins by the addition of 25 µ of serum and 100 µg of immuno-beads conjugated with the anti-CD63 IgG to the sample reservoir forming one confined droplet. The serum sample with the immuno-beads was mixed thoroughly by pipette mixing. After mixing the sample was incubated for 30 minutes at room temperature. The immuno-beads with captured exosomes were then moved towards channel 3, through a wash reservoir (1x PBS) and continuing into an exosome disruption reservoir using a permanent magnet underneath the microfluidic chip. The disruption reservoir holds 30 µL of solution consisting of ~70% EtOH, ~2M guanidine thiocyanate and ~1% Tween-20 surfactant. After pipette mixing, the beads are incubated for 15 minutes at room temperature in the reservoir, after which the beads are removed to the bead collection reservoir through the attached channel. Next 20 µL of 9M GuHCL and 4 µL of 6M KCl were added to the well, then 2 fmol of the exogenous control, *cel-miR*-54, was added and mixed with the sample, followed by the addition of 200 µg of the 1µm magnetic silica beads. After mixing there is another 15 minute incubation to adsorb the RNA. Then the silica beads are removed and travel through a wash reservoir (wash buffer containing 80% ethanol and 1 M guanidine thiocyanate) and into an elution reservoir that contains RNase free ultrapure water. The beads are again thoroughly pipette mixed and again incubated for 15 minutes to release the adsorbed RNA into solution, after which the silica beads are removed into the corresponding bead collection reservoir. Simultaneous extraction of the protein and lipoprotein bound miRNAs was started while the exosomes

were being disrupted and exosomal miRNAs being isolated. After the removal of the exosomes from the serum sample, 30 µL of 9 M GuHCl, 6 µL of 6 M KCl, and 1 µL of 0.1% Tween-20 were added and well mixed with the serum. Then 2 fmol of the exogenous control, *cel-miR*-67, was added and mixed with the sample. Next 200 µg of the magnetic silica beads in 2 µL of water were added, mixed well, and incubated for 15 minutes. Subsequently, the silica beads were magnetically dragged into channel 1. The silica beads then traveled through the channel, passing through the wash well (containing the same wash buffer as above) and continuing to the elution reservoir and incubated for 15 minutes to elute the bound RNA, and finally the beads were removed and collected in the connected bead reservoir. Once the silica beads carrying the protein-bound miRNAs left the sample reservoir, 70 µL of 6 M guanidine thiocyanate, 1 µL of 10% Tween-20, and 15 µL of 100% ethanol were added to the sample and mixed well via pipette. Again 2 fmol of the exogenous control, *cel-miR*-54 this time, was added and mixed with the sample. Then again 200 µg of the magnetic silica beads in 2 µL of water were added, mixed well, and incubated for 15 minutes. The beads were then removed into channel 2 and treated as in channel 1 (wash well, elution well, incubation, and removal of beads). Lastly the three eluents corresponding to the exosome, protein, and lipoprotein associated miRNA fractions were removed from the chip, and then quantified via the optimized pooled RT-qPCR protocol using the commercial Taqman miRNA primer assay kits (Applied Biosystems) specific to each target miRNA.

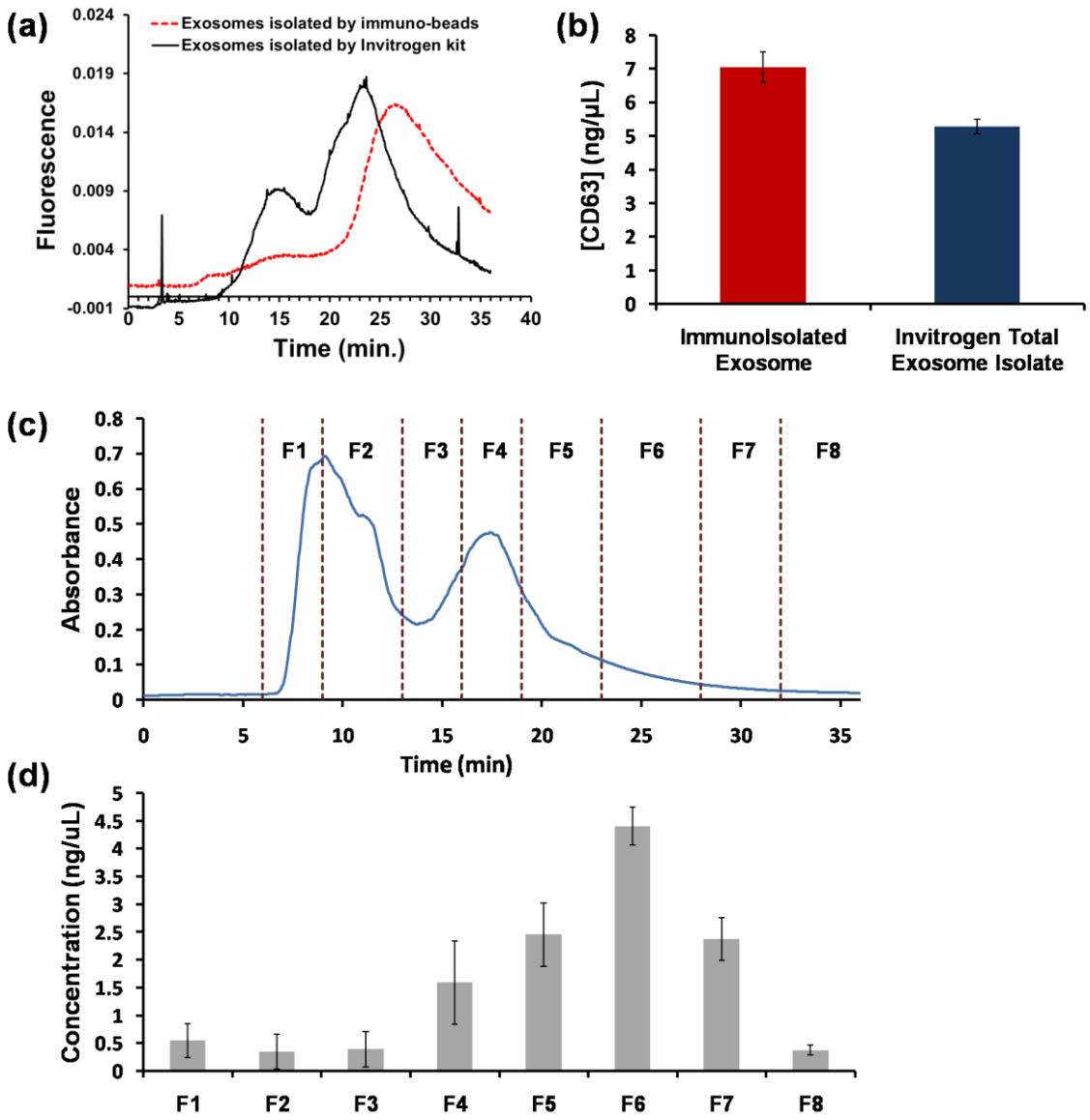

Figure 3.04. (a) AF4 separation traces 9fractograms) collected by fluorescence detector for analysis of exosomes isolated by the immuno-beads as done in our microchip profiling technique (dotted line), and by the Invitrogen kit (solid line). (b) Comparison of the CD63 concentration in exosomes prepared by our immuno-bead isolation method and the Invitrogen kit. (c) Fractogram showing fractions collected during serum separation by AF4 (absorbance detection at 260 nm). (d) Quantification of CD63 using ELISA for all eight collected fractions. The quantities are the average of results from the triplicate testing of each fraction and the error bars represent the standard deviation of those measurements.

3.3: Results and Discussion

3.3.1: Confirmation of Exosome Isolation and Disruption to Release the Exosomal MiRNAs

Isolation of exosomes from serum and extraction of the miRNA using our immuno-bead strategy was confirmed through analyzing the extracted samples with our previously developed asymmetrical flow field-flow fractionation (AF4) technique for separation of serum components and through the comparison of the exosomes prepared by the Invitrogen Exosome Isolation Kit. AF4 separates analytes solely based on their hydration sizes. Previously, we proved the ability of AF4 for the efficient separation of exosomes from proteins and lipoproteins in whole serum with the exception of co-eluted very low-density lipoprotein (VLDL). Thus, we compared the elution profiles of whole serum, exosomes isolated by our immuno-beads on the microfluidic chip, and those prepared by the Invitrogen exosome isolation kit. All the samples were examined by UV-Vis absorbance at 260 nm, and also stained with DiO lipophilic dye and detected by fluorescence for illustration of just the lipid-enriched portions of the separation. As seen in Figure 3.04a, both samples prepared by our on-chip immuno-isolation and by the Invitrogen kit showed significant exosome enrichment shown in the peaks at elution times later than 20 minutes, ELISA results also support this as CD63 was detected at significant amounts in these elution times (Figure 3.04c/ d). The sample prepared by the Invitrogen kit also had a relatively small peak which eluted between 10-17 minutes, which correlates with the lipoprotein complexes which are co-precipitated during the centrifugation. The exosome peak in the sample isolated by our immuno-beads show a

slight shift to a later elution time then the one by the kit which could be the result of lower loading onto the AF4 channel and specific extraction of exosomes. The CD63 concentration found in our method was 7.04 ng/µL (Figure 3.04b), which matches well with the sum of the CD63 concentrations found in fractions 6-8 of whole serum; and the CD63 concentration found with the Invitrogen kit was 5.28 ng/µL, agreeing with the sum CD63 in fractions 5-6. Our method yielded a higher recovery for exosomes from serum as compared to the Invitrogen kit, and we obtained relatively large exosomes which eluted in fraction 7, which was not collected in our previously reported AF4 carrier distribution study.

To confirm the disruption of exosomes using our method, we compared the isolated exosomes before and after disruption using the AF4 separation method. Once isolated using the immuno-beads, they were treated with a solution containing ~75% ethanol and 1 M guanidine isothiocyanate. The high organic content of the solution combined with the guanidine isothiocyanate destroy the membrane structure and solubilize the membrane proteins of the exosomes, releasing the enclosed miRNAs. We can see in figure 3.05 that, after the chemical treatment, the exosome peak disappeared in the AF4 fractogram. In the absorbance fractogram disruption of all proteins is seen, diminishing the trace typically seen before treatment and shifting to lower retention times or small species (Figure 3.05a). Since the DiO lipophilic dye emits strong fluorescence only in a hydrophobic environment and lacks fluorescence in hydrophilic environment, the dramatic decrease in the fluorescence signal indicates the lack of intact hydrophobic structure and the success of the exosome disruption (Figure 3.05b).

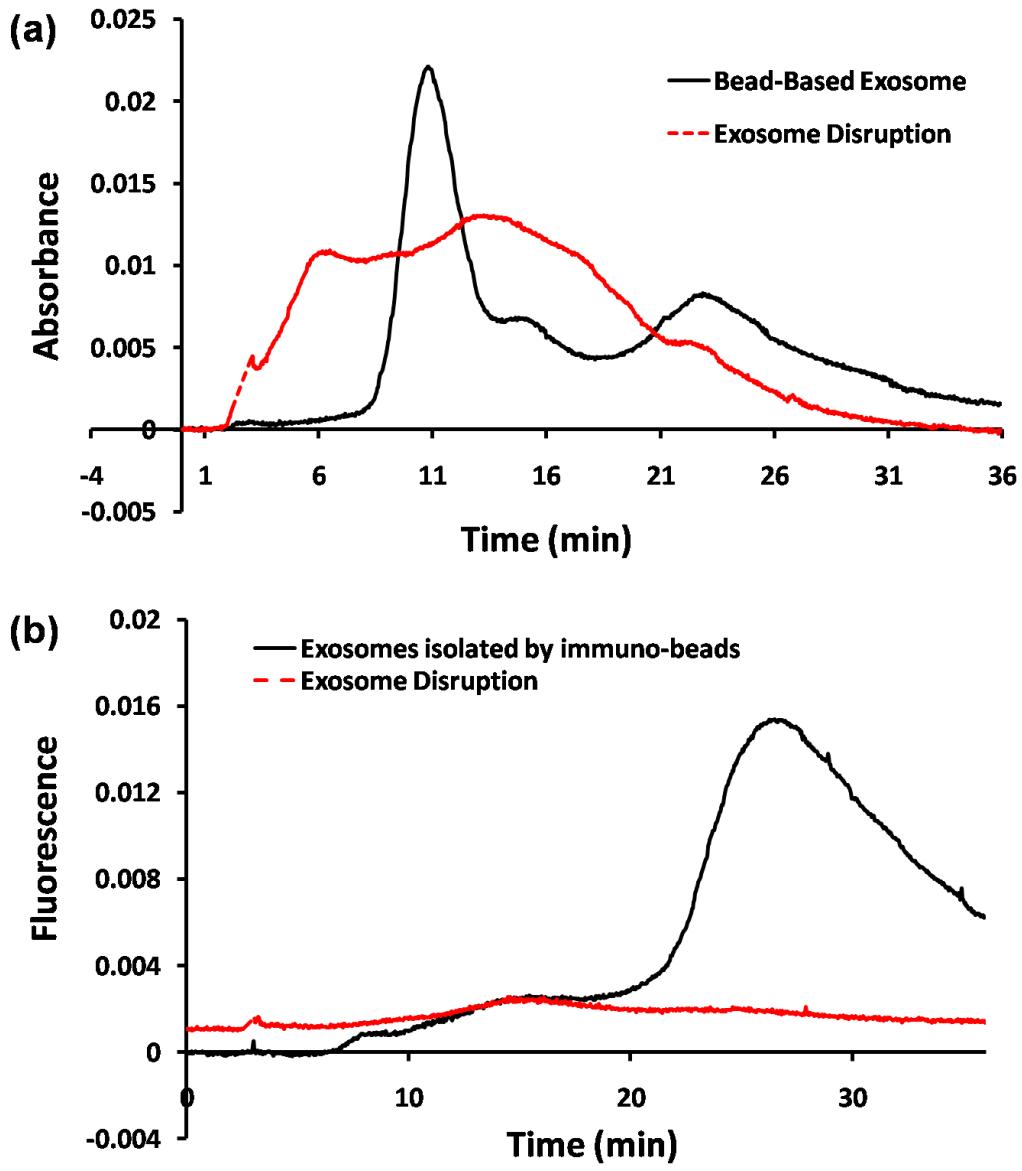

Figure 3.05. Absorbance (a) and fluorescence (b) fractograms for exosomes isolated by the immuno-beads before and after treatment with the disruption solution. Absorbance measured at 260 nmand fluorescence with DiO dye is measured with 480/510 ex/em.

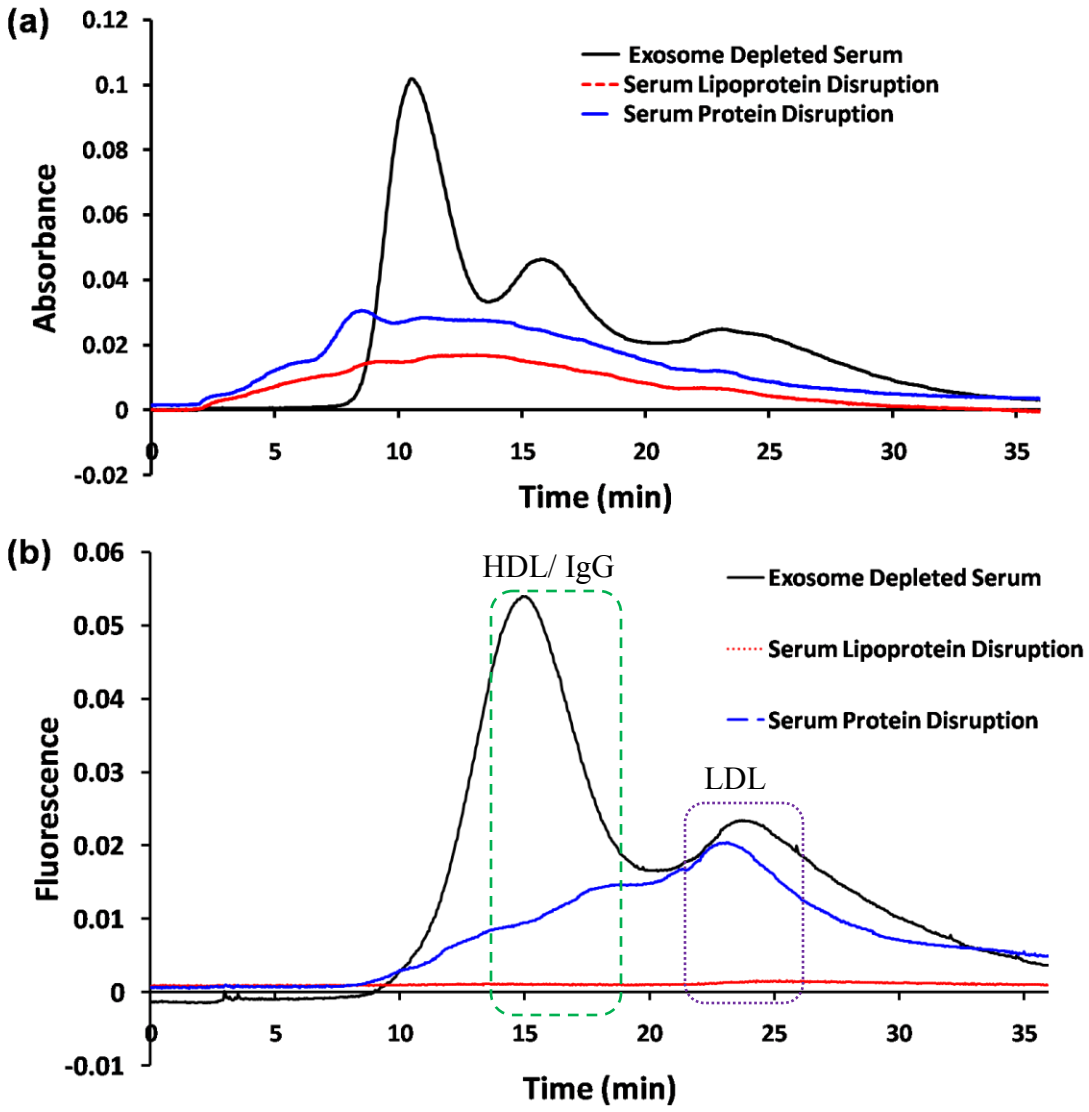

Figure 3.06. Fractograms of exosome-depleted serum before treatment, after treatment with the protein disruption reagents, and after treatment with the lipoprotein disruption reagents.The dashed green box highlights the position where HDL would be eluted (IgG coeluted), and the dotted purple box indicates the elution window for the LDL. Absorbance is measured at 260 nm and the DiO stained fluorescence is measuredad an ex/em of 480/510.

3.3.2: Confirmation of the Disruption of the MiRNA –Protein and -Lipoprotein Complexes

Once the exosomes are extracted, the exosome-depleted serum contains miRNAs mainly bound to lipoprotein complexes or to the proteins like AGO2, GW182, and serum proteins capable of binding miRNA. Protein-RNA interaction relies on H-bonding and electrostatic interactions between the negatively charged phosphate groups on RNA and the positively charged or electropositive primary amines in binding areas of proteins. The presence of chaotropic species work to denature both RNAs and proteins, which would definitely affect the stability of the protein-RNA complexes, leading to dissociation and release of miRNAs. Lipoprotein complexes such as HDL and LDL have compact lipid-protein structure which both aids in protection of the proteins and provide a hydrophobic environment which may aid in binding RNA via the hydrophobic regions of the nucleic acids. In order to disrupt these more compact lipoprotein structures, higher concentrations or stronger denaturants should be employed. For the denaturants used in our study we chose the combination of two chaotropic salts, guanidine hydrochloride (GuHCl) and guanidine isothiocyanate (GuITC), the organic solvent ethanol, and the use of polymeric surfactant Tween-20 which is able to interact with hydrophobic molecules and aid in the disruption of more lipophilic species, such as lipoprotein complexes. To realize consecutive extraction of the protein- and lipoprotein-bound miRNAs from the same serum sample, we treated the exosome depleted serum using a mild solution that contained approximately 0.5 M KCl, 0.0015% Tween-20, and 4 M Guanidine HCl to for relatively gentle disruption and release of the miRNAs bound to proteins. Once these

miRNAs were removed by silica beads, additional Tween-20 and the stronger denaturants, guanidine isothiocyanate and ethanol, were supplied to break-up the compact structures of the lipoprotein complexes and free the associated miRNAs. The final mixture contained approximately 0.5 M KCl, 1.8 M GuHCl. 3 M GuITC, 10% Ethanol, and 1% Tween-20. Again we used our AF4 serum profiling method to investigate the disruption of these species in each case. The absorbance fractogram reveals a loss of the original serum profile as proteins are being denatured with the protein fraction extraction reagents, the fractogram trace is even further decreased upon the addition of the lipoprotein disruption reagents (3.06a). Fluorescence detection of lipoprotein complexes under each denaturing condition offers a more illustrative view of the selective disruption of the lipoprotein complexes. As the DiO lipophilic dye significantly stains HDL and LDL, we can use the dye for fluorescence detection in addition to absorbance detection. Before treatment, exosome depleted serum gives two large peaks stained with DiO (figure 3.06b). Once treated with the mild protein disruption reagents, we see a decrease in the first peak and no significant change in the second peak. According to our previous study and the analysis of human IgG standard, surprisingly IgG can be significantly stained by DiO as well. Therefore the dramatic decrease in the first peak correlates with the protein disruption interfering with DiO staining of denatured IgG, agreeing with our successful protein disruption. The peak corresponding to HDL is still seen after the loss of IgG fluorescence indicating that the structure of HDL remains native in the mild denaturant. After additional treatment of the serum sample with the stronger denaturing solution which contained the GuITC and ethanol, all fluorescence for the HDL and LDL

complexes was lost resulting in a relatively flat fluorescence signal in the fractogram with no distinct peaks (figure 3.06b), indicating that the harsh denaturing environment we provided significantly breaks up and denatures the lipoprotein complexes.

3.3.3: Solid Phase Extraction of the Carrier miRNAs by Magnetic Silica Beads

The disruption and denaturation of the exosomes, lipoprotein-RNA complexes, and protein-RNA complexes release the miRNAs bound to these carriers. These freed miRNAs can then be extracted by binding them to magnetic silica beads. Silica-based solid phase extraction of DNA and RNA has been heavily investigated and widely employed. Chaotropic salts such as guanidine hydrochloride can denature nucleic acids and weaken the hydration effects of nucleic acids in aqueous solutions, promoting interactions with the silica surface, allowing for precipitation of nucleic acids from the solution onto the solid silica support. These interactions include hydrogen-bonding between protonated silanol groups and the negatively charged phosphate backbone of DNA and RNA or salt bridging of deprotonated, negatively charged, silanol groups and the negatively charged phosphate backbone. The dominate interaction in the binding of the nucleic acids to the silica surface depends on the pH and salt concentration of the solutions (either low pH or high salt). Elution can be achieved by depriving favorable conditions for the silica binding and enhancing the solubility and hydration of the nucleic acids (either ultrapure water or a basic, low salt, buffer such as Tris-buffers). In our method the binding is promoted through the chaotropic reagents and high concentration of KCl providing potassium cations for salt bridging provided in the protein or lipoprotein disruption or added during or after the disruption of exosomes. The elution is

therefore achieved by using salt-free ultrapure water to interrupt the silica interactions with the miRNA. However, there is a lot of potential for low recovery of miRNA. Any extraction procedure could experience sample loss due to binding equilibrium and diffusion. Furthermore, miRNA are relatively short nucleic acids and have fewer interactions between each strand and the silica. Also protein and lipid fouling of the silica surface can cause issues with binding, loss in washes, and inefficiency of elution. To evaluate the recovery of our method compared to other methods, we carried out total miRNA extractions using chemical extraction with the TRIzol reagent (Life Technologies) and two different silica-based commercial kits; the GeneJet RNA kit (ThermoScientific) and the PureLink RNA kit (Ambion). These three methods represent those commonly employed to extract RNAs from biological samples. Following the manufacturer's protocols for the kits and optimized TRIzol protocol, only a very small fraction of the cel-miR-67 spiked in the serum was recovered (Figure 3.07). For the commercial kits this could be due to the short length of the miRNAs compared to longer species and mRNA, which does not provide a large interaction surface. Therefore there are binding solution considerations and longer incubations that may be required for miRNAs. The chemical based TRIzol extraction does not work well for miRNAs as they are more difficult to precipitate in alcohol based solutions, requiring long incubation times at low temperatures to achieve significant recovery as seen in Figure 3.07. Our on-chip extraction method led to the highest average recovery of 13.5%, which could be attributed to both the optimization of our extraction conditions, and to the minimal sampling handling and liquid transfer compared to the other methods. Of the methods the

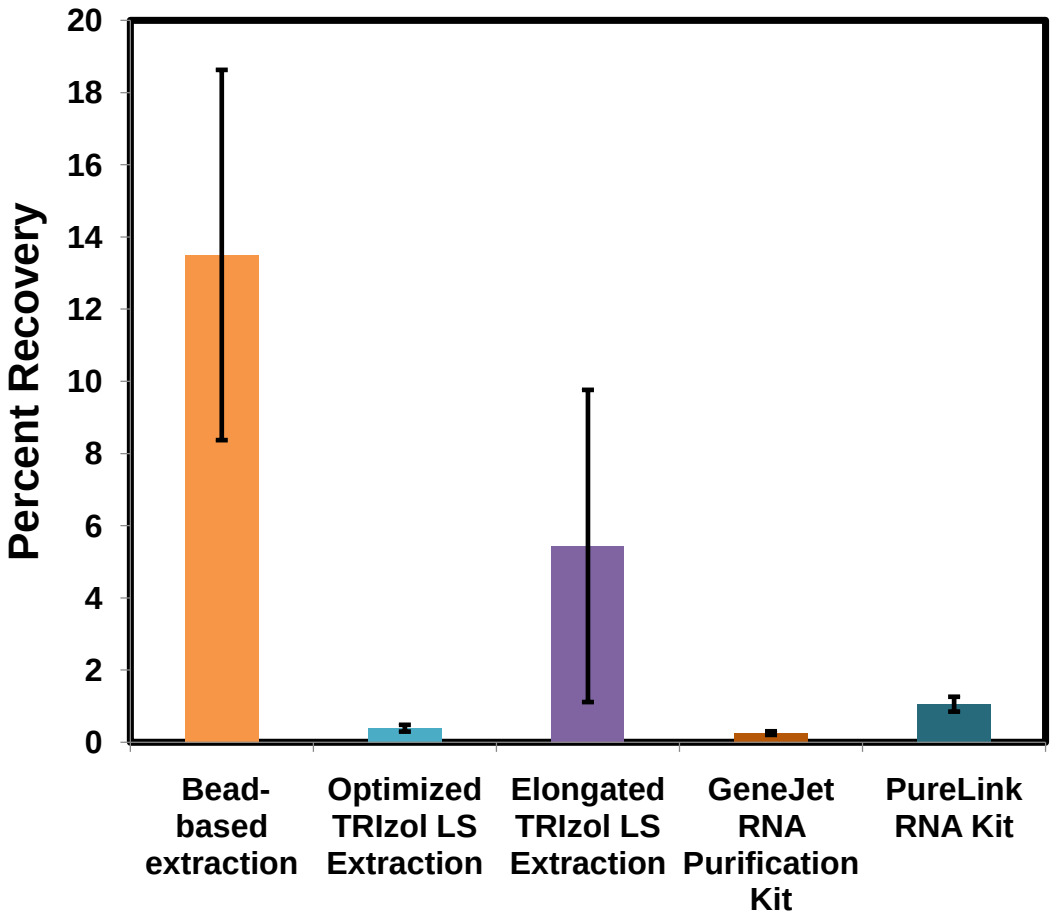

Figure 3.07. Comparison of the percent recovery of spiked exogenous control (cel-mir-67 or cel-miR-54) in serum using our bead-based extraction method and the commercial kits, including the TRIzol LS reagent (the normal protocol with glycogen and a elongated protocol with long incubations at -20 °C, longer and higher speed centrifugations, and glycogen), the GeneJet RNA purification kit, and the PureLink RNA mini kit, all distributed by Thermo Fisher Scientific.

commercial silica-based kits are the least time consuming yet yield the lowest recoveries, whereas our method is not significantly more time consuming and offers higher extraction.

The damage or degradation of nucleic acids during extractions is of concern when optimizing and developing new methods. RNA in particular has a higher possibility of damage and degradation during sample handling and extraction. This can be due to ribonucleases cleaving or completely degrading miRNA and possibly to simple hydrolysis of RNA in aqueous solutions. Therefore we investigated the quality of the total miRNA isolated via our method and comparison to the quality seen in the different commercial methods. We investigated the quality through agarose gel electrophoresis analysis of the pooled RT-qPCR products (figure 3.08a) and gel analysis the total miRNA in each sample using a universal reverse transcription reaction (SuperScript VILO cDNA Synthesis Kit, Thermo Fisher) (Figure 3.08b). According to the TaqMan miRNA Assay from Life Technologies, the RT primers are highly specific such that they only work with mature miRNAs, and have been tested with isomiRs (microRNA with 1-3 base addition or reduction on the 3' end of miRNA), and have <5% cross reactivity with single base mismatched miRNA. When tested with isomiRs, reverse transcription and amplification is only seen with the addition of bases on the 3' end, Loss of bases on the 3' end would result in no product. Therefore fragmentation on the 3' end would fail to produce product, fragmentation on the 5' end would fail to produce full length cDNA. Therefore, fragmentation of the 3' end should result in the lack of cDNA production in the TaqMan miRNA assay, a fragmentation of the 5' end should result in shorter cDNA which would

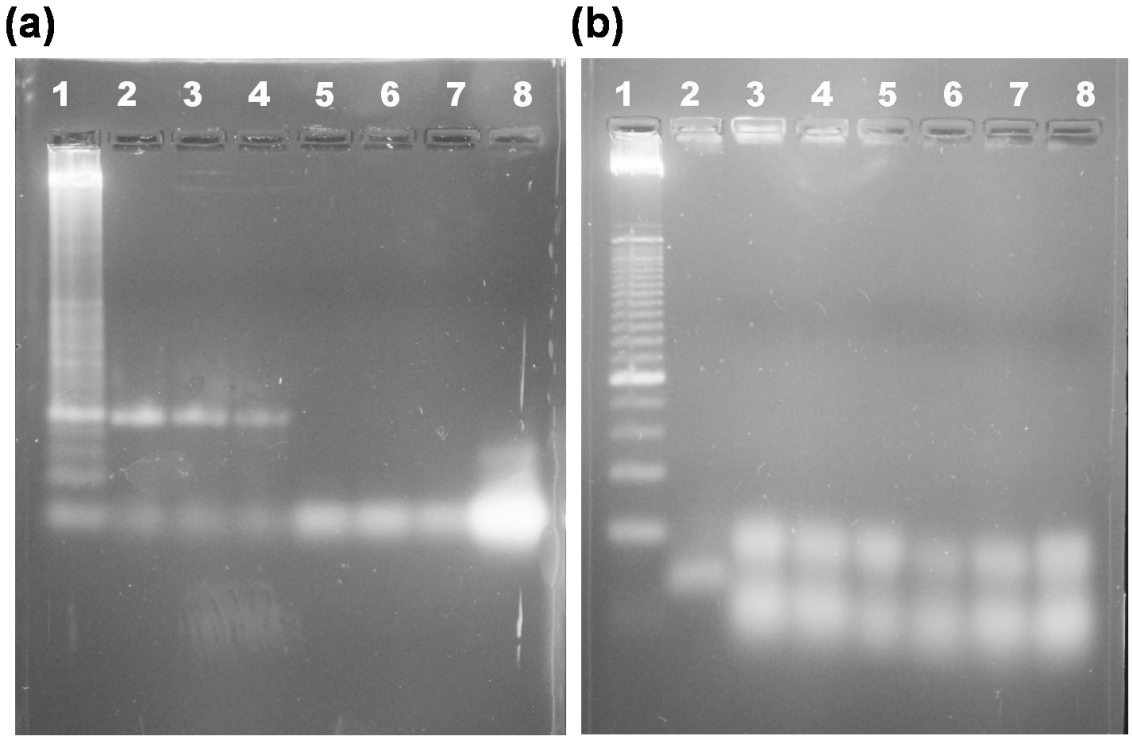

Figure 3.08. (a) Imaged agarose gel containing the following in each well; 1: 25 bp dsDNA ladder, 2: standard (150 amol each of 11 miRNA) after RT-qPCR, 3: standard (1.5 amol each) after RT-qPCR, 4: standard (15 zmol each) after RT-qPCR, 5,6,7: Chip Protein, Lipoprotein, Exosome respectively (after RT and pre-amp), 8: standard miRNA (after RT and pre-amp). (b) Imaged agarose gel containing the following in each well; 1: 25 bp dsDNA ladder, 2: miRNA standard (no RT), 3,4,5: Chip Protein, Lipoprotein, Exosome respectively (Superscript Vilo RT universal cDNA synthesis kit), 6,7,8: TRIzol extract, Purelink kit, Standard miRNA respectively (Superscript Vilo RT universal cDNA synthesis kit). 3 % native agarose gels ran at 110V in 1×TE buffer, imaged with transilluminator and camera with appropriate filter.

not amplify efficiently in the qPCR. Massive degradation should yield no bands in the gel for either the miRNA or the cDNA. As seen in Figure 3.08a a band of the amplified miRNA is visible after pre-amplification, however the cDNA concentration is too low to be visualized on the gel. As seen in figure 3.08b, the SuperScript VILO reverse transcription results however provide visualization of full length products (20-25 nucleotide double stranded miRNA-cDNA). The quality of the miRNA in our method appears sufficient and agrees with the quality of the total miRNA in the commercial methods. Therefore it is sufficient to say that there is no major degradation or damage of the miRNAs to be concerned with in our method.

3.3.4: Evaluation of the Carrier-Bound miRNA Fractionation by Differential Extraction

As seen in the above extraction results, our method results in higher recovery on average while requiring similar or less time for extraction than the commercial methods. The quality of our method is also sufficient and identical to the quality seen in the commercial extraction methods. Furthermore, our method can separately analyze the quantity of miRNA associated with different carrier types; proteins, lipoproteins, and exosomes. In order to further investigate the fractionation effect, we compared the amounts of miRNA isolated from the three carrier fractions recovered from the on-chip extraction to those obtained by the AF4 method we previously reported, the Invitrogen Total Exosome Isolation kit, and immuno-bead isolation of HDL/LDL. TRIzol extractions were used for miRNA recovery in the methods other than our microfluidic method. For these comparisons we analyzed the quantities of four miRNAs; *hsa-miR*-17, *miR*-21, *miR*-155, and *miR*-191. The exogenous controls were used to correct for

differences in recoveries in all the extractions. Fraction 1 obtained by the AF4 method contains proteins and used to represent a majority of the protein-bound miRNA (black bar in Figure 3.09a) and was compared the amount of miRNA in the protein fraction isolated on the microchip (white bar in Figure 3.09a). For exosomal miRNAs, AF4 fraction 6 which mainly contains exosomes (black bar in Figure 3.09b) and the miRNA isolated using the Total Exosome Isolation kit (gray bar in Figure 3.09b) were compared with the exosomal miRNA recovered on-chip (white bar in Figure 3.09b). Fractions 2-5 in the AF4 fractionation were considered as the total lipoprotein-bound miRNAs (black bar) and compared to the on-chip lipoprotein fraction (white bar) in Figure 3.09c). For a more accurate comparison, HDL/LDL complexes were isolated using beads conjugated with anti-HDL and anti-LDL IgGs and the HDL- and LDL- bound miRNAs were extracted for comparison (gray bar in Figure 3.09c).

As seen in Figure 3.09, in general the on-chip isolation of carrier-bound miRNAs agrees with the other methods of isolation and AF4 fractionation. In most cases the on-chip recovered amounts were comparable or greater than the AF4 amounts, likely due to the incomplete collection of all species (elution after fraction 6 or before fraction 1), co-elution of carriers in some fractions, and lower recovery in the large elution volumes during TRIzol extraction. AF4 fractionation followed by TRIzol extraction is less efficient as the recovery is lower than on-chip extraction and requires >2 days for the separation and TRIzol extraction versus 1.5 hours for the on-chip method both from comparable starting volumes of serum. Very small proteins may not be collected as they would come out before fraction 1 affecting the AF4 protein fraction, exosomes are clearly

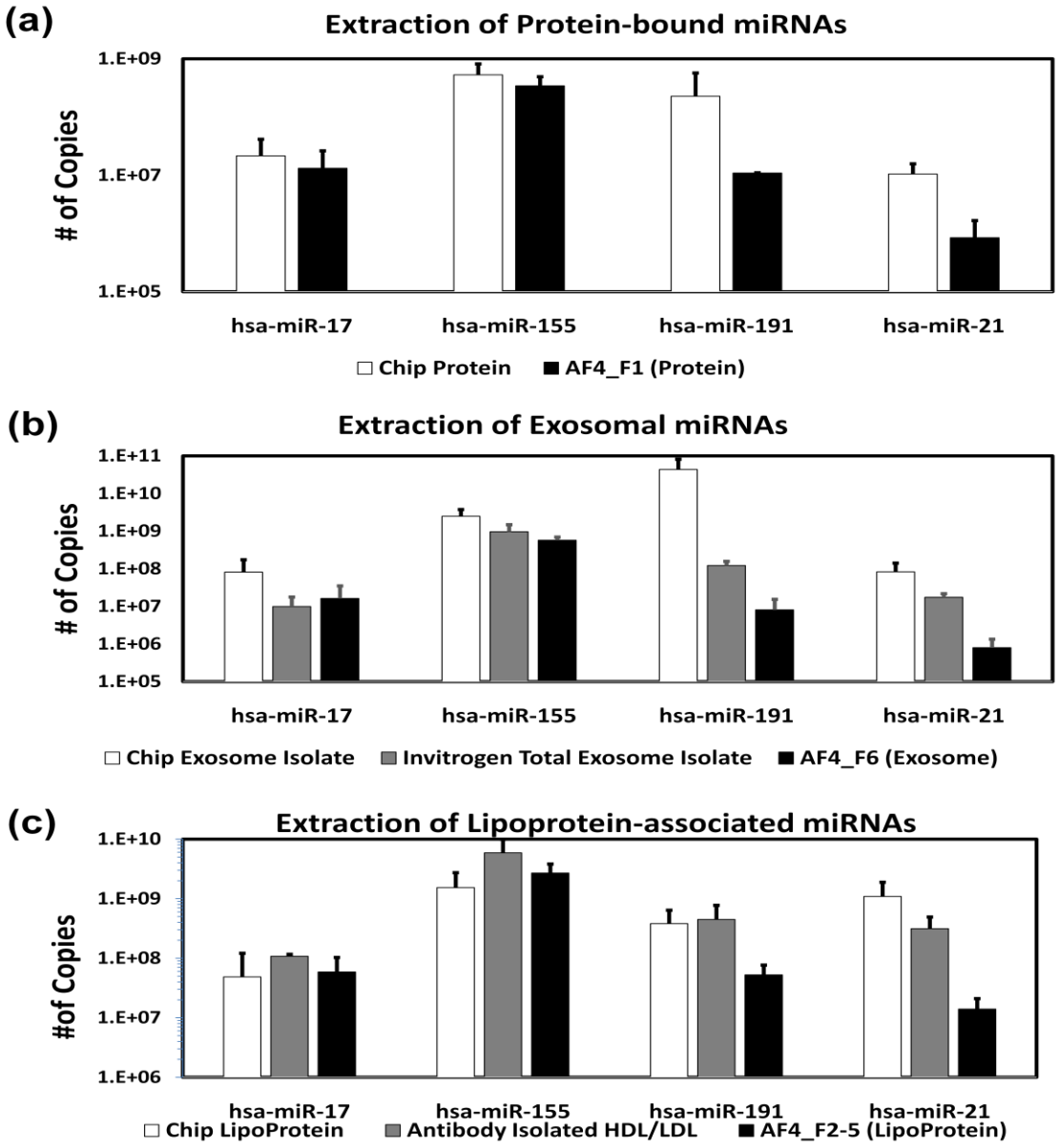

Figure 3.09. Comparison of the miRNA copies obtained from our on-chip technique and the AF4-based distribution profiling method we previously developed, as well as that obtained from immuno-capture of lipoproteins using HDL and LDL antibodies conjugated to magnetic beads, and the Invitrogen Total Exosome Isolation kit. (a) The protein-bound miRNAs recovered from the microchip and Fraction 1 from AF4 separation of pooled healthy serum (Sigma-Aldrich). (b) The exosomal miRNAs recovered from the microchip, Total Exosome Isolation kit, and Fraction 6 from AF4 separation. (c) The lipoprotein-associated miRNAs recovered from the microchip, immuno-capture with antibody conjugated beads, and sum of Fractions 2-5 from AF4 separation.

eluted after fraction 6 according to Figure 3.04d (Fraction 7). Differences in the lipoprotein amounts in AF4 and on-chip may be the main result of co-elution of proteins in earlier fractions and LDL in fraction 6. The amount of exosomal miRNAs from the on-chip fractionation more closely match with that of the Total Exosome Isolation Kit, however differences likely arise again from the miRNA loss during extraction and the poor recovery in the TRIzol extraction. Lastly, very comparable amounts of miRNA were obtained using our on-chip method and the immuno-isolation of HDL/LDL. This re-confirms the successful isolation of lipoprotein-bound miRNA through our differential extraction of protein- and lipoprotein- bound miRNAs on-chip. However, our method is highly advantageous over the immuno-isolation of the lipoprotein complexes as it is less time consuming (15 minutes for extraction and 15 minutes for elution versus 30 minutes for immuno-isolation plus additional time for processing and extraction), and our method does not require the use of the costly HDL and LDL antibodies with more complicated affinity capture. In fact, from this data, our relatively simplistic method can efficiently isolate all three fractions with higher extraction efficiency and comparable or higher recoveries obtained for all three carrier fractions.

3.3.5: Analysis of Serum Samples

We obtained twelve sera samples from our collaborators at the City of Hope Medical Center. These samples, considered as cases in our study, were collected from breast cancer patients prior to treatment. Eleven of the patients have infiltrating ductal carcinoma while one patient has the rarer inflammatory ductal carcinoma, with the cancer stages for the twelve patients ranging from II to IV. We obtained 7 healthy female donor

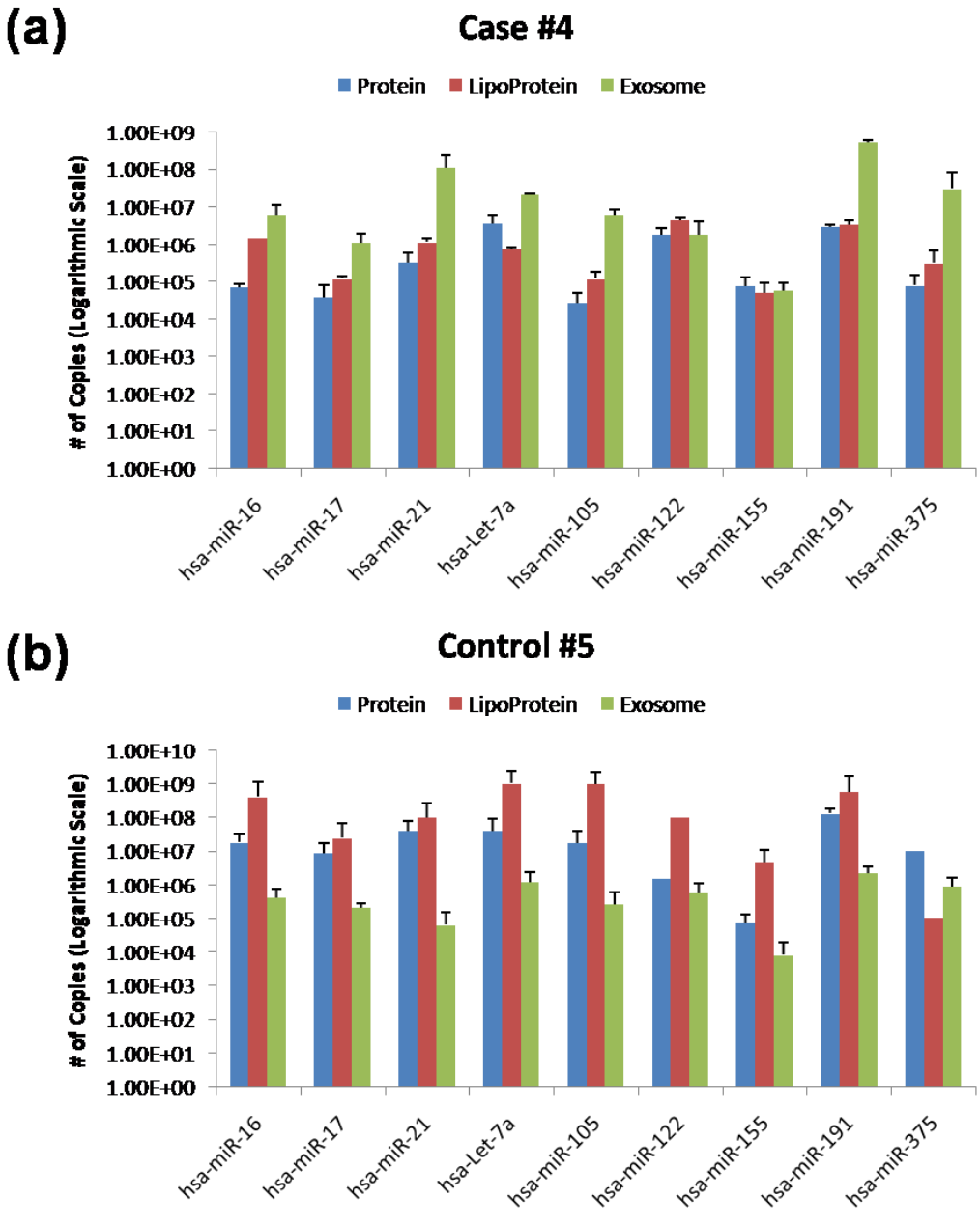

Figure 3.10. Distribution profiles of the sera collected from one breast cancer patient (a) and one healthy donor (b). The case and control shown above are age and race matched.

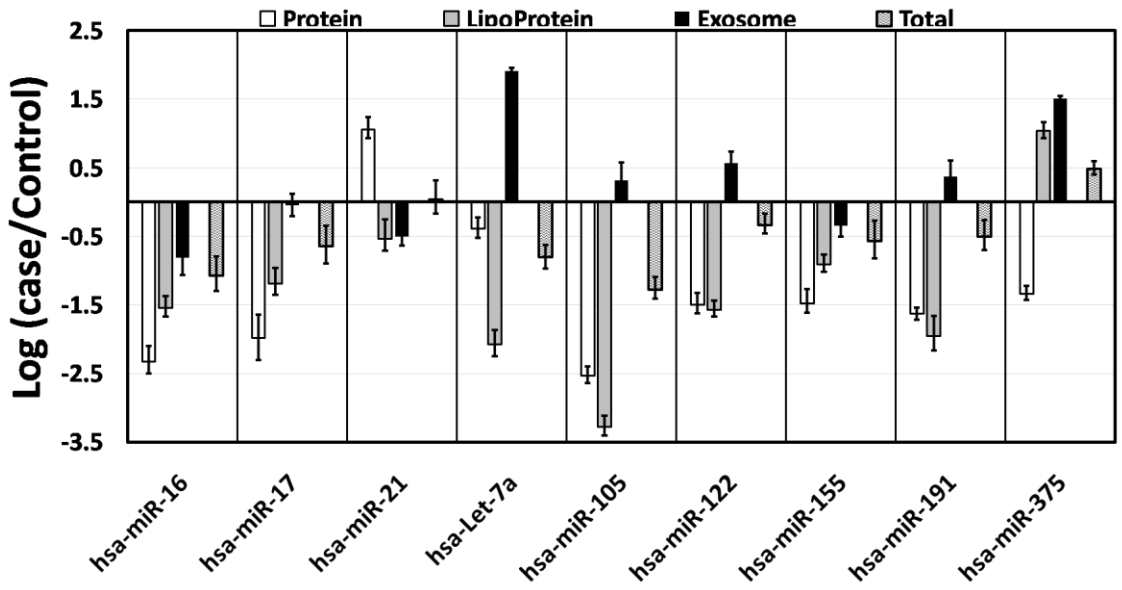

Figure 3.11. Fold changes between miRNA content in breast cancer patient cases and the healthy controls. The log ratio of the average miRNA content in 7 cases over the average from 3 controls

sera samples from Innovative Research Inc. as controls in our study, roughly matching age and race to the cases. The details for the case and control sera samples are shown in Tables 3.1 and 3.2 respectively. We processed these 19 sera samples using our method for the isolation and extraction of miRNAs in the protein, lipoprotein, and exosome fractions. All samples were extracted in triplicate, using a fresh microfluidic chip for each extraction, using 25 µL of sera for each extraction. The results of the pooled RT-qPCR are shown in the miRNA distribution profiles for one case in Figure 3.10a and one control in Figure 3.10b. From this we can see that each miRNA shows distinct patterns in its distribution among the three main carriers, which should be correlated to the process by which they are secreted, transported, and potentially elucidate the normality of the serum sample. Through the comparison of the average miRNA content in each fraction from all of the cases (n=12) with that from all of the controls (n=7), we can reveal larger changes among the individual fractions than could be seen using the changes in the total serum content of each miRNA. Figure 3.11 represents this in the log (case/control) for each miRNA target in each fraction and the total in whole serum for the grouping of 7 cases with 3 controls. As we can see in Figure 3.11, the log (case/control) for most of the total miRNA contents in serum typically fall within the range of ±0.5 and a couple targets giving a total change close to zero. This indicates a fold change less than 1 half order of magnitude, and typically changes this small are considered statistically irrelevant. On the contrary, many of the log (ratio) values for the fractionation of miRNA using our method show changes greater than ±1, indicating large differences between the cases and controls. For instance, it can be seen that the protein associated levels of hsa-miR-16 and

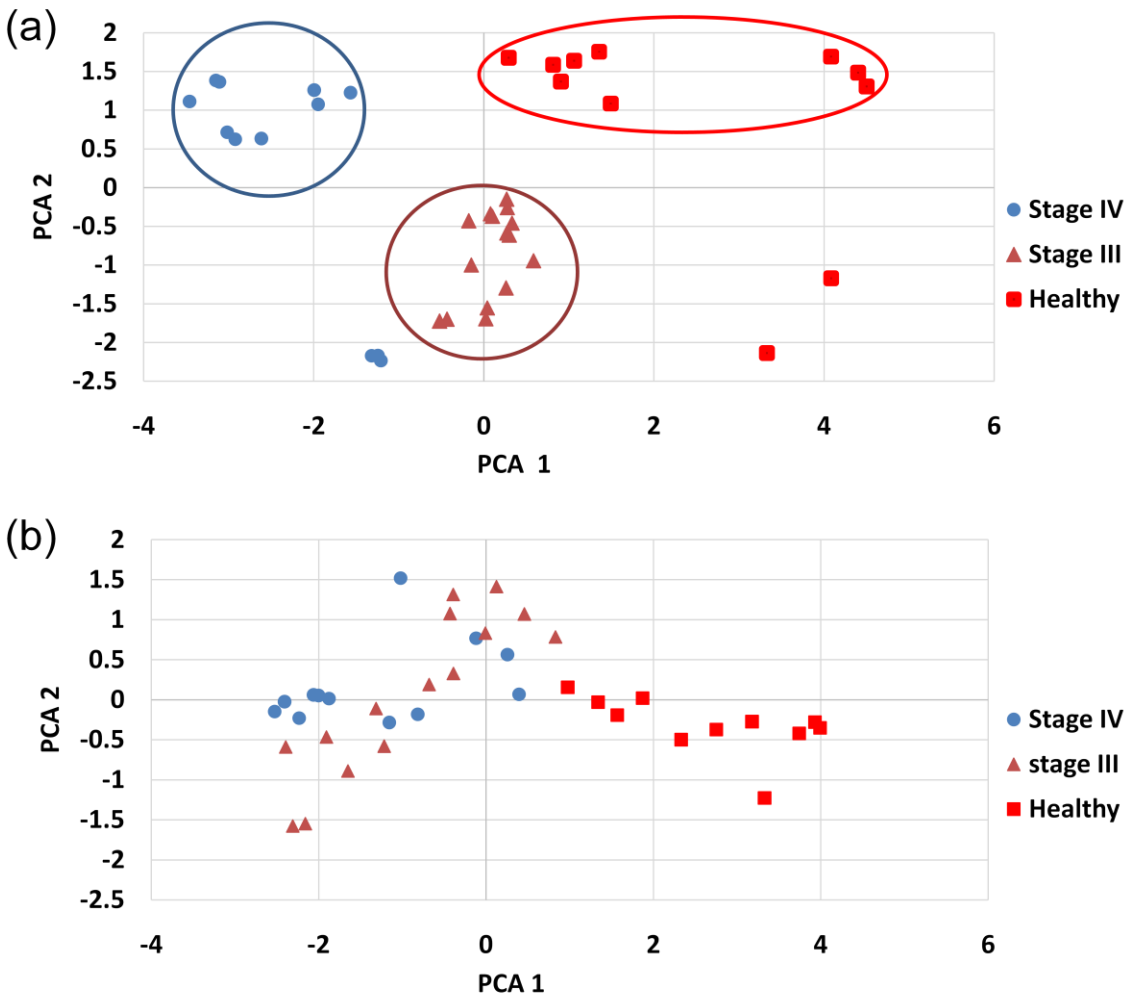

Figure 3.12. Principal component analysis (PCA) score plots of PC1 vs. PC2 for all samples. (a) Score plot using the carrier fraction data from the microfluidic method. (b) Score plot using total summed serum miRNA levels.

miR-155 in the cases are over 100 fold lower than controls, and lipoprotein associated miR-105 is more than 1000 fold lower in breast cancer patients. The exosome associated let-7a and miR-375 are shown to be 2 orders of magnitude greater in the cases over controls. Of even greater interest are the results yielded by subjecting the data to Principle Component Analysis (PCA) which shows clear grouping of cases and of controls with significant grouping of disease stages on a scatter plot (Figure 3.12a). On the contrary, using the total miRNA contents or simply the exosomal miRNA fraction, we lose a good amount of the separation between cases and controls, and no separation of the disease stages is seen in the PCA (Figure 3.12b). These results clearly indicate that the distribution profiling by our method can reveal much larger changes between breast cancer patients and healthy individuals compared to conventional methods. Also our results can clearly provide further distinction between earlier and latter stages of breast cancer, which is not possibly with analysis of total miRNA content.

3.3.6: Discussion

Since the discovery of the fact that circulating miRNAs in blood are bound to various carriers with high affinity, few reports are found to heavily study the distribution among carriers and how it could be related to different diseases. This has been mainly due to the challenges and high technical difficulty in isolating multiple carriers in parallel. The typically employed techniques that have been used for such a process are ultracentrifugation, differential or density-gradients centrifugation, and size-exclusion chromatography (SEC). The ultracentrifugation and centrifugation techniques and exceedingly tedious and time consuming, require large sample volumes, and often suffer

from either poor recovery or impurity. SEC can separate potential carriers by their sizes and the eluted fractions can be collected for the extraction of miRNAs bound by the various carriers. However, the column could damage the binding between proteins and miRNAs, the collection process can also be time consuming with low recovery, and SEC lacks the speed and throughput if a large number of samples are to be analyzed. Our previously developed asymmetrical flow field-flow fractionation (AF4) method uses an open channel for separation, providing gentler conditions that would keep the protein complexes and exosomes intact, but still suffers from many of the same problems as SEC in terms of post-separation collection and processing, speed of separation, and sample throughput. The new microfluidic-based miRNA distribution profiling technique reported in the present work has the ability to rapidly and semi-automatically fractionate miRNAs bound to three distinct types of carriers; proteins, lipoprotein complexes, and exosomes. The technique isolates these carrier-bound miRNAs from small sample volumes through immuno-isolation of exosomes combined with differential extraction of miRNA associated with protein and lipoprotein complexes, eluting them into clean solutions at low volumes for ease of amplification with relatively high recovery and simple operation. These acquired advantages are suitable for analysis of a large number of clinical samples and for the exploration of relationships between carrier distribution profiles and disease development.

The distribution profiles of circulating miRNAs can better the understanding about how they are secreted and how they are stabilized during transportation and within the circulatory system. Also how the miRNAs are carried could be closely related to

whether they can be up-taken by other cells and perhaps what types of cells they could enter. The presented technique provides an unprecedented and simple manner to simultaneously obtain exosomal, protein-bound, and lipoprotein-bound miRNAs. Lipoprotein-bound miRNAs are of interest due to a variety of factors such as their potential to cross the blood-brain barrier; also they may be more significant for patients with distinct levels of HDL or LDL in their blood. Exosomal miRNAs have been studied more often as their secretion is affected in cancer cells and may be related to tumor growth and metastasis. Protein-bound miRNAs have not been widely studied, although they may have potential in disease diagnostics due to abundant export of protein complexes in all cell types. Understanding of their carrier association could then help to understand more about the functions of specific miRNAs in cancer development and enhance the use of miRNAs as reliable biomarkers. For example our preliminary results revealed a higher content of the exosomal miR-122 in cancer patients than in controls. This agrees with the high circulating miR-122 levels found in breast cancer patients as reported in literature[61], and was found to originate from cancer cell secretion associated with metastasis. The cancer-derived miR-122 in exosomes could be transported to recipient cells to reprogram systemic energy metabolism and facilitate disease progression.[62] However, if we look at the overall level of circulating miR-122, its content dropped in patients due to the significant decrease of this miRNA in the lipoprotein and protein fractions. This is even more interesting as most cancer lines show reduced intracellular miR-122 with non-detectable levels in the protein portion, as reported in the same paper. Let-7a also exhibited a similar phenomenon as miR-122, with a much higher

content detected in cancer patients but lower detected in the lipoprotein-bound fraction. Therefore its relation with cancer metastasis may be worthy of further investigation.

Another clear trend revealed in our study, is that the patient samples generally contained significantly lower levels of protein-bound miRNAs in the circulatory system. This difference may be caused by cancer condition or by sample handling before the analysis. As there is no significant difference in the collection and storage procedures from the two serum sources, it is more likely related to cancer condition. Therefore, the further investigation of the protein-associated levels of miRNA may be worthwhile in cancer diagnostics. Future investigation can include investigating the key proteins with their relative abundance in the protein fractions between patients and healthy controls and the relation to protein-bound miRNA levels.

3.4: Conclusion

The microfluidic-based miRNA distribution profiling technique provides a quick and rather simplistic method of isolating miRNAs associated to different carriers, unseen in previously explored methods and in out previously investigated AF4 technique. The information provided is certainly valuable to further understand the functions of circulating miRNAs and reveal their relationships with disease development and progression. The technique can also help identify more effectively miRNA biomarkers and enable more proper usage of these markers in disease diagnosis and prognosis. Our platform is small and the whole process can be completely automated through the use of computer programming and robotics. Through the combination of automatic microfluidic

processing with mature miRNA quantification techniques, a promising disease diagnostic device with high sensitivity can be realized.

References:

(1) Chowdhury, D.; Choi, Y. E.; Brault, M. E. Charity Begins at Home: Non-Coding RNA Functions in DNA Repair. *Nat. Rev. Mol. Cell Biol.* **2013**, *14* (3), 181–189.

(2) Wahlestedt, C. Targeting Long Non-Coding RNA to Therapeutically Upregulate Gene Expression. *Nat. Rev. Drug Discov.* **2013**, *12* (6), 433–446.

(3) Dontu, G.; Rinaldis, E. de. MicroRNAs: Shortcuts in Dealing with Molecular Complexity? *Breast Cancer Res.* **2010**, *12* (1), 301.

(4) Iqbal, J.; Shen, Y.; Liu, Y.; Fu, K.; Jaffe, E. S.; Liu, C.; Liu, Z.; Lachel, C. M.; Deffenbacher, K.; Greiner, T. C.; Vose, J. M.; Bhagavathi, S.; Staudt, L. M.; Rimsza, L.; Rosenwald, A.; Ott, G.; Delabie, J.; Campo, E.; Braziel, R. M.; Cook, J. R.; Tubbs, R. R.; Gascoyne, R. D.; Armitage, J. O.; Weisenburger, D. D.; McKeithan, T. W.; Chan, W. C. Genome-Wide miRNA Profiling of Mantle Cell Lymphoma Reveals a Distinct Subgroup with Poor Prognosis. *Blood* **2012**, *119* (21), 4939–4948.

(5) Ma, L.; Weinberg, R. A. Micromanagers of Malignancy: Role of microRNAs in Regulating Metastasis. *Trends Genet. TIG* **2008**, *24* (9), 448–456.

(6) Ventura, A.; Jacks, T. MicroRNAs and Cancer: Short RNAs Go a Long Way. *Cell* **2009**, *136* (4), 586–591.

(7) Creemers, E. E.; Tijsen, A. J.; Pinto, Y. M. Circulating microRNAs: Novel Biomarkers and Extracellular Communicators in Cardiovascular Disease? *Circ. Res.* **2012**, *110* (3), 483–495.

(8) Laganà, A.; Russo, F.; Veneziano, D.; Bella, S. D.; Giugno, R.; Pulvirenti, A.; Croce, C. M.; Ferro, A. Extracellular Circulating Viral microRNAs: Current Knowledge and Perspectives. *Front. Genet.* **2013**, *4*, 120.

(9) Olivieri, F.; Rippo, M. R.; Procopio, A. D.; Fazioli, F. Circulating Inflamma-miRs in Aging and Age-Related Diseases. *Front. Genet.* **2013**, *4*, 121.

(10) Rykova, E. Y.; Laktionov, P. P.; Vlassov, V. V. Circulating Nucleic Acids in Health and Disease. In *Extracellular Nucleic Acids*; Kikuchi, Y., Rykova, E. Y., Eds.; Nucleic Acids and Molecular Biology; Springer Berlin Heidelberg, 2010; pp 93–128.

(11) Cortez, M. A.; Welsh, J. W.; Calin, G. A. Circulating microRNAs as Noninvasive Biomarkers in Breast Cancer. *Recent Results Cancer Res. Fortschritte Krebsforsch. Prog. Dans Rech. Sur Cancer* **2012**, *195*, 151–161.

(12) Mar-Aguilar, F.; Mendoza-Ramírez, J. A.; Malagón-Santiago, I.; Espino-Silva, P. K.; Santuario-Facio, S. K.; Ruiz-Flores, P.; Rodríguez-Padilla, C.; Reséndez-Pérez, D. Serum Circulating microRNA Profiling for Identification of Potential Breast Cancer Biomarkers. *Dis. Markers* **2013**, *34* (3), 163–169.

(13) Samantarrai, D.; Dash, S.; Chhetri, B.; Mallick, B. Genomic and Epigenomic Cross-Talks in the Regulatory Landscape of miRNAs in Breast Cancer. *Mol. Cancer Res. MCR* **2013**, *11* (4), 315–328.

(14) Hagen, J. W.; Lai, E. C. microRNA Control of Cell-Cell Signaling during Development and Disease. *Cell Cycle Georget. Tex* **2008**, *7* (15), 2327–2332.

(15) Nicoloso, M. S.; Spizzo, R.; Shimizu, M.; Rossi, S.; Calin, G. A. MicroRNAs--the Micro Steering Wheel of Tumour Metastases. *Nat. Rev. Cancer* **2009**, *9* (4), 293–302.

(16) Shi, M.; Liu, D.; Duan, H.; Shen, B.; Guo, N. Metastasis-Related miRNAs, Active Players in Breast Cancer Invasion, and Metastasis. *Cancer Metastasis Rev.* **2010**, *29* (4), 785–799.

(17) Volinia, S.; Galasso, M.; Costinean, S.; Tagliavini, L.; Gamberoni, G.; Drusco, A.; Marchesini, J.; Mascellani, N.; Sana, M. E.; Abu Jarour, R.; Desponts, C.; Teitell, M.; Baffa, R.; Aqeilan, R.; Iorio, M. V.; Taccioli, C.; Garzon, R.; Di Leva, G.; Fabbri, M.; Catozzi, M.; Previati, M.; Ambs, S.; Palumbo, T.; Garofalo, M.; Veronese, A.; Bottoni, A.; Gasparini, P.; Harris, C. C.; Visone, R.; Pekarsky, Y.; de la Chapelle, A.; Bloomston, M.; Dillhoff, M.; Rassenti, L. Z.; Kipps, T. J.; Huebner, K.; Pichiorri, F.; Lenze, D.; Cairo, S.; Buendia, M.-A.; Pineau, P.; Dejean, A.; Zanesi, N.; Rossi, S.; Calin, G. A.; Liu, C.-G.; Palatini, J.; Negrini, M.; Vecchione, A.; Rosenberg, A.; Croce, C. M. Reprogramming of miRNA Networks in Cancer and Leukemia. *Genome Res.* **2010**, *20* (5), 589–599.

(18) Williams, Z.; Ben-Dov, I. Z.; Elias, R.; Mihailovic, A.; Brown, M.; Rosenwaks, Z.; Tuschl, T. Comprehensive Profiling of Circulating microRNA via Small RNA Sequencing of cDNA Libraries Reveals Biomarker Potential and Limitations. *Proc. Natl. Acad. Sci. U. S. A.* **2013**, *110* (11), 4255–4260.

(19) Mitchell, P. S.; Parkin, R. K.; Kroh, E. M.; Fritz, B. R.; Wyman, S. K.; Pogosova-Agadjanyan, E. L.; Peterson, A.; Noteboom, J.; O'Briant, K. C.; Allen, A.; Lin, D. W.; Urban, N.; Drescher, C. W.; Knudsen, B. S.; Stirewalt, D. L.; Gentleman, R.; Vessella, R. L.; Nelson, P. S.; Martin, D. B.; Tewari, M. Circulating microRNAs as Stable Blood-Based Markers for Cancer Detection. *Proc. Natl. Acad. Sci.* **2008**, *105* (30), 10513–10518.

(20) Russo, F.; Di Bella, S.; Nigita, G.; Macca, V.; Laganà, A.; Giugno, R.; Pulvirenti, A.; Ferro, A. miRandola: Extracellular Circulating MicroRNAs Database. *PLoS ONE* **2012**, *7* (10), e47786.

(21) Heneghan, H. M.; Miller, N.; Lowery, A. J.; Sweeney, K. J.; Newell, J.; Kerin, M. J. Circulating microRNAs as Novel Minimally Invasive Biomarkers for Breast Cancer. *Ann. Surg.* **2010**, *251* (3), 499–505.

(22) Davoren, P. A.; McNeill, R. E.; Lowery, A. J.; Kerin, M. J.; Miller, N. Identification of Suitable Endogenous Control Genes for microRNA Gene Expression Analysis in Human Breast Cancer. *BMC Mol. Biol.* **2008**, *9*, 76.

(23) Zhu, W.; Qin, W.; Atasoy, U.; Sauter, E. R. Circulating microRNAs in Breast Cancer and Healthy Subjects. *BMC Res. Notes* **2009**, *2* (1), 89.

(24) Roth, C.; Rack, B.; Müller, V.; Janni, W.; Pantel, K.; Schwarzenbach, H. Circulating microRNAs as Blood-Based Markers for Patients with Primary and Metastatic Breast Cancer. *Breast Cancer Res.* **2010**, *12* (6), R90.

(25) Hu, Z.; Dong, J.; Wang, L.-E.; Ma, H.; Liu, J.; Zhao, Y.; Tang, J.; Chen, X.; Dai, J.; Wei, Q.; Zhang, C.; Shen, H. Serum microRNA Profiling and Breast Cancer Risk: The Use of miR-484/191 as Endogenous Controls. *Carcinogenesis* **2012**, *33* (4), 828–834.

(26) Sieuwerts, A. M.; Mostert, B.; Bolt-de Vries, J.; Peeters, D.; de Jongh, F. E.; Stouthard, J. M. L.; Dirix, L. Y.; van Dam, P. A.; Van Galen, A.; de Weerd, V.; Kraan, J.; van der Spoel, P.; Ramírez-Moreno, R.; van Deurzen, C. H. M.; Smid, M.; Yu, J. X.; Jiang, J.; Wang, Y.; Gratama, J. W.; Sleijfer, S.; Foekens, J. A.; Martens, J. W. M. mRNA and microRNA Expression Profiles in Circulating Tumor Cells and Primary Tumors of Metastatic Breast Cancer Patients. *Clin. Cancer Res. Off. J. Am. Assoc. Cancer Res.* **2011**, *17* (11), 3600–3618.

(27) Wu, Q.; Wang, C.; Lu, Z.; Guo, L.; Ge, Q. Analysis of Serum Genome-Wide microRNAs for Breast Cancer Detection. *Clin. Chim. Acta Int. J. Clin. Chem.* **2012**, *413* (13-14), 1058–1065.

(28) Wang, F.; Zheng, Z.; Guo, J.; Ding, X. Correlation and Quantitation of microRNA Aberrant Expression in Tissues and Sera from Patients with Breast Tumor. *Gynecol. Oncol.* **2010**, *119* (3), 586–593.

(29) Guo, L.-J.; Zhang, Q.-Y. Decreased Serum miR-181a Is a Potential New Tool for Breast Cancer Screening. *Int. J. Mol. Med.* **2012**, *30* (3), 680–686.

(30) Wu, Q.; Lu, Z.; Li, H.; Lu, J.; Guo, L.; Ge, Q. Next-Generation Sequencing of microRNAs for Breast Cancer Detection. *J. Biomed. Biotechnol.* **2011**, *2011*, 597145.

(31) Heneghan, H. M.; Miller, N.; Kelly, R.; Newell, J.; Kerin, M. J. Systemic miRNA-195 Differentiates Breast Cancer from Other Malignancies and Is a Potential Biomarker for Detecting Noninvasive and Early Stage Disease. *The Oncologist* **2010**, *15* (7), 673–682.

(32) Jonsdottir, K.; Janssen, S. R.; Da Rosa, F. C.; Gudlaugsson, E.; Skaland, I.; Baak, J. P. A.; Janssen, E. A. M. Validation of Expression Patterns for Nine miRNAs in 204 Lymph-Node Negative Breast Cancers. *PLoS ONE* **2012**, *7* (11), e48692.

(33) Ng, E. K. O.; Li, R.; Shin, V. Y.; Jin, H. C.; Leung, C. P. H.; Ma, E. S. K.; Pang, R.; Chua, D.; Chu, K.-M.; Law, W. L.; Law, S. Y. K.; Poon, R. T. P.; Kwong, A. Circulating microRNAs as Specific Biomarkers for Breast Cancer Detection. *PloS One* **2013**, *8* (1), e53141.

(34) Pigati, L.; Yaddanapudi, S. C. S.; Iyengar, R.; Kim, D.-J.; Hearn, S. A.; Danforth, D.; Hastings, M. L.; Duelli, D. M. Selective Release of MicroRNA Species from Normal and Malignant Mammary Epithelial Cells. *PLoS ONE* **2010**, *5* (10), e13515.

(35) Asaga, S.; Kuo, C.; Nguyen, T.; Terpenning, M.; Giuliano, A. E.; Hoon, D. S. B. Direct Serum Assay for microRNA-21 Concentrations in Early and Advanced Breast Cancer. *Clin. Chem.* **2011**, *57* (1), 84–91.

(36) Jarry, J.; Schadendorf, D.; Greenwood, C.; Spatz, A.; van Kempen, L. C. The Validity of Circulating microRNAs in Oncology: Five Years of Challenges and Contradictions. *Mol. Oncol.* **2014**, *8* (4), 819–829.

(37) Leidner, R. S.; Li, L.; Thompson, C. L. Dampening Enthusiasm for Circulating microRNA in Breast Cancer. *PloS One* **2013**, *8* (3), e57841.

(38) Etheridge, A.; Lee, I.; Hood, L.; Galas, D.; Wang, K. Extracellular microRNA: A New Source of Biomarkers. *Mutat. Res. Mol. Mech. Mutagen.* **2011**, *717* (1–2), 85–90.

(39) Turchinovich, A.; Weiz, L.; Burwinkel, B. Extracellular miRNAs: The Mystery of Their Origin and Function. *Trends Biochem. Sci.* **2012**, *37* (11), 460–465.

(40) Wang, K.; Zhang, S.; Weber, J.; Baxter, D.; Galas, D. J. Export of microRNAs and microRNA-Protective Protein by Mammalian Cells. *Nucleic Acids Res.* **2010**, gkq601.

(41) Hoy, A. M.; Buck, A. H. Extracellular Small RNAs: What, Where, Why? *Biochem. Soc. Trans.* **2012**, *40* (4), 886–890.

(42) Kosaka, N.; Iguchi, H.; Yoshioka, Y.; Takeshita, F.; Matsuki, Y.; Ochiya, T. Secretory Mechanisms and Intercellular Transfer of MicroRNAs in Living Cells. *J. Biol. Chem.* **2010**, *285* (23), 17442–17452.

(43) Ohshima, K.; Inoue, K.; Fujiwara, A.; Hatakeyama, K.; Kanto, K.; Watanabe, Y.; Muramatsu, K.; Fukuda, Y.; Ogura, S.; Yamaguchi, K.; Mochizuki, T. Let-7 microRNA Family Is Selectively Secreted into the Extracellular Environment via Exosomes in a Metastatic Gastric Cancer Cell Line. *PloS One* **2010**, *5* (10), e13247.

(44) Vickers, K. C.; Remaley, A. T. Lipid-Based Carriers of microRNAs and Intercellular Communication. *Curr. Opin. Lipidol.* **2012**, *23* (2), 91–97.

(45) Yang, M.; Chen, J.; Su, F.; Yu, B.; Su, F.; Lin, L.; Liu, Y.; Huang, J.-D.; Song, E. Microvesicles Secreted by Macrophages Shuttle Invasion-Potentiating microRNAs into Breast Cancer Cells. *Mol. Cancer* **2011**, *10*, 117.

(46) Vickers, K. C.; Palmisano, B. T.; Shoucri, B. M.; Shamburek, R. D.; Remaley, A. T. MicroRNAs Are Transported in Plasma and Delivered to Recipient Cells by High-Density Lipoproteins. *Nat. Cell Biol.* **2011**, *13* (4), 423–433.

(47) Wang, J.; Zhang, Y.; Zhang, W.; Jin, Y.; Dai, J. Association of Perfluorooctanoic Acid with HDL Cholesterol and Circulating miR-26b and miR-199-3p in Workers of a Fluorochemical Plant and Nearby Residents. *Environ. Sci. Technol.* **2012**, *46* (17), 9274–9281.

(48) Wang, H.; Eckel, R. H. What Are Lipoproteins Doing in the Brain? *Trends Endocrinol. Metab.* **2014**, *25* (1), 8–14.

(49) Wagner, J.; Riwanto, M.; Besler, C.; Knau, A.; Fichtlscherer, S.; Röxe, T.; Zeiher, A. M.; Landmesser, U.; Dimmeler, S. Characterization of Levels and Cellular Transfer of Circulating Lipoprotein-Bound MicroRNAs. *Arterioscler. Thromb. Vasc. Biol.* **2013**, *33* (6), 1392–1400.

(50) Diehl, P.; Fricke, A.; Sander, L.; Stamm, J.; Bassler, N.; Htun, N.; Ziemann, M.; Helbing, T.; El-Osta, A.; Jowett, J. B. M.; Peter, K. Microparticles: Major Transport Vehicles for Distinct microRNAs in Circulation. *Cardiovasc. Res.* **2012**, *93* (4), 633–644.

(51) McDonald, M. K.; Capasso, K. E.; Ajit, S. K. Purification and microRNA Profiling of Exosomes Derived from Blood and Culture Media. *J. Vis. Exp. JoVE* **2013**, No. 76, e50294.

(52) Xu, J.; Chen, Q.; Zen, K.; Zhang, C.; Zhang, Q. Synaptosomes Secrete and Uptake Functionally Active microRNAs via Exocytosis and Endocytosis Pathways. *J. Neurochem.* **2013**, *124* (1), 15–25.

(53) Palma, J.; Yaddanapudi, S. C.; Pigati, L.; Havens, M. A.; Jeong, S.; Weiner, G. A.; Weimer, K. M. E.; Stern, B.; Hastings, M. L.; Duelli, D. M. MicroRNAs Are Exported from Malignant Cells in Customized Particles. *Nucleic Acids Res.* **2012**, *40* (18), 9125–9138.

(54) Kosaka, N.; Iguchi, H.; Yoshioka, Y.; Hagiwara, K.; Takeshita, F.; Ochiya, T. Competitive Interactions of Cancer Cells and Normal Cells via Secretory microRNAs. *J. Biol. Chem.* **2012**, *287* (2), 1397–1405.

(55) Rayner, K. J.; Hennessy, E. J. Extracellular Communication via microRNA: Lipid Particles Have a New Message. *J. Lipid Res.* **2013**, *54* (5), 1174–1181.

(56) Umezu, T.; Ohyashiki, K.; Kuroda, M.; Ohyashiki, J. H. Leukemia Cell to Endothelial Cell Communication via Exosomal miRNAs. *Oncogene* **2013**, *32* (22), 2747–2755.

(57) Pegtel, D. M.; Cosmopoulos, K.; Thorley-Lawson, D. A.; van Eijndhoven, M. A. J.; Hopmans, E. S.; Lindenberg, J. L.; de Gruijl, T. D.; Würdinger, T.; Middeldorp, J. M. Functional Delivery of Viral miRNAs via Exosomes. *Proc. Natl. Acad. Sci. U. S. A.* **2010**, *107* (14), 6328–6333.

(58) Kosaka, N.; Ochiya, T. Unraveling the Mystery of Cancer by Secretory microRNA: Horizontal microRNA Transfer between Living Cells. *Front. Genet.* **2011**, *2*, 97.

(59) Ashby, J.; Flack, K.; Jimenez, L. A.; Duan, Y.; Khatib, A.-K.; Somlo, G.; Wang, S. E.; Cui, X.; Zhong, W. Distribution Profiling of Circulating microRNAs in Serum. *Anal. Chem.* **2014**, *86* (18), 9343–9349.

(60) Zhong, R.; Flack, K.; Zhong, W. Automatic Extraction and Processing of Small RNAs on a Multi-Well/multi-Channel (M&M) Chip. *The Analyst* **2012**, *137* (23), 5546–5552.

(61) Fong, M. Y.; Zhou, W.; Liu, L.; Alontaga, A. Y.; Chandra, M.; Ashby, J.; Chow, A.; O'Connor, S. T. F.; Li, S.; Chin, A. R.; Somlo, G.; Palomares, M.; Li, Z.; Tremblay, J. R.; Tsuyada, A.; Sun, G.; Reid, M. A.; Wu, X.; Swiderski, P.; Ren,

X.; Shi, Y.; Kong, M.; Zhong, W.; Chen, Y.; Wang, S. E. Breast-Cancer-Secreted miR-122 Reprograms Glucose Metabolism in Premetastatic Niche to Promote Metastasis. *Nat. Cell Biol.* **2015**, *17* (2), 183–194.

(62) Fong, M. Y.; Zhou, W.; Liu, L.; Alontaga, A. Y.; Chandra, M.; Ashby, J.; Chow, A.; O'Connor, S. T. F.; Li, S.; Chin, A. R.; Somlo, G.; Palomares, M.; Li, Z.; Tremblay, J. R.; Tsuyada, A.; Sun, G.; Reid, M. A.; Wu, X.; Swiderski, P.; Ren, X.; Shi, Y.; Kong, M.; Zhong, W.; Chen, Y.; Wang, S. E. Breast-Cancer-Secreted miR-122 Reprograms Glucose Metabolism in Premetastatic Niche to Promote Metastasis. *Nat. Cell Biol.* **2015**, *17* (2), 183–194.

Chapter 4: Development and Optimization of Isothermal Techniques for Sensitive and Selective Analysis of MicroRNA

4.1: Introduction

Serum concentrations of miRNA can vary from relatively high to minute amounts.[1] For determination of miRNA levels in smaller serum volumes equal to only a couple drops of blood, the determination of many miRNAs becomes difficult.[2] Sensitive detection of these miRNA biomarkers requires amplification strategies to increase the total number of detectable species correlating to each target miRNA.[3,4] These amplification strategies can either amplify the measurable signal through means of generating many fluorescent or luminescent species for each target or through means of replicating the target to increase the number of species that can be tagged with reporter probes or molecules. Specificity is also an important aspect of amplification strategies used in miRNA determination as many miRNAs exist which have sequences that may differ by only one or two base mismatches.

Conventional analytical methods, such as reverse transcription quantitative PCR (RT-qPCR) for analysis of miRNA requires advance lab facilities and can be expensive and time consuming.[5] Moving from conventional lab bench techniques to point of care settings requires simpler, cost effective, and rapid assays for miRNA determination. Development of simple yet efficient target and signal amplification techniques that can detect very few miRNA copies (<1 zmol) in a single sample is essential for miRNA determination in serum. This is critical in the development of a microfluidic total analysis system (μ-TAS) for the detection of miRNA. Traditional miRNA amplification strategies

require complex configuration for microfluidic applications. Achieving optimal thermal transfer is essential to traditional PCR based amplification. Also a detection method applicable to qPCR amplification (such as a fluorescence detector) require complex set-up and can suffer from light scattering and transmittance of light through the device if the device is made of transparent materials. Creating multiplexed detection of several different targets simultaneously also adds complexity to the device. The cost of performing qPCR on microfluidic devices is another important consideration in keeping the overall cost of the device and analysis low. The use of droplet based PCR or digital PCR techniques miniaturized on a microfluidic device have also been explored, however still can add complexity and cost to the system.

Isothermal target amplification strategies have been developed that do not require thermocycling and can be done at lower temperatures, and therefore can be more easily applied to a simple point of care set-ups.[6–10] Many isothermal amplification strategies are highly applicable to a microarray for multiplexed and high throughput analysis of miRNA. Isothermal amplification techniques have been developed at elevated temperatures as well as relatively low temperatures below 37 degrees Celsius, some even at room temperature reducing the need for heating elements in the design of the microfluidic system. Common isothermal amplification strategies include strand displacement amplification (SDA), rolling circle amplification (RCA), helicase-dependent amplification (HDA), loop-mediated amplification (LAMP), and hybridization chain reaction (HCR). For miRNA determination, RCA allows for efficient synthesis of long single stranded DNA with high simplicity,[11] SDA is efficient at linear production of

single stranded cDNA,[12,13] and HCR efficiently builds long double stranded DNA scaffolds without the need for enzymes.[14]

4.2: Rolling Circle Amplification with Cation Exchange Amplification (CXAmp) for MicroRNA Detection

4.2.1: RCA combined with CXAmp

In RCA, a circular probe formed from the target strand serves as the template for generation of ssDNA with repeated sequences of the circular probe[15] at an ultrafast rate up to 1 kilobase per min.[16,17] The longer the ssDNA product the more repeated sequences that can be used for detection. Recognition of the rolling circle product (RCP) with oligonucleotides complimentary to tandem regions allows for labeling with dye or nanoparticles for optical or electrochemical detection.[18] In addition, different sequences, such as digestion sites for target endonuclease[19,20] and DNAzyme,[21–23] can be inserted to the circular probe to facilitate RCP detection without lowering the RCP synthesis rate, owing to the high strand displacement capability of the phi29 polymerase enzyme. Alternatively, hapten-modified dNTPs can be used in RCA to label the RCP.[24] However, the operation of attaching or triggering the signaling units is not very straightforward, difficult to control and reproduce, and may yield unsatisfactory results. This is because the long single-stranded RCP is highly likely to become super-coiled with complex secondary structure, leaving limited places for attachment of reporters or preventing proper functioning of the related enzymes. The use of RCA for detection of small RNA and siRNA in a mixture was previously investigated by Ni Li et al,[20] which used RCA to produce long RCPs which were digested by endonucleases, followed by separation and

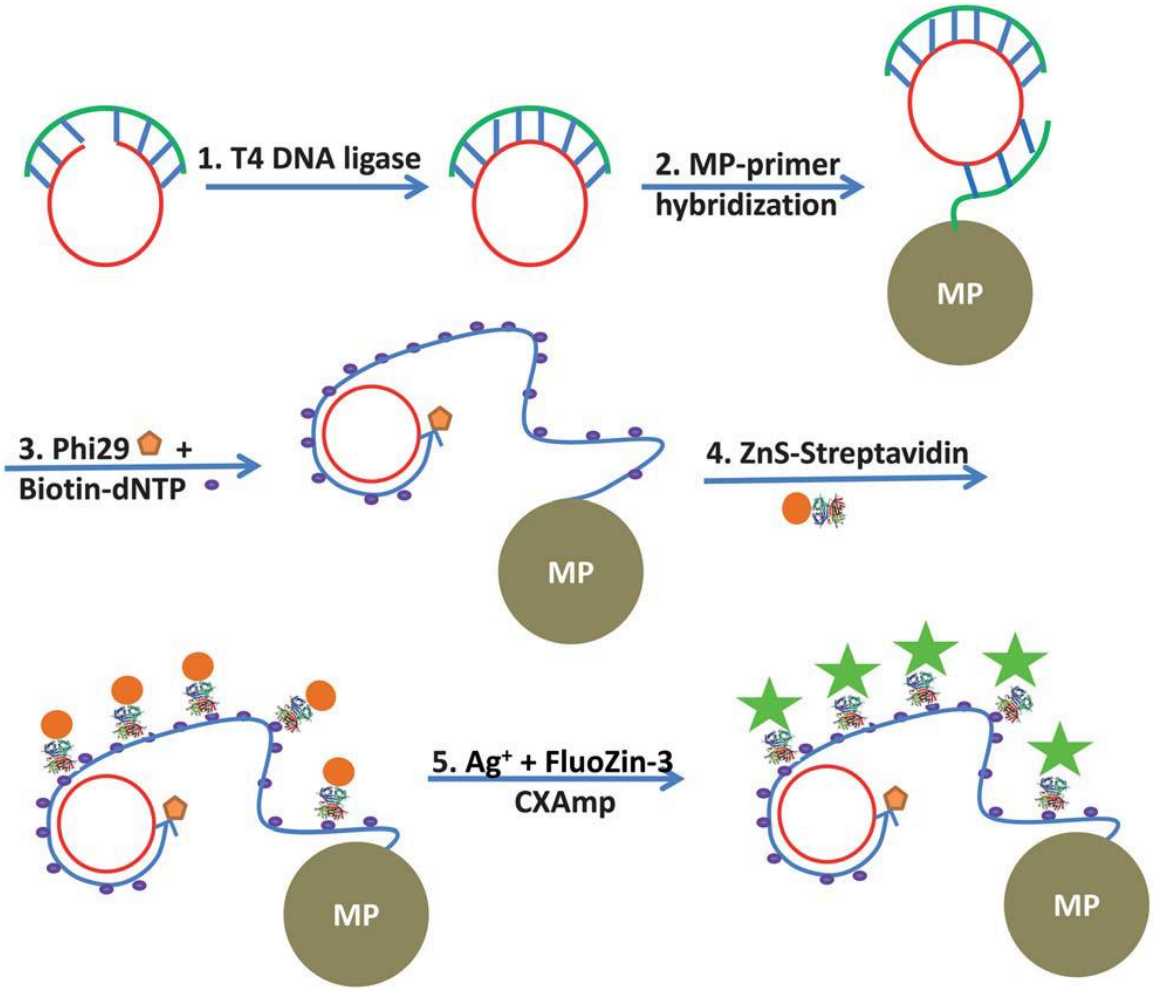

Figure 4.01. Schematic illustration for the RCA process combined with labeling the long RCPs with ZnS NCCs and detection by CXAmp.

detection of RCP fragments using capillary electrophoresis. Previously in our group we have developed and optimized methods of signal amplification which we termed cation exchange amplification (CXAmp) based on the exchange of metal cations in nanocrystals with cations in solution which has been utilized for sensitive detection of proteins and nucleic acids in bioassays.[25–28] In the past we have employed single small crystals (<10 nm) as well as large nanocrystal clusters (>40 nm), including CdSe, ZnSe, and ZnS nanocrystals. Incubation of the nanocrystals in a solution containing a relatively high concentration of competing cations, the cadmium or zinc will exchange with the competitor and become free cations in solution which can then be detected via metal sensitive colorimetric or fluorescent dye molecules.

Here we used RCA combined with a novel method of labeling and detecting RCPs with the achievement of cascade signal amplification using cation exchange of zinc containing nanocrystal clusters (NCCs) as seen in Figure 4.01. First the circular probe is generated through the hybridization of a padlock DNA probe with the target miRNA which is complementary to portions of the 3' and 5' ends of the padlock probe. The 3' and 5' ends of the padlock probe can then be linked together by T4 DNA ligase creating a circular DNA strand (Step 1). The circular probe can then be captured through hybridization with primers conjugated to the surface magnetic particles (MPs) (Step 2). Then through the use of phi29 enzyme and a mixture of dNTPs containing biotinylated dATP, long RCPs containing biotin are synthesized (Step 3). Subsequently, streptavidin-conjugated ZnS NCCs could be captured by the RCP-MPs through the strong biotin-streptavidin binding (Step 4). After washing the MPs to remove excess NCCs, signal

amplification can be achieved through the cation exchange reaction between Ag(I) ions in the solution and Zn(II) encapsulated in the NCCs. The individual NCCs, which there may be numerous NCCs per RCP, can then release millions of Zn(II) ions each and trigger the intense fluorescence from FluoZin-3, a sensitive Zn(II)-responsive dye (Step 5). Through the use of RCA, for each target miRNA, if *m* long RCPs can be produced with each RCP capturing *n* NCCS, an improvement factor equal to $m \times n$ in addition to the million-fold signal enhancement of the CXAmp.

4.2.2: Materials and Methods

All oligonucleotides and standard miRNAs were purchased from Integrated DNA Technologies (Coralville, IA) with desired modifications. The 5' end of the padlock probe was phosphorylated for the ligation reaction to occur and the primer was modified with an amine group on the 5' end for conjugation to the polystyrene beads. Phi29 DNA polymerase and T4 DNA ligase was from New England Biolabs Inc. (Ipswich, MA). Carboxyl polystyrene magnetic particles (25 mg/mL) with a diameter of 4.35 μm were acquired from Spherotech Inc. (Lake Forest, IL). 1-(3-dimethylaminopropyl)-3-ethylcarbodiimide hydrochloride (EDC), and silver nitrate were purchased from Acros Organics (Pittsburgh, PA). Streptavidin, sulfo-N-hydroxysuccinimide (sulfo-NHS), dithiothreitol (DTT), and the salts used to prepare buffer solutions were supplied by Fisher Scientific (Pittsburg, PA). Bovine serum albumin (BSA) and Tween-20 were obtained from Sigma Aldrich (St. Louis, MO). Biotin-14-dATP, Human Brain Total RNA, deoxyribonucleotides (dNTPs), and FluoZin-3 were from Invitrogen (Carlsbad, CA).

Conjugation of polystyrene microspheres with RCA primers was performed using conventional carbodiimide coupling. First, 2 nmol of the primer was added to 1 mL of 2.5 mg/mL 4.35 um polystyrene particles suspended in the linking buffer (0.02 M phosphate buffer, pH~7.2). The carboxyl groups were activated with the addition of 0.1 mg EDC and 0.1 mg sulfo-NHS. The reaction was incubated at RT for 3 hours on a tube rotator to keep beads well suspended. The microbeads were then pulled down with a permanent magnet and the supernatant was removed. The microspheres were then dispersed in 100 µL (25 mg/mL bead concentration) of the linking buffer and stored at 4 °C until use.

The ZnS NCCs containing carboxyl groups on their surface were conjugated with streptavidinthrough conventional carbodiimide chemistry. Forty microliters of the stock ZnS NCCs (~ 4 x 10^{11} particles) were activated with 5 mg EDC and 5 mg sulfo-NHS, then centrifuged at 16.1 rcf for 12 minutes, washed, and resuspended in 100 µL of linking buffer. Then 40 µg of streptavidin was added and incubated on a rotator for 3 hours at room temperature. Excess reactive sites were quenched with 2-mercaptoethanol. The ZnS NCC-streptavidin conjugate was pelleted by centrifugation at 16.1k X g for 12 min and dispersed in 100 µL of linking buffer containing 5% BSA and stored at 4°C until further use.

In a typical experiment, solutions of synthetic hsa-let-7a at different concentrations were hybridized to the complementary sequences at the 5’ and 3’ ends of the padlock probe. The reaction conditions are described below. Let-7a solution was mixed with 100 nM of the padlock probe in 20 µL of ligation buffer (50 mM Tris-HCl, pH 7.5, 10 mM $MgCl_2$, 10 mM DTT, and 1 mM ATP) and denatured at 85 °C for 3 min

to ensure the availability of linear sequences for hybridization, slowly cooled to room temperature, and then incubated at RT for 1 hr. After the incubation 2 mM ATP and 0.1 U T4 DNA ligase were added, mixed, and incubated for 1 hour at RT for ligation of the probe. After ligation, 1 μL of primer conjugated magnetic beads was added, the mixture was then denatured at 85 °C for 3 min and incubated at RT for 1 hr. Using a magnet, the beads were pulled down along with the captured probes and dispersed in 40 μL of reaction buffer (40 mM Tris-HCl, pH 7.5, 50 mM KCl, 10 mM $MgCl_2$, 5 mM $(NH_4)_2SO_4$, 4mM DTT) containing 5% BSA and incubated for 30 min at RT to prevent non-specific interactions. With the addition of phi29 polymerase and dNTPs, including biotin-dATP, elongation of the bead-bound primers with the captured probes was carried out at 37 °C for 50 min forming long biotinylated ssDNA. The RCA products were tagged by dispersing the pelleted beads in 100 μL of 1× PBS with 5% BSA containing ZnS NCCs for 1 hour at RT on a tube rotator. The beads were once again pulled down and washed with 1× PBS containing 0.01% Tween-20 to remove unbound NCCs. Cation exchange with fluorescence detection was then performed by dispersion of RCA product beads in a 100 μL solution consisting of 500 μM silver nitrate and 3μM FluoZin-3, and then placing in a 700W microwave for 2 minutes at full power. The beads are pulled down and the supernatant is transferred to a 96-well microtiter plate and the fluorescence is measured in a Victor II Microplate reader (Perkin-Elmer, Waltham, MA) equipped with an excitation and emission filter wavelength of 485 nm and 530/30 nm respectively.

4.2.3: Detection of MiRNA by RCA-CXAmp

For the detection of miRNA via RCA-CXAmp the target miRNA is used as a template to form the circular probe through ligation of the linear padlock strand hybridized to the miRNA. This formed circular probe is then used to perform RCA elongating the primer strands on the MPs. This technique circumvents issues with miRNA degradation during the RCA process as the circular probe is already formed in the first step of the method. After the RCA reaction, ZnS NCCs with an average diameter of 40 nm and streptavidin conjugated on the surface bind to the RCPs and microwave-assisted cation exchange in carried out producing fluorescent FluoZin-3 dye molecules for detection. For proof-of-principle, the reaction was carried out using *hsa-let*-7a as the miRNA target. *Hsa-let*-7a is a relevant miRNA for many cancers, being a heavily expressed miRNA in all tissues normally regulating gene expression and a tumor-suppressive miRNA, which would block the expression of oncogenes and is therefore under-expressed in cancer cells. Many miRNAs, especially those in the same family, such as the *let*-7 family of miRNAs, can share high similarity in their sequences. This allows us to choose other *let*-7 family members as naturally occurring miRNAs with one or two base mismatches to test the specificity of our assay. The specificity in our assay arises from the ligation step as the circular probe is only formed if the linear probe can fold properly through perfect hybridization of the fully complementary miRNA target to allow the ligase to link the 3’ and 5’ end of the probe. Imperfect hybridization would destabilize the linear padlock probe folding and depending on the location of the mismatch base(s), either a very low number or no circular probes would be formed

leading to, at most, a weak signal after CXAmp. To examine our specificity, we compared the signal produced from 1 fmol of *let*-7a, *let*-7e, *let*-7i, and the blank using the assay designed for *let*-7a. The sequences of *let*-7e and *let*-7i differ from that of *let*-7a by one and four bases respectively. Figure 4.02a shows the relative increase in the fluorescence signal intensity over the blank (I/I_0). The I/I_0 for *let*-7a was over twice that of *let*-7e which was comparable to the blank, and over three times greater than that of *let*-7i which was actually lower than the blank on average. The multiple base mismatch of the *let*-7i likely hybridizes to one end of the linear padlock probe which prevents any incidental interactions of padlock probes with each other and blocks the padlock probe from interacting with the primers on the MPs. The fluorescent signals of the mismatched strand were still not distinguishable from the blank/background at 10 fmol (Figure 4.02b) demonstrating the high specificity of our assay for discrimination of single-base mismatches.

Using prepared *let*-7a standard solutions, we obtained a linear calibration curve for our RCA-CXAmp assay which showed high linearity ($R^2 = 0.998$) over triplicate assay results (Figure 4.02b). From the standard data we calculated a detection limit of 91 amol (using the definition of blank + 3SD). To test the applicability of the assay to real sample analysis, we applied the assay to the determination of the amount of *hsa-let*-7a in Human Brain Total RNA (Ambion) (Figure 4.02c). The amount of *let*-7a determined through the direct RCA-CXAmp assay was 217±16 amol in 50 ng of the total RNA. We then employed a standard addition method to confirm quantification accuracy. For this assay we spiked 500 amol of synthetic *hsa-let*-7a into the 50 ng sample of total RNA and

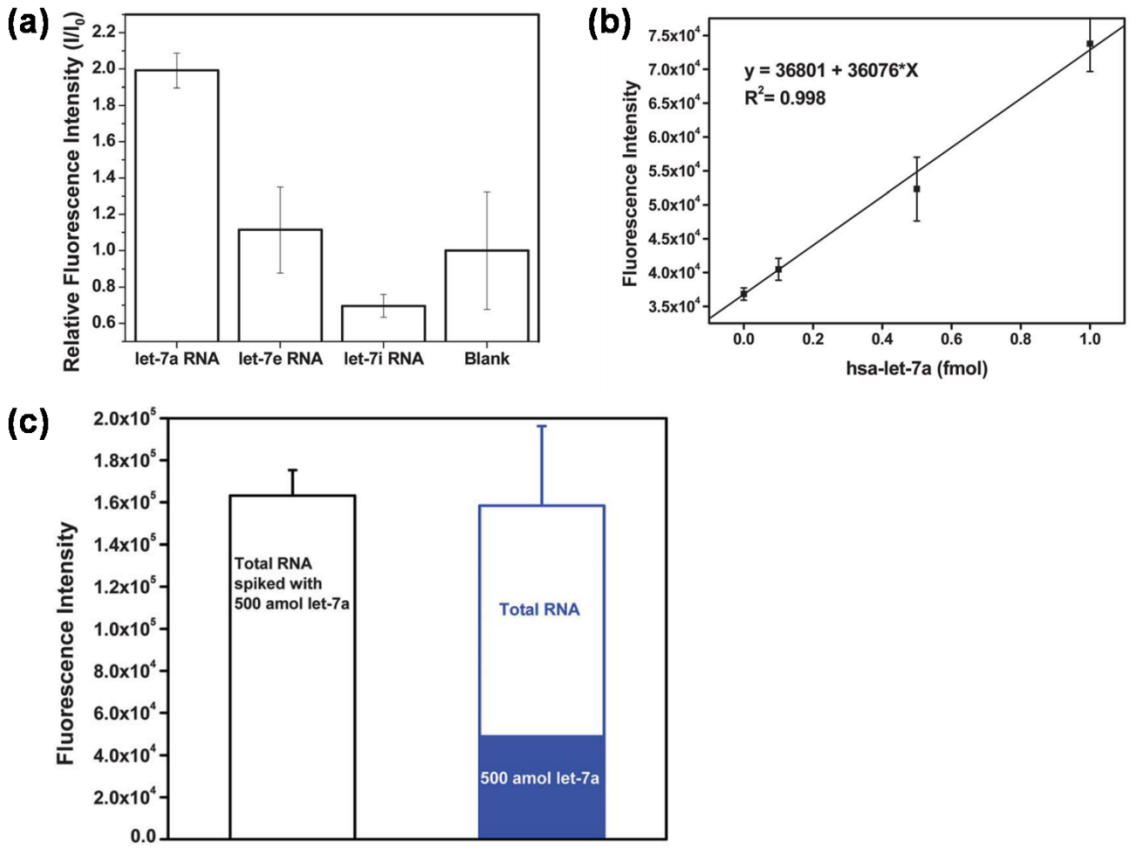

Figure 4.02. (a) The relative fluorescence intensities acquired for the target hsa-let-7a and mismatched strands let-7e and let-7i at an amount of 1 fmol each for measure of assay specificity. (b) Calibration curve of the fluorescence intensity vs. the amount of let-7a miRNA for the RCA-CXAmp. Error bars represent the standard deviation of triplicate measurements. (c) Determination of let-7a in the Human Brain Total RNA sample using standard addition.

performed the assay normally. The spiked total RNA yielded a fluorescence intensity value very similar to the sum of the intensities of the 500 amol standard and total brain RNA. Therefore the quantification accuracy of our assay is sufficient to detect attomole levels of miRNA in 50 ng of total RNA sample. This presents the ability of the assay in determination of low abundance targets such as miRNAs from relatively small sample sizes (~2.5×10^3 cells for 50 ng of total RNA or around ~30-35 ug of tissue sample).

4.2.4: Conclusions on RCA-CXAmp for MiRNA Detection

In summary, we demonstrated ability for tagging the RCPs with ZnS NCCs, and combining the RCA with CXAmp can lead to achievement of cascade signal amplification yielding superior detection performance compared to RCA or CXAmp alone. This combination, RCA-CXAmp holds promise for detection of trace biomarkers such as miRNA. Through the use of RCA in increasing specificity and target amplification and CXAmp to further assist through signal enhancement, low detection limits are achievable. Through further optimization and exploration of more isothermal techniques, an assay may be developed and optimized to push the sensitivity further to achieve even lower detection limits for the detection of trace biomarkers in disease diagnosis.

4.3: Hybridization Chain Reaction (HCR) of Strand Displacement Amplification (SDA) Products for Sensitive Detection of MicroRNA

4.3.1: Introduction to SDA and HCR

Strand displacement amplification is an isothermal nucleic acid amplification technique which relies on target or primer strand recycling for linear amplification.[12,29]

SDA has been employed in both protein and small molecule and biomolecule analysis using aptamers[30–32] and for nucleic acid amplification using capture strands or primers.[29,33] The technique simply requires a template and primers for the polymerase enzyme to extend. The template can be the target nucleic acid or a capture probe which can bind the target. The polymerase enzyme used is one which displays strand displacement capability, meaning the enzyme is able to displace DNA or RNA strands hybridized with the template being replicated during the extension of the primer strand. The amplification is the result of the displaced nucleic acid initiating further rounds of polymerization and displacement.

Hybridization chain reaction is a non-enzymatic method of amplification through the growth of a double stranded oligonucleotide scaffold for increasing detectable signal, which can be performed at room temperature.[14,34] HCR was originally developed by Dirks and Pierce[14] at the California Institute of Technology and introduced in 2004. The technique only requires two DNA hairpin strands in addition to the HCR initiator strand which could be the target nucleic acid, aptamer, or other target sensing oligonucleotide. The key to the technique is the careful design of the two hairpin species in terms of their energies, stable stem-loop structure, and minimal cross reactivity with each other. The design in the size of their loop, stem, and overhung tail are critical in efficient HCR. The method is simple; the two hairpins are stable and non-reactive with each other, in the presence of an initiator one of the hairpin species is opened, causing cascade reaction of the first strand hybridizing to the second hairpin through the complementary sequence which will then hybridize with and open the first hairpin. The reaction would continue

until the hairpin species are consumed or removed, producing a DNA duplex thousands to tens of thousands of nucleotides in length. Dirks and Pierce[14] illustrated colorimetric detection using gold nanoparticles.[35] Other simple methods of detection can be employ DNA binding or intercalating molecules for fluorescent or electrochemical detection.[36–40] Over the years since its inception, HCR has grown and has been optimized for favorable stability and hybridization rate, as well as modified for a variety of detection methods.[41] These include modifications on the DNA hairpin with reporter molecules and moieties for attachment of biological species and enzymes.[33,38]

4.3.2: Experimental Design of SDA-HCR

Utilized separately, SDA and HCR typically yield linear amplification of target species which can have limitations on detection limits and linear range of detection. Through the combination of these two techniques and the optimization of the method we can realize an isothermal detection method with quadratic amplification enabling low detection limits with larger ranges of detection.[42,43] Furthermore, the method of signal production and detection can be optimized to amplify target detection further to yield extremely low detection limits over a large linear range similar to quantitative PCR methods.[25–27,44–46] Through the careful design of initial steps of the method, high selectivity can be achieved. In our method, we utilize stem-loop capture probes for the selection of the target miRNA of interest. Stem-loop probes have highly stable structure which requires oligonucleotide sequences which are able to hybridize with a significant portion of the stem and loop in order to destabilize its structure.[5] This enables high selectivity with possibility of single-base mismatch differentiation.

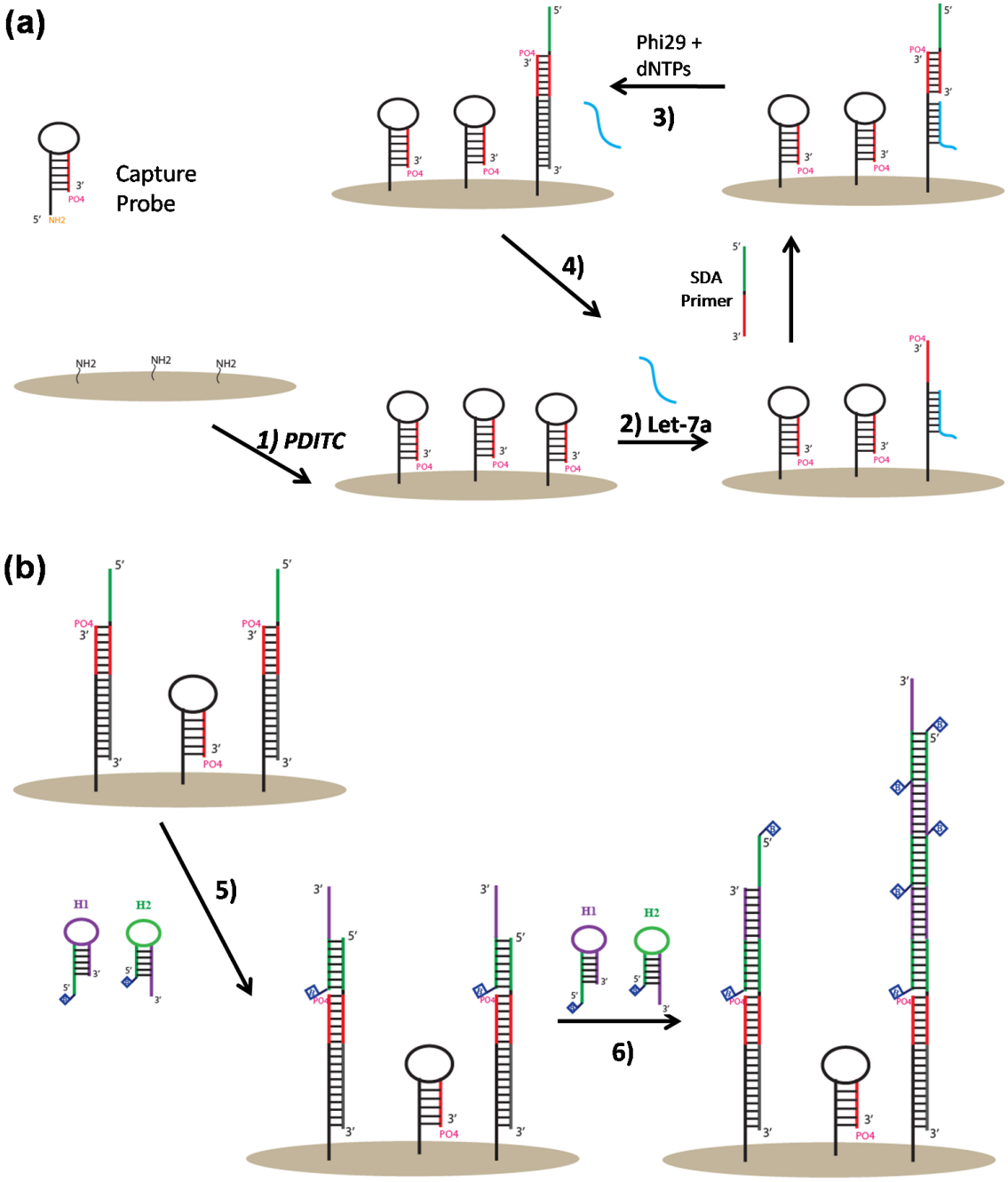

Figure 4.03. Schematic illustration of the SDA-HCR process in the detection of hsa-let-7a miRNA. (a) Target capture and strand displacement amplification. (b) Hybridization chain reaction using the SDA product as the initiator. H1 and H2 are biotin modified.

As illustrated in Figure 4.03, we utilize stem-loop probes for the selective capture of the target miRNA, *hsa-let*-7a, along with dual stage amplification; using SDA in the first stage to recycle the target miRNA and produce initiator sequences allowing for the employment of HCR in the second stage of amplification. The capture probes are designed to have high affinity with the target in a portion of its sequence which causes destabilization of the stem-loop nature of this probe. This capture probe has an amine modification on its 5' end allowing for covalent surface attachment (Step 1) for easy removal of solutions during different steps in the method. The 3' end of the capture probe was blocked by a phosphate modification to inhibit extension of the capture probe during the SDA process. A SDA primer sequence was designed to be complementary to a short sequence at the 3' end of the capture probe and a significant overhang off the 3' end of the probe. However, care was taken in its design to prevent destabilization of the capture probe stem-loop structure through the high energy loss require for the process, therefore only allowing for sufficient hybridization of the primer to capture probes opened by *let*-7a (Step 2). During the SDA process, the primer is elongated in the 5' to 3' direction toward the attachment surface through the activity causing the displacement of the internally hybridized *let*-7a (Step 3). The displaced *let*-7a is then capable of hybridizing with and opening another nearby capture probe on the surface (Step 4), and the SDA process continues with primer hybridization and *let*-7a release. Through this process we realize recycling of our target, resulting in multiple SDA products for each target strand. The 5' end of the SDA primer, which overhangs from the capture probe, acts as an initiator for HCR. This initiator sequence is complementary to the 5' overhang of the

stem-loop sequence of hairpin 1 (H1) (Step 5). Once opened, the previously hybridized portion of H1 is exposed, which is complementary to the 3' overhang on hairpin 2 (H2) (Step 6). The newly exposed portion at the 5' end of H2 is complementary to the overhang of H1, resulting in the cascade hybridization of H1 and H2 elongating the formed double stranded DNA complex. H1 and H2 contain biotinylated modifications on their 5' ends, allowing for attachment of reporter molecules, enzymes, or nanoparticles.

4.3.3: Materials and Methods

All oligonucleotides were purchased with desired modifications from Integrated DNA Technologies (Coralville, IA). Sequence information and other relevant information for all oligonucleotides used are provided in Table 4.1. Klenow fragment (3'→5' exo-) and phi29 DNA polymerase were purchased from New England Biolabs (Ipswich, MA). P-phenylene diisothiocyanate (PDITC) and pyridine were obtained from Sigma Aldrich (St. Louis, MO). Horseradish peroxidase (HRP)-streptavidin conjugate, SYBR Gold nucleic acid gel stain, and deoxynucleotides (dNTPs) were from Invitrogen (Carlsbad, CA). Phosphate salts, sodium chloride, potassium chloride, magnesium chloride, sodium hydroxide, 3-aminopropyl-triethoxysilane (APTES), 2-propanol, ethanol, tris base, boric acid, EDTA, and Pierce enhanced ehemiluminescence substrate were purchased from ThermoFisher (Pittsburgh, PA). Polydimethylsiloxane (PDMS) was purchased as Sylgard 184 from Dow Corning (Midland, MI).

All experiments were either performed on an amino-modified PDMS-Glass multi-well chip. Cured PDMS substrate was cut to the size of a standard microscope slide (25 mm × 75 mm). Holes were then punched in the PDMS in the spacing of a 96-well plate

using a 5mm stainless steel cylinder for a total of 16 wells per chip. The PDMS substrate was then covalently attached to a standard glass microscope slide; The PDMS and glass slide were placed in a plasma oxidation chamber (Harrick Plasma Cleaner) for 1 minute and immediately joined together forming permanent Si-O-Si bonds between the PDMS and the glass. The multi-well chip then contained PDMS wells with glass bottoms. The bottom of the wells were then modified; wells were washed with 1 M NaOH, water, 100% ethanol and air dried, then 10% (v/v) APTES in ethanol was incubated in the wells for 10 minutes and removed, then washed several times with ethanol and dried. Capture probes were attached through amine-amine coupling using PDITC. An isopropanol (IPA) solution containing 10% pyridine and 0.5% PDITC was added to the wells and incubated for 2 hours at room temperature. The wells were then washed with IPA, ethanol, and then dried. The DNA capture probe is then incubated in 50 mM borate buffer (pH~9) in the wells overnight at room temperature. The wells are then washed with borate and then ultrapure water.

For klenow fragment the SDA conditions are as follows; 1x Tris-HCl buffer, 400 uM dNTPs, 500 nM SDA primer and 5U klenow fragment exo- for 1 hour at 37 °C. For phi29 the SDA conditions are as follows; 1x phi29 buffer (NEB), 200 ug/mL BSA, 400 uM dNTPs, 250 nM SDA primer, and 5U phi29 for 1 hour @ 37 degrees C. For each experiment, the *let*-7a standard or blank was loaded into the well (50 µL total volume in 1× PBS with 5mM $MgCl_2$) and incubated for 90 minutes at 37 °C. Wells were then washed twice with PBS buffer and the SDA reagents were added. After SDA, the wells were washed twice with PBS and the HCR solution consisting of 500 nM each hairpin 1

Identity	**Sequence (5'-3')**
Target: hsa-let-7a	rUrGrA rGrGrU rArGrU rArGrG rUrUrG rUrArU rArGrU rU
Capture Probe	NH_2-AAA AAA AAA ACC GTC CTA ***TAC AAC CTA CTA CCT CAA ATT*** AGG ACG G-PO4
Capture Probe Blocker	CCG TCC TAA TTT GAG GTA GTA GGT TGT ATA GGA CGG T
SDA Primer	AGT CTA GGA TTC GGC GTG GGT TAA TTT TTC CGT CCT A
Hairpin 1	Biotin-TTA ACC CAC GCC GAA TCC TAG ACT ***CAA AGT*** AGT CTA GGA TTC GGC GTG
Hairpin 2	Biotin-AGT CTA GGA TTC GGC GTG ***GGT TAA*** CAC GCC GAA TCC TAG ACT ACT TTG

Table 4.1. Sequence information for all synthesized oligonucleotides used in this study.Matching colors indicate complementary sequences. Bolded regions in sequences represent the loop regions and underlined portions represent the self complementary stem regions. The capture probe blocker is complementary to the entire capture probe sequence minus the poly A tail on the 5' end.

and hairpin 2 in 5x PBS buffer was loaded in the well and incubated for 2 hours at room temperature. Detection with SYBR Gold was achieved by a 10 minute incubation in pH~ 8.0 TBE buffer (1.5× dye concentration) and detected using a Victor2 plate reader (Perkin Elmer). Detection using luminescence was performed as follows; horseradish peroxidase (HRP) conjugated streptavidin in a 1:5000 dilution in 1× PBS was added and incubated for 1 hour at room temperature with gentle shaking. The supernatant was discarded and the plate was washed 3 times with 1× PBS. Next 50 μL of the Pierce enhanced chemiluminescence (ECL) substrate (Thermo Fisher) was added, and incubated for 5 minutes. The resulting chemiluminescence was immediately detected on the Victor2 plate reader. Analysis by gel electrophoresis was completed on an 8% polyacrylamide gel (native-PAGE). The gel electrophoresis was run in 1× TBE at 200 V. The gel was then stained with SYBR Gold gel stain for detection using an UV transilluminator and camera with appropriate filter.

4.3.4: Results and Discussion

Optimization of the SDA involved the choice of enzyme, as the enzymatic activity and strand displacement capability are essential for successful SDA. We chose to test two commonly employed isothermal enzymes with strand displacement capability, Klenow fragment and phi29 polymerase. As can be seen in Figure 4.04(a, b), both enzymes exhibited amplification yet Klenow fragment gave more inconsistent results and had much higher background as compared to phi29 (Figure 4.04a). Therefore phi29 was chosen in all following experiments (Figure 4.04b). We performed gel electrophoresis to investigate if the hybridization chain reaction was indeed growing double stranded chains

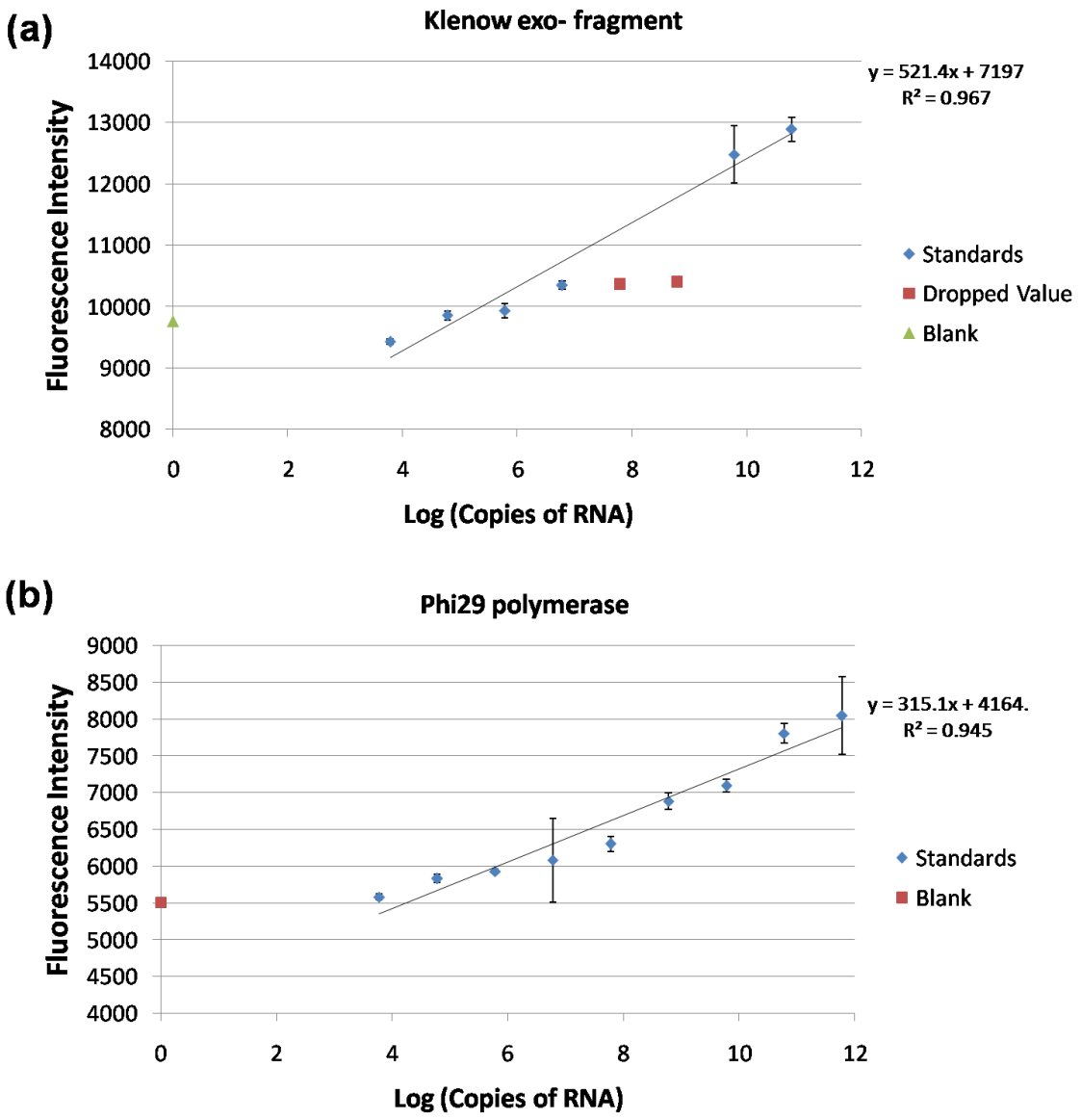

Figure 4.04. Standard calibration curves for the SDA-HCR method using Sybr Gold for detection with Klenow exo- fragment (a) and phi29 polymerase (b) chosen as SDA enzymes.

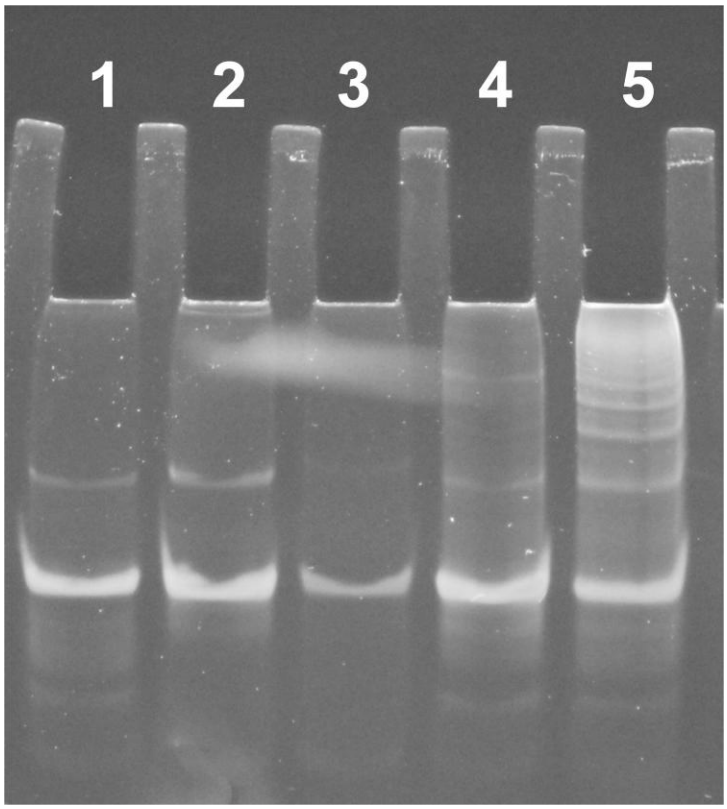

Figure 4.05. Image of native polyacrylamide gel (10%). The contents of each well/lane is as follows; 1: Hairpin 1, 2: Hairpin 2, 3: SDA primer, 4: Hairpin 1 and Hairpin 2 mixed, 5: Hairpin 1 and Hairpin 2 with SDA primer mixed. All samples were made respectively in 1× PBS buffer and incubated for 1 hour at room temperature prior to loading gel for electrophoresis. Gel was dyed using Sybr Gold staining and imaged using a transilluminator and camera with an appropriate filter.

of significant length and to test stability of the stem-loop secondary structure of the hairpins to prevent reaction in the absence of initiator. The same method for HCR portion of the experiment was used in tube as on chip. We found that minimal cross reactivity between the two hairpins was seen in the absence of the SDA primer, however in the presence of the SDA primer the HCR was initiated yielding product of much higher molecular weight (Figure 4.05).

Testing for successful SDA with minimal nonspecific amplification due to binding of the SDA primer to unopened capture probes was investigated through the use of a capture probe blocker strand for comparison to the blank (no *let*-7a). The capture probe blocker is fully complementary to the entire capture probe sequence and therefore blocks any species (*let*-7a, SDA primer) from hybridizing with the capture probe. The SDA-HCR method, with SYBR Gold detection, was used with two standard solutions towards the higher and lower detection limits, one blank, and then a well incubated with a saturating amount of capture probe blocker during the sample incubation period (Figure 4.06). We see that the blank signal is slightly lower than the blocked signal, both of which are well below the signal for 1 amol *let*-7a. This illustrates that there is essentially no HCR reaction produced by reaction of the SDA primer with unopened capture probes as this would cause the signal to be higher for the blank. The elevated signal of the blocked capture probe is due to the increased DNA material on the surface due to the double stranded DNA formed versus the shorter stem-loop capture probes present in the blank.

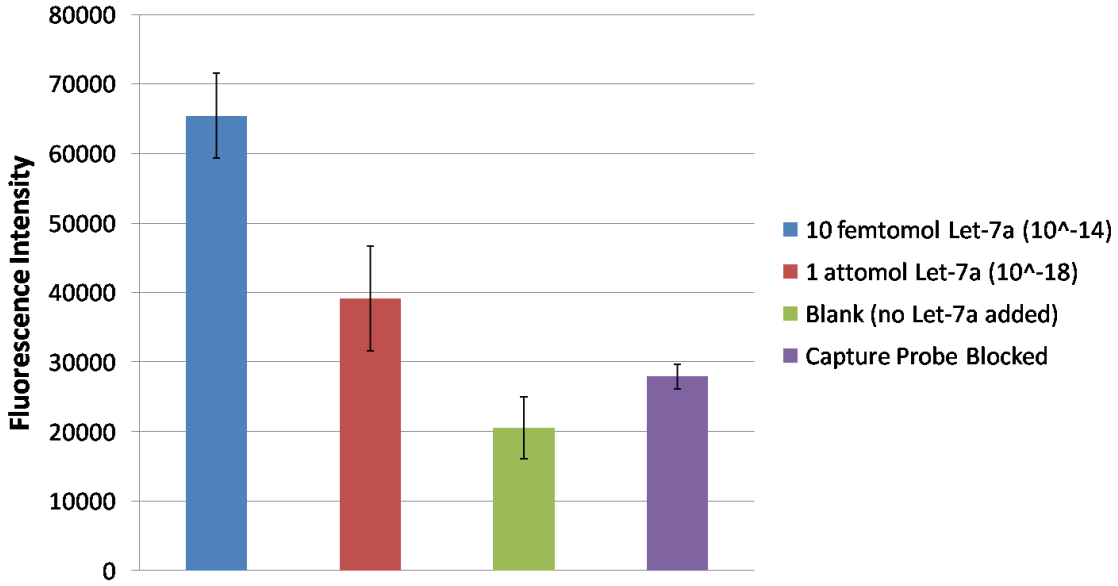

Figure 4.06. SDA-HCR for quantization of standard hsa-let-7a using SYBR Gold for fluorescent detection. The calculated LOD is 1.31 fmol (S/N=5).

In order to push the detection limits lower, we investigated the use of streptavidin-HRP to tag the HCR products. As both HCR primers contain a 5' biotin group, an HCR product can bind several streptavidin-HRP yielding greater signal. Figure 4.07 shows the result of HRP luminescence coupled with SDA-HCR. We see a significant amplification of the signal in this case. Using SYBR Gold based detection the signal of 1 attomole of *let*-7a standard is less than twice that of the blank, and even closer when taking the standard deviation into account. This experimental data correlates with a calculated limit of detection (LOD), with signal-to-noise ratio (S/N) of 5, of 1.31 fmol. When HRP-based luminescence in used, the signal of the 1 attomole of *let*-7a standard is over three times the blank with smaller error bars. Again, the calculated LOD (S/N=5) gives a value of 2.02 amol, which is nearly 3 orders of magnitude lower than using direct nucleic detection with SYBR dye.

As we can see in the above results, the current method is capable of detecting 1 attomole in a 10 µL volume, equal to 100 femtomolar, with satisfactory signal to background ratio using conventional HRP-based detection. This can be further improved through the optimization of background signal through controlling the binding of SDA primer in absence of *let*-7a. This can be achieved through the modification of the SDA primer, by reducing the portion complementary to the capture probe by one base. Also the target incubation conditions such as the buffer composition and temperature can be optimized to increase the stability of the capture probe stem-loop structure and reduce SDA primer binding. Further optimization of the SDA reaction conditions could further

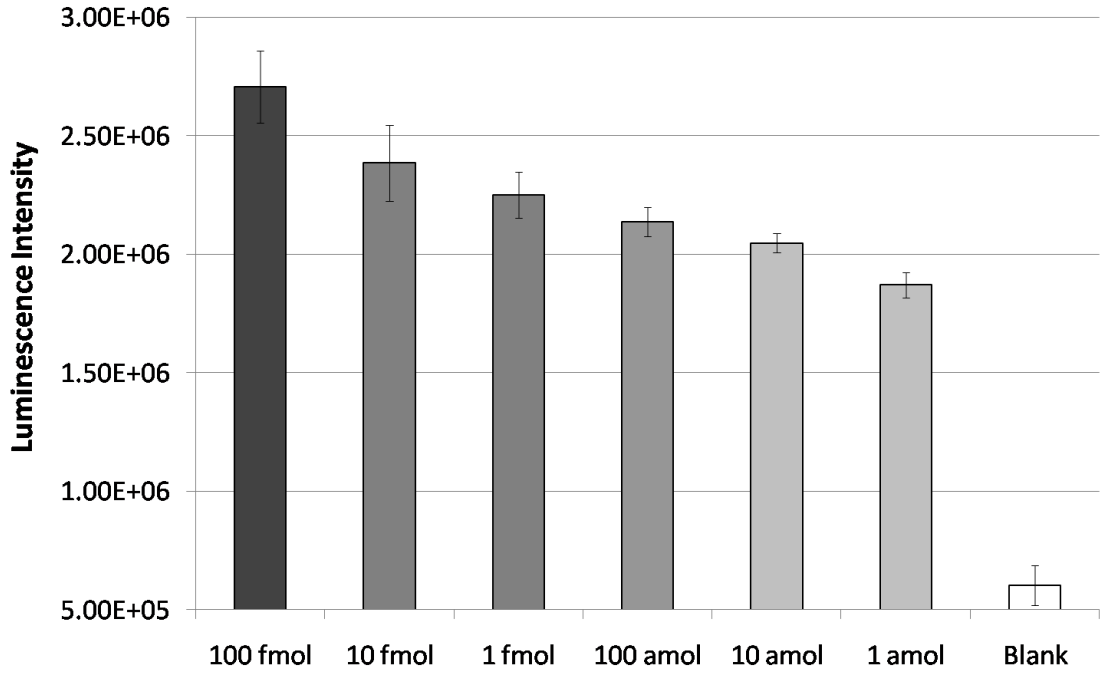

Figure 4.07. SDA-HCR for quantization of standard hsa-let-7a using streptavidin-HRP for tagging of the HCR product and amplified luminescent signal. The LOD is calculated at 234 zmol (S/N=3.3).

reduce the background and increase the signal through more specific and highly efficient amplification.

4.3.5: Conclusions

In this research, we successfully combined two isothermal amplification techniques, SDA and HCR, to detect the miRNA *hsa-let*-7a. The developed method has the potential for high specificity, provided by a stem-loop capture probe, and only relies on miRNA stability through the first stage of amplification. Used alone, the SDA reaction yields poor detection limits in our technique. The combination of SDA with HCR decreases the limit of detection significantly. Using SYBR Gold for detection the LOD (S/N=5) of 1.31 femtomole is achieved. Adding signal amplification through the utilization of HRP-based luminescence by tagging the HCR products yields LODs at 2.02 attomole and 234 zeptomole, with S/N of 5 and 3.3 respectively. Therefore the developed method provides much desirable detection limits with great potential for use as an isothermal miRNA quantification method competitive with real-time quantitative PCR after additional optimization.

4.4: Isothermal Amplification Conclusions

In this chapter, two isothermal amplification methods for the quantification of miRNA, *hsa-let*-7a, have been introduced; RCA-CXAmp and SDA-HCR. The RCA-CXAmp offers a relatively quick method with high selectivity of the target miRNA, while yielding an LOD (S/N =3) of 91 attomole. The SDA-HCR method was developed in hopes of improving the detection limits further by achieving quadratic amplification, with products of the SDA-HCR having biotin moieties for tagging of the products similar

to RCA tagged for CXAmp. In SDA-HCR, a LOD (greater S/N=5) of 1.31 femtomole and 2.02 attomole is achieved for direct SYBR-based detection and HRP tagged detection respectively. In the RCA-CXAmp work, we found that the CXAmp offers greater sensitivity than HRP in the detection of the RCA product. The improvement by utilizing CXAmp was about 2 orders of magnitude over HRP-luminescence. Although a different luminescence substrate reagent is employed in the SDA-HCR work, we could expect similar results. Therefore, utilizing CXAmp by tagging the SDA-HCR products could improve the detection limits even further, possibly achieving detection of just a few hundred copies of miRNA.

References:

(1) Wang, K.; Yuan, Y.; Cho, J.-H.; McClarty, S.; Baxter, D.; Galas, D. J. Comparing the MicroRNA Spectrum between Serum and Plasma. *PLoS ONE* **2012**, *7* (7), e41561.

(2) McDonald, J. S.; Milosevic, D.; Reddi, H. V.; Grebe, S. K.; Algeciras-Schimnich, A. Analysis of Circulating MicroRNA: Preanalytical and Analytical Challenges. *Clin. Chem.* **2011**, *57* (6), 833–840.

(3) Johnson, B. N.; Mutharasan, R. Biosensor-Based microRNA Detection: Techniques, Design, Performance, and Challenges. *The Analyst* **2014**, *139* (7), 1576.

(4) Catuogno, S.; Esposito, C. L.; Quintavalle, C.; Cerchia, L.; Condorelli, G.; De Franciscis, V. Recent Advance in Biosensors for microRNAs Detection in Cancer. *Cancers* **2011**, *3* (2), 1877–1898.

(5) Chen, C.; Ridzon, D. A.; Broomer, A. J.; Zhou, Z.; Lee, D. H.; Nguyen, J. T.; Barbisin, M.; Xu, N. L.; Mahuvakar, V. R.; Andersen, M. R.; Lao, K. Q.; Livak, K. J.; Guegler, K. J. Real-Time Quantification of microRNAs by Stem–loop RT–PCR. *Nucleic Acids Res.* **2005**, *33* (20), e179–e179.

(6) Gill, P.; Ghaemi, A. Nucleic Acid Isothermal Amplification Technologies—A Review. *Nucleosides Nucleotides Nucleic Acids* **2008**, *27* (3), 224–243.

(7) Jia, H.; Li, Z.; Liu, C.; Cheng, Y. Ultrasensitive Detection of microRNAs by Exponential Isothermal Amplification. *Angew. Chem. Int. Ed.* **2010**, *49* (32), 5498–5501.

(8) Kim, J.; Easley, C. J. Isothermal DNA Amplification in Bioanalysis: Strategies and Applications. *Bioanalysis* **2011**, *3* (2), 227–239.

(9) Kim, J.; Easley, C. J. Isothermal DNA Amplification in Bioanalysis: Strategies and Applications. *Bioanalysis* **2011**, *3* (2), 227–239.

(10) Asiello, P. J.; Baeumner, A. J. Miniaturized Isothermal Nucleic Acid Amplification, a Review. *Lab. Chip* **2011**, *11* (8), 1420–1430.

(11) Demidov, V. V. Rolling-Circle Amplification in DNA Diagnostics: The Power of Simplicity. *Expert Rev. Mol. Diagn.* **2002**, *2* (6), 542–548.

(12) Walker, G. T.; Fraiser, M. S.; Schram, J. L.; Little, M. C.; Nadeau, J. G.; Malinowski, D. P. Strand Displacement Amplification—an Isothermal, in Vitro DNA Amplification Technique. *Nucleic Acids Res.* **1992**, *20* (7), 1691–1696.

(13) Detter, J. C.; Jett, J. M.; Lucas, S. M.; Dalin, E.; Arellano, A. R.; Wang, M.; Nelson, J. R.; Chapman, J.; Lou, Y.; Rokhsar, D.; Hawkins, T. L.; Richardson, P. M. Isothermal Strand-Displacement Amplification Applications for High-Throughput Genomics. *Genomics* **2002**, *80* (6), 691–698.

(14) Dirks, R. M.; Pierce, N. A. Triggered Amplification by Hybridization Chain Reaction. *Proc. Natl. Acad. Sci. U. S. A.* **2004**, *101* (43), 15275–15278.

(15) Fire, A.; Xu, S. Q. Rolling Replication of Short DNA Circles. *Proc. Natl. Acad. Sci.* **1995**, *92* (10), 4641–4645.

(16) Dean, F. B.; Nelson, J. R.; Giesler, T. L.; Lasken, R. S. Rapid Amplification of Plasmid and Phage DNA Using Phi29 DNA Polymerase and Multiply-Primed Rolling Circle Amplification. *Genome Res.* **2001**, *11* (6), 1095–1099.

(17) Hutchison, C. A.; Smith, H. O.; Pfannkoch, C.; Venter, J. C. Cell-Free Cloning Using φ29 DNA Polymerase. *Proc. Natl. Acad. Sci. U. S. A.* **2005**, *102* (48), 17332–17336.

(18) Zhao, W.; Ali, M. M.; Brook, M. A.; Li, Y. Rolling Circle Amplification: Applications in Nanotechnology and Biodetection with Functional Nucleic Acids. *Angew. Chem. Int. Ed.* **2008**, *47* (34), 6330–6337.

(19) Li, N.; Li, J.; Zhong, W. CE Combined with Rolling Circle Amplification for Sensitive DNA Detection. *ELECTROPHORESIS* **2008**, *29* (2), 424–432.

(20) Li, N.; Jablonowski, C.; Jin, H.; Zhong, W. Stand-Alone Rolling Circle Amplification Combined with Capillary Electrophoresis for Specific Detection of Small RNA. *Anal. Chem.* **2009**, *81* (12), 4906–4913.

(21) Tang, L.; Liu, Y.; Ali, M. M.; Kang, D. K.; Zhao, W.; Li, J. Colorimetric and Ultrasensitive Bioassay Based on a Dual-Amplification System Using Aptamer and DNAzyme. *Anal. Chem.* **2012**, *84* (11), 4711–4717.

(22) Bi, S.; Cui, Y.; Li, L. Dumbbell Probe-Mediated Cascade Isothermal Amplification: A Novel Strategy for Label-Free Detection of microRNAs and Its Application to Real Sample Assay. *Anal. Chim. Acta* **2013**, *760*, 69–74.

(23) Dong, H.; Wang, C.; Xiong, Y.; Lu, H.; Ju, H.; Zhang, X. Highly Sensitive and Selective Chemiluminescent Imaging for DNA Detection by Ligation-Mediated

Rolling Circle Amplified Synthesis of DNAzyme. *Biosens. Bioelectron.* **2013**, *41*, 348–353.

(24) Lena Linck, E. R. Direct Labeling Rolling Circle Amplification as a Straightforward Signal Amplification Technique for Biodetection Formats. *Anal Methods* **2012**, *4* (5), 1215–1220.

(25) Li, J.; Zhang, T.; Ge, J.; Yin, Y.; Zhong, W. Fluorescence Signal Amplification by Cation Exchange in Ionic Nanocrystals. *Angew. Chem. Int. Ed.* **2009**, *48* (9), 1588–1591.

(26) Yao, J.; Han, X.; Zeng, S.; Zhong, W. Detection of Femtomolar Proteins by Nonfluorescent ZnS Nanocrystal Clusters. *Anal. Chem.* **2012**, *84* (3), 1645–1652.

(27) Yao, J.; Schachermeyer, S.; Yin, Y.; Zhong, W. Cation Exchange in ZnSe Nanocrystals for Signal Amplification in Bioassays. *Anal. Chem.* **2011**, *83* (1), 402–408.

(28) Li, T.; Wang, E.; Dong, S. G-Quadruplex-Based DNAzyme as a Sensing Platform for Ultrasensitive Colorimetric Potassium Detection. *Chem. Commun.* **2009**, No. 5, 580–582.

(29) Guo, Q.; Yang, X.; Wang, K.; Tan, W.; Li, W.; Tang, H.; Li, H. Sensitive Fluorescence Detection of Nucleic Acids Based on Isothermal Circular Strand-Displacement Polymerization Reaction. *Nucleic Acids Res.* **2009**, *37* (3), e20.

(30) He, J.-L.; Wu, Z.-S.; Zhou, H.; Wang, H.-Q.; Jiang, J.-H.; Shen, G.-L.; Yu, R.-Q. Fluorescence Aptameric Sensor for Strand Displacement Amplification Detection of Cocaine. *Anal. Chem.* **2010**, *82* (4), 1358–1364.

(31) Fang, Z.; Wu, W.; Lu, X.; Zeng, L. Lateral Flow Biosensor for DNA Extraction-Free Detection of Salmonella Based on Aptamer Mediated Strand Displacement Amplification. *Biosens. Bioelectron.* **2014**, *56*, 192–197.

(32) Zhu, C.; Wen, Y.; Li, D.; Wang, L.; Song, S.; Fan, C.; Willner, I. Inhibition of the In Vitro Replication of DNA by an Aptamer–Protein Complex in an Autonomous DNA Machine. *Chem. – Eur. J.* **2009**, *15* (44), 11898–11903.

(33) Wang, C.; Zhou, H.; Zhu, W.; Li, H.; Jiang, J.; Shen, G.; Yu, R. Ultrasensitive Electrochemical DNA Detection Based on Dual Amplification of Circular Strand-Displacement Polymerase Reaction and Hybridization Chain Reaction. *Biosens. Bioelectron.* **2013**, *47*, 324–328.

(34) Yamaguchi, T.; Kawakami, S.; Hatamoto, M.; Imachi, H.; Takahashi, M.; Araki, N.; Yamaguchi, T.; Kubota, K. In Situ DNA-Hybridization Chain Reaction (HCR): A Facilitated in Situ HCR System for the Detection of Environmental Microorganisms. *Environ. Microbiol.* **2015**, *17* (7), 2532–2541.

(35) Yang, W.-J.; Li, X.-B.; Li, Y.-Y.; Zhao, L.-F.; He, W.-L.; Gao, Y.-Q.; Wan, Y.-J.; Xia, W.; Chen, T.; Zheng, H.; Li, M.; Xu, S. Quantification of microRNA by Gold Nanoparticle Probes. *Anal. Biochem.* **2008**, *376* (2), 183–188.

(36) Chen, Y.; Xu, J.; Su, J.; Xiang, Y.; Yuan, R.; Chai, Y. In Situ Hybridization Chain Reaction Amplification for Universal and Highly Sensitive Electrochemiluminescent Detection of DNA. *Anal. Chem.* **2012**, *84* (18), 7750–7755.

(37) Deng, Y.; Nie, J.; Zhang, X.; Zhao, M.-Z.; Zhou, Y.-L.; Zhang, X.-X. Hybridization Chain Reaction-Based Fluorescence Immunoassay Using DNA Intercalating Dye for Signal Readout. *Analyst* **2014**, *139* (13), 3378–3383.

(38) Ge, Z.; Lin, M.; Wang, P.; Pei, H.; Yan, J.; Shi, J.; Huang, Q.; He, D.; Fan, C.; Zuo, X. Hybridization Chain Reaction Amplification of MicroRNA Detection with a Tetrahedral DNA Nanostructure-Based Electrochemical Biosensor. *Anal. Chem.* **2014**, *86* (4), 2124–2130.

(39) Liu, S.; Wang, Y.; Ming, J.; Lin, Y.; Cheng, C.; Li, F. Enzyme-Free and Ultrasensitive Electrochemical Detection of Nucleic Acids by Target Catalyzed Hairpin Assembly Followed with Hybridization Chain Reaction. *Biosens. Bioelectron.* **2013**, *49*, 472–477.

(40) Qiu, X.; Wang, P.; Cao, Z. Hybridization Chain Reaction Modulated DNA-Hosted Silver Nanoclusters for Fluorescent Identification of Single Nucleotide Polymorphisms in the Let-7 miRNA Family. *Biosens. Bioelectron.* **2014**, *60*, 351–357.

(41) Choi, H. M. T.; Beck, V. A.; Pierce, N. A. Next-Generation in Situ Hybridization Chain Reaction: Higher Gain, Lower Cost, Greater Durability. *ACS Nano* **2014**, *8* (5), 4284–4294.

(42) Duan, R.; Zuo, X.; Wang, S.; Quan, X.; Chen, D.; Chen, Z.; Jiang, L.; Fan, C.; Xia, F. Lab in a Tube: Ultrasensitive Detection of MicroRNAs at the Single-Cell Level and in Breast Cancer Patients Using Quadratic Isothermal Amplification. *J. Am. Chem. Soc.* **2013**, *135* (12), 4604–4607.

(43) Duan, R.; Zuo, X.; Wang, S.; Quan, X.; Chen, D.; Chen, Z.; Jiang, L.; Fan, C.; Xia, F. Quadratic Isothermal Amplification for the Detection of microRNA. *Nat. Protoc.* **2014**, *9* (3), 597–607.

(44) Tian, Y.; He, Y.; Mao, C. Cascade Signal Amplification for DNA Detection. *ChemBioChem* **2006**, *7* (12), 1862–1864.

(45) Adams, J. C. Biotin Amplification of Biotin and Horseradish Peroxidase Signals in Histochemical Stains. *J. Histochem. Cytochem.* **1992**, *40* (10), 1457–1463.

(46) Gao, W.; Dong, H.; Lei, J.; Ji, H.; Ju, H. Signal Amplification of Streptavidin–horseradish Peroxidase Functionalized Carbon Nanotubes for Amperometric Detection of Attomolar DNA. *Chem. Commun.* **2011**, *47* (18), 5220–5222.

Chapter 5: Development and Optimization of Techniques for Solid Phase Extraction of miRNA

5.1: Introduction

Reliable methods for isolation and purification of miRNA from complex liquid samples are essential for detection and analysis of miRNA as biomarkers.[1–5] MiRNA is poorly extracted using traditional chemical separation techniques due to its small size and moderate solubility in ethanol-water solutions. Furthermore, many commercial kits for solid phase extraction of miRNA employ the same silicon dioxide (silica) membranes and similar binding solutions used to extract longer RNA species. Since miRNA is only 20-25 nucleotides in length, the number of interactions between the silica surface and each miRNA strand are limited and lead to weaker binding of the miRNA on the silica, yielding poor recovery of miRNA. Non-specific adsorption of other biological molecules and proteins in complex matrices can cause fouling of these silica membranes and reduce miRNA binding further. The binding solutions are initially designed and optimized for general RNA extraction on silica and could be optimized further. Therefore the choice of a solid-phase material along with development and optimization on the binding conditions is needed to improve recovery.

Silica or glass beads were originally employed in nucleic acid extractions[6,7], although the use of porous silica gels and monolithic silica became more heavily used due to the greater surface areas of these species[8–10], becoming the basis of commercial silica membrane spin columns.[11] Silica exhibits a high density of silanol groups on its surface giving it the ability to create salt bridges or hydrogen bonds with negatively

charged, and electronegative, phosphate groups on DNA and RNA bases. Silanol groups on silica surfaces are fairly acidic with a pKa of about 4.8 and therefore deprotonated in aqueous environments unless the solution is acidic enough to protonate them.[12,13] For this reason the main mode of nucleic acid binding above the pKa will be salt bridging, or hydrogen bonding when below the pKa. Silica is not the only material that display pervasive hydroxyl like groups on the surface which exhibit binding to phosphate groups. Silicon carbide has been recently used in nucleic acid binding (NorgenBiotek). Also titanium dioxide (titania) and zirconium dioxide (zirconia) have been investigated and utilized for their favorable interactions with phosphate groups on modified peptides and proteins for enrichment, as well as with DNA for drug delivery.[14–22]

Nucleic acids are known to adsorb silica through the use of high salt concentration, low pH, chaotropic reagents, or a combination of these.[6,23–25] Most silica-based extraction techniques use a solution that is neutral or slightly basic and therefore utilize high concentrations of sodium or potassium chloride, guanidine hydrochloride (GuHCl) or guanidine isothiocyanate (GuITC) for DNA or RNA respectively, ethanol, and surfactants such as Triton X-100 for lysis and binding of nucleic acids while minimizing protein contamination. Specific optimization of the binding solution components is necessary for extracting DNA, RNA, and small RNAs. The binding solution also requires some modification based on sample type and choice of solid-phase material to achieve high recovery. Wash steps are typically necessary to remove contaminants and usually utilize ethanol or isopropanol with other chaotropic reagents to maintain adsorption of nucleic acid while solubilizing and removing proteins and lipids.

5.2: Silica Microbeads for Extraction of MicroRNA

5.2.1: Introduction

Silica-based extraction is the conventional method for solid-phase extraction of nucleic acids.[6] Commercial nucleic acid binding beads and columns provided in DNA or RNA extraction kits are most typically pure silica; either a solid silica coating or porous silica is utilized. The binding of nucleic acids to these materials relies on the reagents supplied in a binding buffer solution. However the nature of the nucleic acid also has a significant impact on binding and therefore recovery in the extraction. DNA and RNA require different conditions for adequate binding and the conditions need to be optimized for the length of the DNA or RNA being extracted.[26] Further, the amount of silica material used in the extraction will affect the upper extraction limit (loading limit) and the elution volume will impact the efficiency of the elution. Extraction of miRNA on silica coated magnetic beads offers a simple method for recovery of miRNA from a solution.[8] Such a method can be efficiently utilized on a microfluidic device to bind miRNA and transport the miRNA across channels to other isolated areas on the device.[9,27,28] However, binding of miRNA to silica is weaker by nature of its small size and high solubility in solution, and requires specifically optimized protocol for successful extraction with high efficiency.

5.2.2: Materials and Methods

Taq 5× master mix was purchased from New England Biolabs. TaqMan MicroRNA Assays specific for each target, RNase-free ultrapure water, and TRIzol LS reagent were purchased from Life Technologies (Carlsbad, CA). Synthesized MicroRNA

standards and exogenous control were purchased from Integrated DNA Technologies (Coralville, IA). Sodium chloride, potassium chloride, magnesium chloride, sodium hydroxide, ethylene glycol, dimethylsulfoxide (DMSO), 2-propanol, ethanol, urea, guanidine hydrochloride, and guanidine isothiocyanate were purchased from ThermoFisher (Pittsburgh, PA). Polydimethylsiloxane (PDMS) was purchased as Sylgard 184 from Dow Corning (Midland, MI). Superparamagnetic silica particles with a nominal diameter of 1.0 μm were purchased from Bioclone Inc. (San Diego, CA).

Recipes varied as they were being optimized for the extractions. The Final optimized extraction conditions of standard miRNA from water were 4.5 M GuHCl and 1.0 M KCl and 0.1% Tween 20. For serum miRNA extractions we used the Total Exosome Isolation kit (Invitrogen) to separate the exosome fraction from the other serum components. Then a variety of recipes were used for optimization of miRNA extraction from the exosome fraction and exosome depleted serum fraction. To 50μL of sample 400 μg of silica beads were added along with appropriate amounts of binding reagents. After a 15 minute incubation for binding, the beads were pulled down and washed 2 times with ethanol, isolated and dried, then the beads were incubated for 15 minutes in ultrapure water for elution of miRNA.

An optimized RT-qPCR protocol was used for analysis employing the individual TaqMan MicroRNA Assay kits (Applied Biosystems). In each RT reaction, 5 μL of sample extract (1 μL for endogenous control) was mixed with 3 μL of a reverse transcription master mix and 2 μL of a corresponding stem-loop RT primer for each miRNA target strand. The RT master mix consisted of 1.1 μL nuclease-free water, 1 μL

of a 10× RT buffer, 0.13 μL of RNAse inhibitor, 0.1 μL of a dNTP mix, and 0.67 μL reverse transcriptase (all components were provided in a TaqMan reverse transcription kit). After mixing and brief centrifugation, 5 μL of silicone oil was layered on top of the RT mixture, and reverse transcription conducted on a Perkin-Elmer 2400 GeneAmp PCR Thermocycler. The RT reaction consisted of a 30-minute annealing step at 16°C, a 32-minute reverse transcription step at 42°C, and a 5-minute denaturing step at 85°C. After RT, the samples underwent quantitative PCR (qPCR). On the qPCR plate, 1 μL of the RT product was mixed with 9 μL of qPCR master mix for a final volume of 10μL. As an overlay, 5 μL of silicone oil was added to the top of each sample to limit evaporation. The PCR master mix consisted of 4.9 μL of nuclease-free water, 1 μL of ethylene glycol, 0.1 μL of DMSO, 0.5 μL of 25 mM magnesium chloride, 2 μL of Taq 5× master mix, and 0.5 μL of 20× qPCR primer mix (specific forward and reverse PCR primers, and specific TaqMan fluorescent probe). Each sample RT product was plated in triplicate, and standards corresponding to the samples analyzed (high- versus low-abundance) were plated in singlet. The qPCR analysis was conducted on a Bio-Rad CFX real-time instrument, with an initial activation step at 95 °C for 90s followed by an initial annealing step at 59°C for 50s, followed by a 40-cycle PCR with 30s denaturation at 95 °C and 70s annealing/extension at 53 °C in each cycle.

5.2.3: Results and Discussion

Figure 5.01 shows the recoveries of hsa-miR-16 and cel-miR-67 standards from a water sample using the optimized protocol employing 4.5 M GuHCl with 1 M KCl. From this data we see that high recoveries the concentration range over 4 orders of magnitude

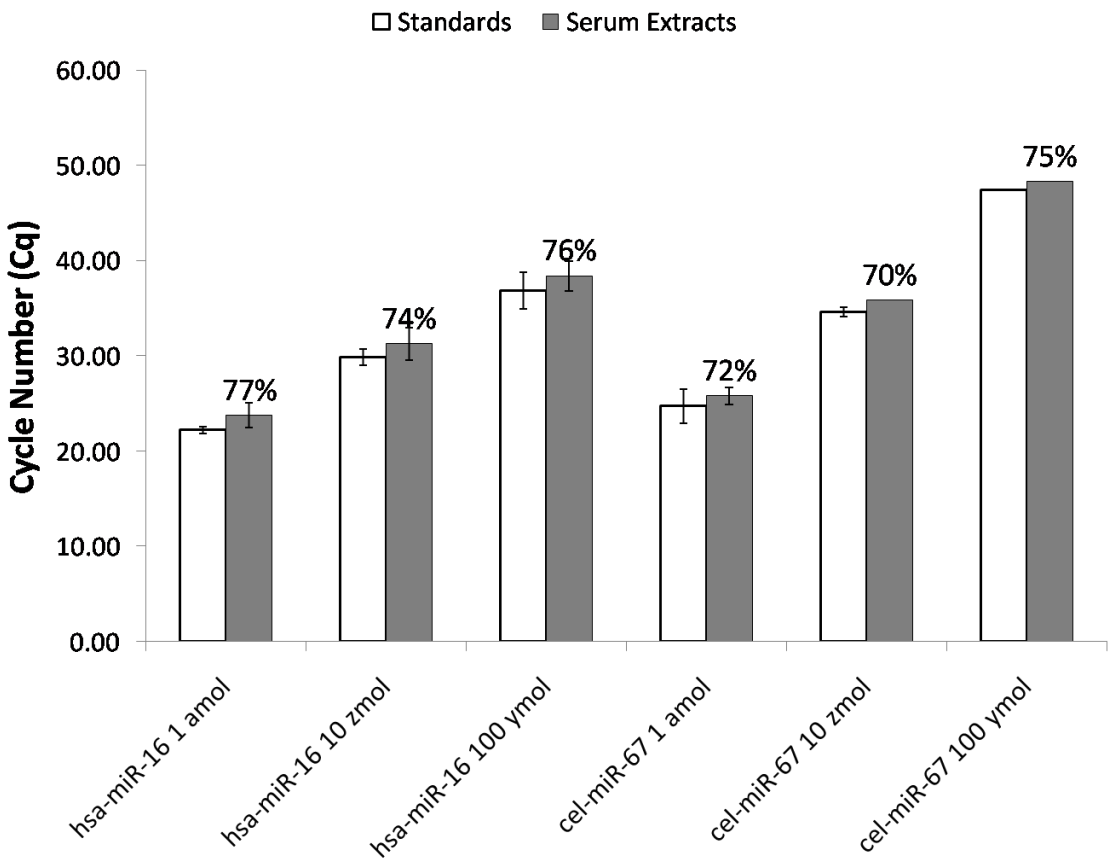

Figure 5.01. RT-qPCR results for the extraction of standards hsa-miR-16 and cel-miR-67 from water on a simple microfluidic device using silica-magnetic beads. Percentages indicate the recovery of the target at that concentration using the standards to calculate the recovery.

from 100 ymol to 1 amol in 5 microliters. Extraction of miRNA from serum is more difficult due to the complex nature of serum; containing many salts and ions which could interfere with extraction, containing proteins and lipids which might cause fouling of the surface, and the necessary denaturation of miRNA binding with proteins and lipoproteins as well as disruption of exosomes. As seen in Figure 5.02 from the optimization of miR-16 extraction from exosome and exosome depleted serum fractions, the GuHCl based recipe used in water extractions fails to extract all of the serum miRNA in each fraction as compared to the conventional TRIzol extractions. This is due to the poor ability of GuHCl to disrupt lipoprotein complexes and exosomes. With the addition of GuITC and Tween-20 we see higher recovery in the exosome depleted serum, which correlates to the harsher conditions in those situations enabling denaturation of all protein-miRNA and most of lipoprotein-miRNA complexes. With the exosome fraction we also see an increase with the GuITC, and a further increase with the use of higher concentration surfactants. However, the silica bead-based method of extraction was not able to extract all of the miR-16 found by TRIzol extraction, indicating that the addition of organic solvents or harsher conditions may be necessary for disruption of those vesicles lipid bilayer structure. The extraction efficiency as calculated by the recovery of the exogenous control cel-miR-67 dropped well below 1 percent for the original GuHCl recipe and was as high as 20% for the more optimized extractions.

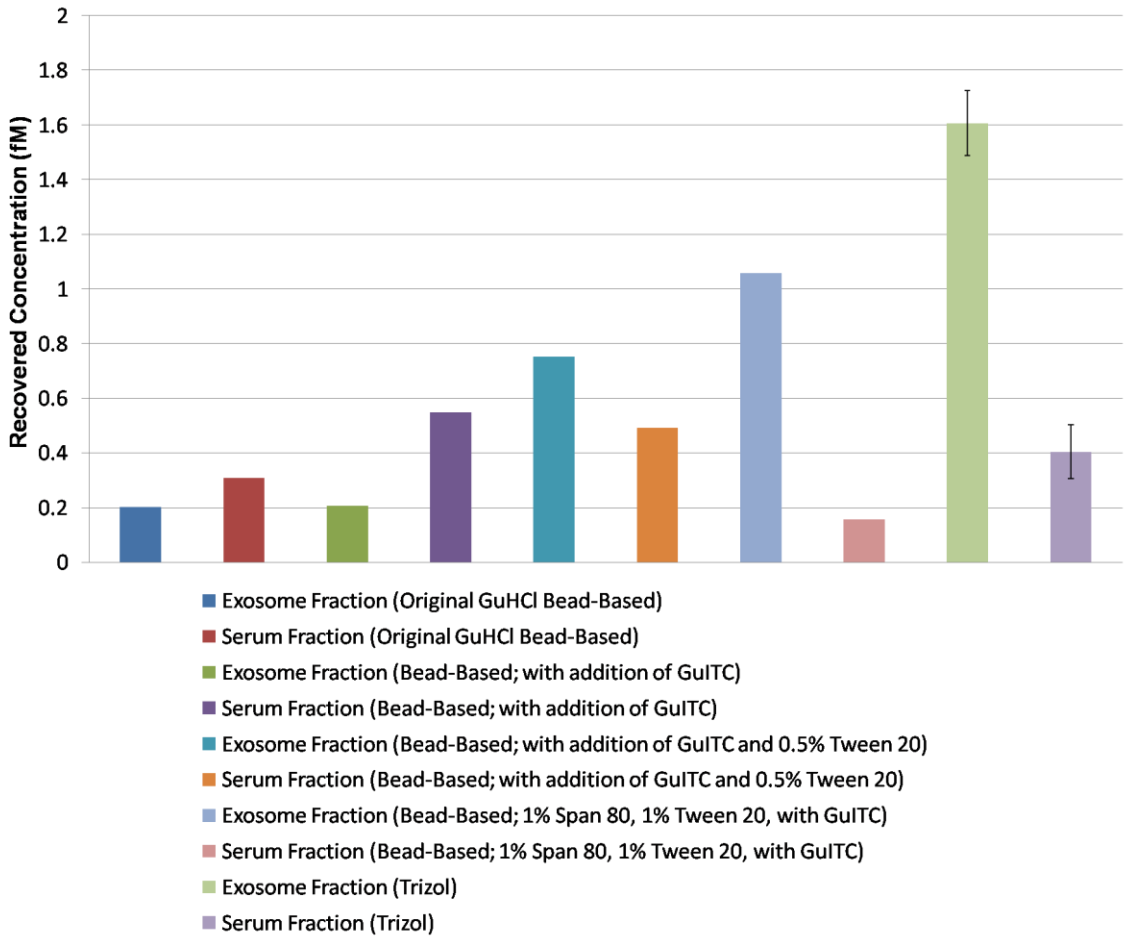

Figure 5.02. Optimization results for recovering hsa-miR-16 from serum using silica magnetic bead based extraction. Serum was split into two fractions using the Invitrogen Total Exosome Isolation kit; exosomes and exosome depleted serum (supernatant in the exosome isolation. The miR-16 recovered from each fraction using the TRIzol chemical extraction was used to identify the absolute levels. In all cases, cel-miR-67 was used as an exogenous spiked standard for correction of extraction efficiency.

5.3: MicroRNA Extraction Using Titania Fibers

5.3.1: Introduction

Similar to silicon dioxide (silica), titanium dioxide (titania), has the potential ability to bind to phosphate through hydrogen bonding or salt bridging of the surface hydroxyl or oxide groups respectively.[15,18] Titanium dioxide nanomaterials have been investigated recently for binding of DNA for targeted delivery into cells.[18] However, there has been little to no investigation on the use and optimization of titania materials for the extraction of nucleic acids. This may be the result of the assumption that it would yield similar results to silica. Yet titania does show favorable properties for the extraction of nucleic acids, and further investigation into the use of titania for nucleic acid extraction can potentially yield better recoveries. Titanium nanofibers are easily fabricated via electro-spinning based on literature protocols[18,29,30], with controllable diameters less than 500 nm. Titania is also less acidic then silica with a pKa of 6.6 for the surface Ti-OH groups[31] compared to 4.8 for silanol groups.

5.3.2: Materials and Methods

Titanium isopropoxide and polyvinylpyrrolidone (PVP) were purchased from Sigma-Aldrich (St. Louis, MO). Isopropanol, glacial acetic acid, ethanol, guanidine hydrochloride, guanidine isothiocyanate, potassium acetate, potassium chloride, dimethylsulfoxide, ethylene glycol, and PureLink RNA mini kit were acquired from Thermo Fisher (Waltham, MA). Taq 5× master mix was purchased from New England Biolabs (Ipswich, MA). TaqMan MicroRNA Assay for *cel-miR*-54 was purchased from

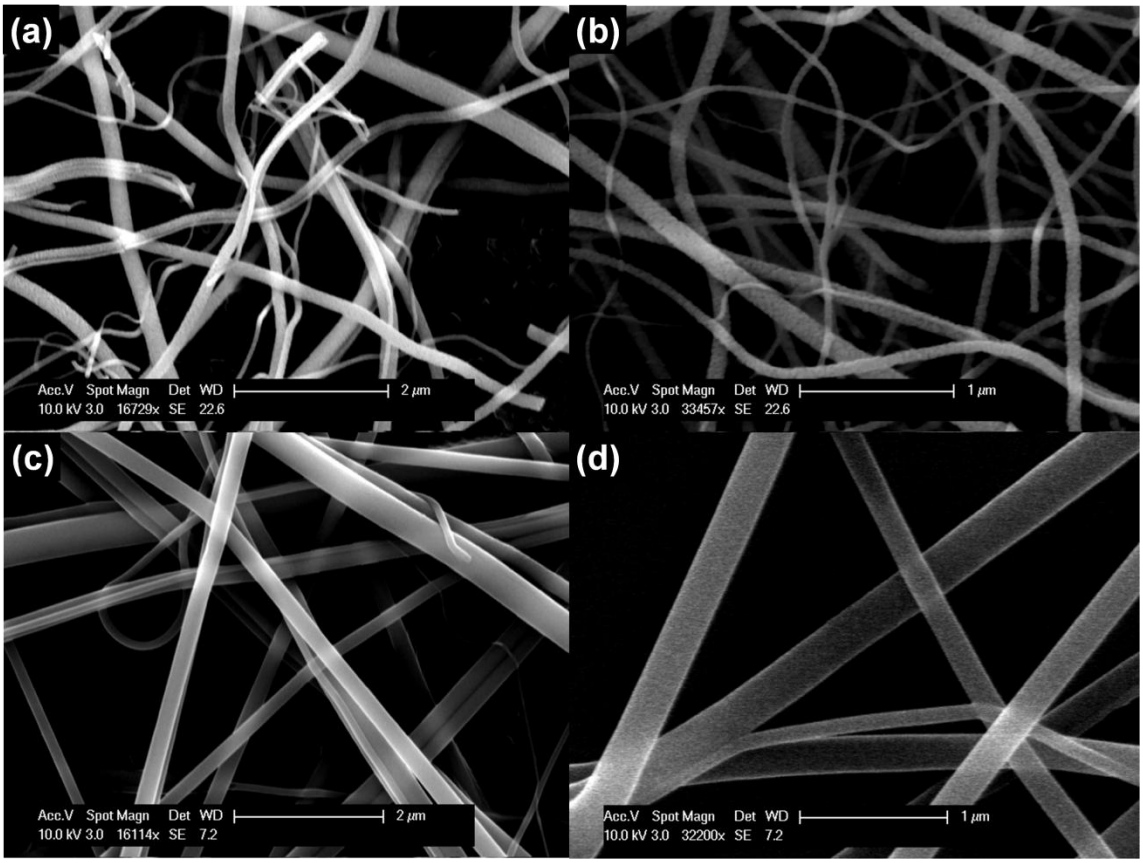

Figure 5.03. SEM images of titania nanofibers using our fabrication method. (a)(b) The titania nanofibers after calcination. (c)(d) The titania fibers prior to calcination. Shrinkage of fibers is seen after calcination indicating the loss of organic material.

Life Technologies (Carlsbad, CA). Synthesized *cel-miR*-54 microRNA was purchased from Integrated DNA Technologies (Coralville, IA).

Titania nanofibers were fabricated using electro-spinning based on previously published methods.[29,30] Two solutions were made; a 12% PVP polymer solution in ethanol (7.5 mL total volume), and a titania precursor solution consisting of 1.5 g of titanium isopropoxide in 6 mL of 1:1 mixture of ethanol:acetic acid. The titania precursor solution was stirred at room temperature for 20 minutes and then added to the dissolved PVP solution. The mixture was then stirred for 30 minutes at room temperature before loading into a syringe for electro-spinning. The syringe was placed on a syringe pump set up to deliver a flow rate of 3.6 mL/hour during electro-spinning. The fibers were spun at an electric field strength of 3.0 kV/cm (positive at needle and grounded to collection surface) onto a rotating cylinder collector at a distance of 5 cm between the syringe tip and collector. After electro-spinning, the fibers were removed from the collector and placed in a glass dish and calcinated by heating in a furnace at 600 °C for 2 hours and then slowly cooled. The calcination process removes the polymer and produces pure titania nanofibers which are suspended in water (100 mg/mL) when ready for use. The fibers were characterized using scanning electron microscopy (SEM) (Figure 5.03) indicating the shrinkage of fibers after calcination correlating to the removal of organic material within the fibers. The final diameter of the calcinated fibers was approximated to be around 100-150 nm versus >200 nm for the non-calcinated fibers.

For the quantification of extracted miRNA, the same optimized RT-qPCR protocol given in section 5.2.2 of this chapter was used. For extraction, the miRNA

sample was incubated for 15 minutes with the appropriate extraction reagents followed by isolation of the fiber using a 0.22 µm Costar centrifugal filter (Corning). The fibers were then washed with 500 µL of ethanol and incubated for 15 minutes in 20 mM phosphate buffer for elution of bound miRNA. The eluent was then isolated through centrifugal filtration into a fresh tube and used for RT-qPCR analysis.

5.3.3: Results and Discussion

For the investigation of the extraction ability of the titania nanofibers, we compared our recoveries to the recovery in a commercial silica-based kit (Purelink RNA mini kit, Thermo Fisher). We investigated the titania-based extraction using four buffer solutions; binding buffer 1-3 (BB1, BB2, BB3) and the buffer included in the Purelink kit. All three binding buffers contained 0.4 M potassium acetate buffer (pH~9), 1 M KCl, 0.2% Tween-20, and in addition; BB1 contained 6 M GuHCl, BB2 contained 4.5 M GuITC, and BB3 contained 3.5 M GuITC and 1.5 M GuHCl. Previously we investigated the use of buffer conditions on the elution of DNA from titania and found that inorganic phosphate buffer is more efficient then Tris-buffer or water typically used in elution from titania. We suspected this from previous literature reports of phosphate destabilizing DNA interactions with titania nanoparticles in biological systems. We optimized the concentration of the phosphate buffer used to maximize the elution without inhibiting PCR amplification (Figure 5.04). From this we found that the increase of phosphate concentration up to 20 mM increased dissociation of nucleic acids from titania, while higher concentration had effect on PCR inhibition. For this study we used a 24 base miRNA from *Caenorhabditis elagan, cel-miR*-54 our exogenous standard, to demonstrate

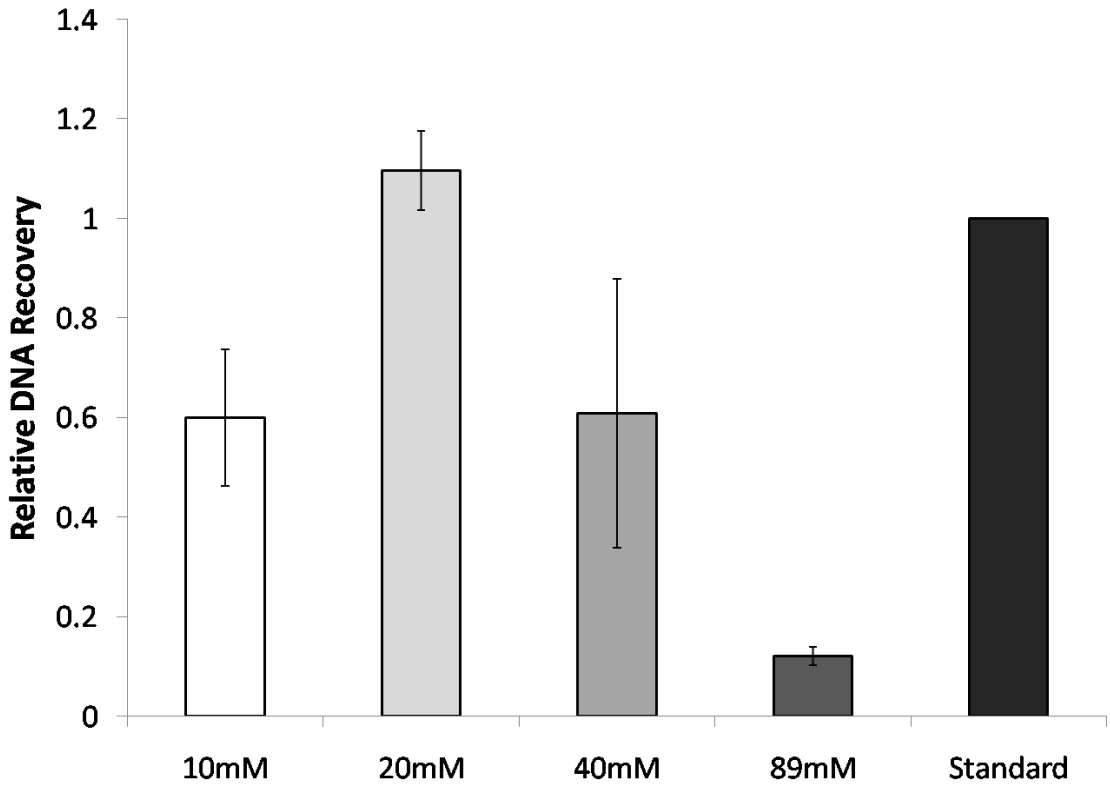

Figure 5.04. Optimization of the concentration of phosphate buffer used in the elution of an 80 base DNA from titania nanofibers from 10 mM-89 mM phosphate (pH~8.0). Maximum DNA release is seen at 20 mM while higher concentration causes PCR inhibition. Relative recoveries are calculated with SYBR-based qPCR quantification of recovered quantity in comparison to the expected quantity.

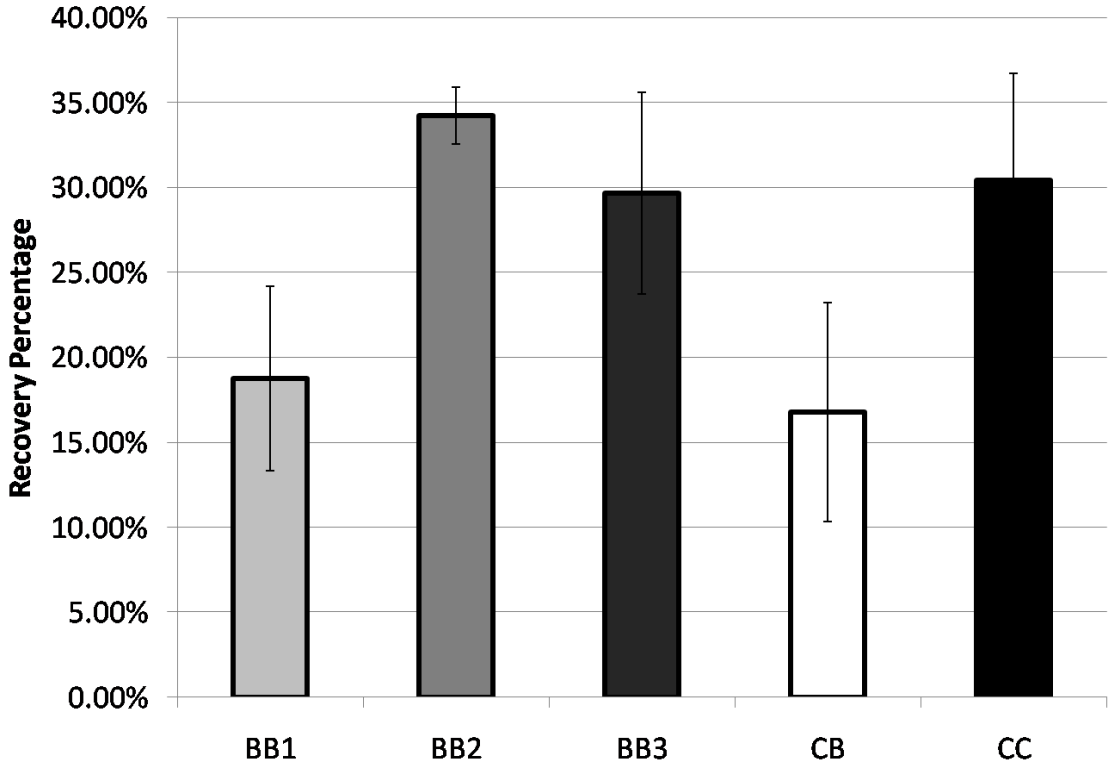

Figure 5.05. Optimization of binding buffer recipe for extraction of microRNA with titania nanofibers. Three custom recipes (BB1-BB3) were tested in addition to the use of a buffer included in the Purelink mini RNA kit (Thermo Fisher) with titania (CB) in comparison to the recovery using the silica-based column in the Purelink kit according to the manufacturer's protocol. All extraction samples were 500 amol cel-miR-54 in 100 µL of ultrapure water.

the extraction of miRNA and other small RNA. 500 amol of *miR*-54 was diluted in 100 µL of ultrapure water and mixed with 200 µL of buffer and 50 µL of ethanol, after extraction the bound miRNA was eluted in 100 µL of 20 mM phosphate. As shown in Figure 5.05, the investigation of our binding buffer recipes and the effect of the guanidine species used reveal that GuITC outperforms GuHCl or the mixture of the two, demonstrating that GuITC is ideal for extraction of RNA on titania at basic pH values which is similar to that demonstrated for silica in literature. Further, the BB2 recipe outperformed the buffer included in the commercial column extraction kit when used with our titania fibers and also has higher recovery than that achieved by using the commercial kit as directed by the manufacturer's protocol. This indicates that our recipe thus far is optimized for titania binding, and with further optimization has the potential to well surpass the ability of commercial silica columns in the extraction of miRNA.

5.4: Conclusion

In this study we investigated titania as an alternative nucleic acid binding material for SPE of miRNA. Our work demonstrates the ability of titania to bind and elute miRNA under similar conditions to silica for extraction purposes. Comparing to a commercial silica-based column extraction kit for RNA, our technique is superior in its currently optimized state showing a relative recovery of 34.2% versus 30.4% for the commercial kit with our method showing greater reproducibility. Further optimization of our extraction reagent composition may improve this extraction efficiency further. Also the investigation of titania's ability to extract miRNA via hydrogen bonding at lower pH (<6) in low salt conditions needs to be studied and the optimization of the incubation periods

for binding and elution is necessary to achieve higher recovery of miRNA. Then we hope to further optimize these conditions to complex sample matrices such as serum. Lastly we hope to integrate the titania fibers on a simple microfluidic device for efficient extraction of miRNAs for more commercial and clinical applications.

References:

(1) McDonald, J. S.; Milosevic, D.; Reddi, H. V.; Grebe, S. K.; Algeciras-Schimnich, A. Analysis of Circulating MicroRNA: Preanalytical and Analytical Challenges. *Clin. Chem.* **2011**, *57* (6), 833–840.

(2) McAlexander, M. A.; Phillips, M. J.; Witwer, K. W. Comparison of Methods for miRNA Extraction from Plasma and Quantitative Recovery of RNA from Cerebrospinal Fluid. *Front. Genet.* **2013**, *4*.

(3) De Guire, V.; Robitaille, R.; Tétreault, N.; Guérin, R.; Ménard, C.; Bambace, N.; Sapieha, P. Circulating miRNAs as Sensitive and Specific Biomarkers for the Diagnosis and Monitoring of Human Diseases: Promises and Challenges. *Clin. Biochem.* **2013**, *46* (10–11), 846–860.

(4) Ach, R. A.; Wang, H.; Curry, B. Measuring microRNAs: Comparisons of Microarray and Quantitative PCR Measurements, and of Different Total RNA Prep Methods. *BMC Biotechnol.* **2008**, *8* (1), 69.

(5) Eldh, M.; Lötvall, J.; Malmhäll, C.; Ekström, K. Importance of RNA Isolation Methods for Analysis of Exosomal RNA: Evaluation of Different Methods. *Mol. Immunol.* **2012**, *50* (4), 278–286.

(6) Boom, R.; Sol, C. J.; Salimans, M. M.; Jansen, C. L.; Dillen, P. M. W.; Noordaa, J. van der. Rapid and Simple Method for Purification of Nucleic Acids. *J. Clin. Microbiol.* **1990**, *28* (3), 495–503.

(7) Marko, M. A.; Chipperfield, R.; Birnboim, H. C. A Procedure for the Large-Scale Isolation of Highly Purified Plasmid DNA Using Alkaline Extraction and Binding to Glass Powder. *Anal. Biochem.* **1982**, *121* (2), 382–387.

(8) Berensmeier, S. Magnetic Particles for the Separation and Purification of Nucleic Acids. *Appl. Microbiol. Biotechnol.* **2006**, *73* (3), 495–504.

(9) Cady, N. C.; Stelick, S.; Batt, C. A. Nucleic Acid Purification Using Microfabricated Silicon Structures. *Biosens. Bioelectron.* **2003**, *19* (1), 59–66.

(10) Christel, L. A.; Petersen, K.; McMillan, W.; Northrup, M. A. Rapid, Automated Nucleic Acid Probe Assays Using Silicon Microstructures for Nucleic Acid Concentration. *J. Biomech. Eng.* **1999**, *121* (1), 22–27.

(11) Karp, A.; Isaac, P. G.; Ingram, D. S. Isolation of Nucleic Acids Using Silica-Gel Based Membranes: Methods Based on the Use of QIAamp Spin Columns. In

Molecular Tools for Screening Biodiversity; Karp, A., Isaac, P. G., Ingram, D. S., Eds.; Springer Netherlands, 1998; pp 59–63.

(12) Alberto Méndez, E. B. Comparison of the Acidity of Residual Silanol Groups in Several Liquid Chromatography Columns. *J. Chromatogr. A* **2003**, *986* (1), 33–44.

(13) Campos, A. F. C.; Marinho, E. P.; Ferreira, M. de A.; Tourinho, F. A.; Paula, F. L. de O.; Depeyrot, J. X-DLVO Interactions between Nanocolloidal Magnetic Particles: The Quantitative Interpretation of the pH-Dependent Phase Diagram of EDL-MF. *Braz. J. Phys.* **2009**, *39* (1A), 230–235.

(14) Bian, J.; Xue, Y.; Yao, K.; Gu, X.; Yan, C.; Wang, Y. Solid-Phase Extraction Approach for Phospholipids Profiling by Titania-Coated Silica Microspheres prior to Reversed-Phase Liquid Chromatography-Evaporative Light Scattering Detection and Tandem Mass Spectrometry Analysis. *Talanta* **2014**, *123*, 233–240.

(15) Cleaves, H. J.; Jonsson, C. M.; Jonsson, C. L.; Sverjensky, D. A.; Hazen, R. M. Adsorption of Nucleic Acid Components on Rutile (TiO2) Surfaces. *Astrobiology* **2010**, *10* (3), 311–323.

(16) Ji, L.; Wu, J.-H.; Luo, Q.; Li, X.; Zheng, W.; Zhai, G.; Wang, F.; Lü, S.; Feng, Y.-Q.; Liu, J.; Xiong, S. Quantitative Mass Spectrometry Combined with Separation and Enrichment of Phosphopeptides by Titania Coated Magnetic Mesoporous Silica Microspheres for Screening of Protein Kinase Inhibitors. *Anal. Chem.* **2012**, *84* (5), 2284–2291.

(17) Richardson, B. M.; Soderblom, E. J.; Thompson, J. W.; Moseley, M. A. Automated, Reproducible, Titania-Based Phosphopeptide Enrichment Strategy for Label-Free Quantitative Phosphoproteomics. *J. Biomol. Tech. JBT* **2013**, *24* (1), 8–16.

(18) Zhang, X.; Wang, F.; Liu, B.; Kelly, E. Y.; Servos, M. R.; Liu, J. Adsorption of DNA Oligonucleotides by Titanium Dioxide Nanoparticles. *Langmuir* **2014**, *30* (3), 839–845.

(19) Rappsilber, J.; Mann, M.; Ishihama, Y. Protocol for Micro-Purification, Enrichment, Pre-Fractionation and Storage of Peptides for Proteomics Using StageTips. *Nat. Protoc.* **2007**, *2* (8), 1896–1906.

(20) Sugiyama, N.; Masuda, T.; Shinoda, K.; Nakamura, A.; Tomita, M.; Ishihama, Y. Phosphopeptide Enrichment by Aliphatic Hydroxy Acid-Modified Metal Oxide Chromatography for Nano-LC-MS/MS in Proteomics Applications. *Mol. Cell. Proteomics MCP* **2007**, *6* (6), 1103–1109.

(21) Wan, H.; Yan, J.; Yu, L.; Zhang, X.; Xue, X.; Li, X.; Liang, X. Zirconia Layer Coated Mesoporous Silica Microspheres Used for Highly Specific Phosphopeptide Enrichment. *Talanta* **2010**, *82* (5), 1701–1707.

(22) Wang, S.-T.; Chen, D.; Ding, J.; Yuan, B.-F.; Feng, Y.-Q. Borated Titania, a New Option for the Selective Enrichment of Cis-Diol Biomolecules. *Chem. – Eur. J.* **2013**, *19* (2), 606–612.

(23) Vandeventer, P. E.; Lin, J. S.; Zwang, T. J.; Nadim, A.; Johal, M. S.; Niemz, A. Multiphasic DNA Adsorption to Silica Surfaces under Varying Buffer, pH, and Ionic Strength Conditions. *J. Phys. Chem. B* **2012**, *116* (19), 5661–5670.

(24) Vandeventer, P. E.; Mejia, J.; Nadim, A.; Johal, M. S.; Niemz, A. DNA Adsorption to and Elution from Silica Surfaces: Influence of Amino Acid Buffers. *J. Phys. Chem. B* **2013**, *117* (37), 10742–10749.

(25) Melzak, K. A.; Sherwood, C. S.; Turner, R. F. B.; Haynes, C. A. Driving Forces for DNA Adsorption to Silica in Perchlorate Solutions. *J. Colloid Interface Sci.* **1996**, *181* (2), 635–644.

(26) Gitig, D. Life Science Technologies: Moving Beyond DNA. *Science* **2009**.

(27) Breadmore, M. C.; Wolfe, K. A.; Arcibal, I. G.; Leung, W. K.; Dickson, D.; Giordano, B. C.; Power, M. E.; Ferrance, J. P.; Feldman, S. H.; Norris, P. M.; Landers, J. P. Microchip-Based Purification of DNA from Biological Samples. *Anal. Chem.* **2003**, *75* (8), 1880–1886.

(28) Price, C. W.; Leslie, D. C.; Landers, J. P. Nucleic Acid Extraction Techniques and Application to the Microchip. *Lab. Chip* **2009**, *9* (17), 2484.

(29) Tekmen, C.; Suslu, A.; Cocen, U. Titania Nanofibers Prepared by Electrospinning. *Mater. Lett.* **2008**, *62* (29), 4470–4472.

(30) Li, D.; Xia, Y. Fabrication of Titania Nanofibers by Electrospinning. *Nano Lett.* **2003**, *3* (4), 555–560.

(31) Brunette, D. M.; Tengvall, P.; Textor, M.; Thomsen, P. *Titanium in Medicine: Material Science, Surface Science, Engineering, Biological Responses and Medical Applications*; Springer Science & Business Media, 2012.

Chapter 6: Conclusion and Future Outlook

The focus of my research presented in this dissertation has been the development and optimization of methods for total extraction, processing, and analysis of microRNA. This includes the development of novel strategies for the separation of potential miRNA carriers in serum, development of optimization of miRNA from serum, and novel detection strategies.

In Chapter 2, a method for serum miRNA carrier separation based on the open channel separation method, asymmetrical flow field-flow fractionation (AF4), is presented. We optimized the separation of all potential carriers in serum such as proteins, high- and low-density lipoprotein complexes, and exosomes. High reproducibility of peak elution windows allowed for automated collection of carrier fractions with high confidence in recovery of each carrier species. Based on the RT-qPCR results of serum flow through, minimal loss of miRNA was seen in the AF4 channel. After its development, we applied the method to the fractionation of sera from breast cancer patients and individuals in order to investigate the prospective advantages of carrier-based serum miRNA profiling over total miRNA content in serum. For the proof-of-concept in the potential of serum miRNA profiling, we analyzed two case sera (BC patients) and two control sera (healthy donors) and performed statistical analysis on the acquired absolute quantification data. From the fold changes between cases and controls we clearly see that there are times which the profiling method provides clear indication of altered miRNA content whereas the total content seems statistically unchanged.

Furthermore, principal component analysis (PCA) using our profiling method shows differentiation of case and control.

In Chapter 3, a novel microfluidic technique for simultaneous profiling of microRNA into three fractions from a whole serum sample is presented. These three fractions which are sequentially extracted are exosomal-associated, protein-bound, and lipoprotein-bound miRNA. The presented technique is much more rapid, less tedious, and relatively simplistic as compared to conventional methods for isolation of serum components. In addition, the newly developed microfluidic technique has advantages over our previously developed asymmetrical flow field-flow fractionation (AF4) technique while providing clearer distinction of the fractions and offering a potentially high-throughput operation. We successfully optimized the microfluidic fractionation employing immuno-isolation of exosome combined with our differential extraction of protein and lipoprotein complexes. The successful selective disruption of protein and lipoprotein complexes and disruption of exosomes for miRNA release was shown through DiO staining and AF4 fractionation. The exosomes and associated miRNA isolated by our method agrees with or outperforms those isolated by other techniques. The miRNA content isolated for the protein and lipoprotein fractions agree with those obtained in the AF4 method or those from immuno-isolation of HDL and LDL. We evaluated the ability of our microfluidic profiling technique through the triplicate fractionation of 12 breast cancer patient sera samples (cases) and 7 healthy donor sera (controls). From the qPCR quantification and the following statistical analysis we showed that our technique indicates much greater changes for miRNA associated with different

carriers than the total miRNA content. Also the fold changes seen in this technique were greater than our previous AF4 method. Through PCA analysis of the data, we illustrated the ability of the microfluidic profiling technique in distinct differentiation of case and control sera. In addition, we were able to visualize clear separation of the stage of the breast cancer patients through PCA scatter plots. The future directions of this work include further optimization and automation of the device and potential integration of microarray assay for direct detection within the microfluidic device. Through the integration of robotics and computer programs the chip has potential for automation.[1–3] Further the use of efficient extraction columns could be employed for a pressure or pump driven microfluidic format which could be desirable for high-throughput analysis of larger sample volumes. Additionally the integration of microarrays for amplification of miRNA within the device could lead to total analysis on-chip, simplifying the total process further and limiting any need for transferring eluted miRNAs off-chip for quantification.

In Chapter 4, two techniques for isothermal amplification of miRNA were discussed. The first is rolling circle amplification (RCA) combined with tagging of the product for signal amplification. The presented RCA method utilizes a linear padlock probe with 3’ and 5’ end sequences complimentary to *has-miR*-7a, causing the linear probe to fold into a circular sequence, yielding the specificity in the method. After ligation of the 3’ and 5’ ends, a circular probe for RCA is formed which is utilized in the amplification of primer sequences conjugated to magnetic polystyrene beads. Through the use of biotin-ATP, biotin moieties are integrated into the sequence of the product

allowing for tagging through biotin-avidin interactions. Through the use of a cation-exchange amplification (CXAmp) technique developed in our lab, we are able to tag the RCA product with streptavidin conjugated ZnS nanocrystal clusters (NCCs) which will produce thousands of Zn(II) ions to be released upon exchange with Ag(I). Using a zinc sensitive fluorophore, FluoZin-3, we are able to turn on thousands of fluorophores for each NCC tagged on the product. Although the technique was efficient, the limit of detection was relatively high for miRNA detection at 91 amol (S/N=3). In order to push the detection limit lower and detect more relevant quantities of miRNA, we explored an additional method for isothermal amplification in detection of *has-let*-7a.

This led to the second technique presented, which combines strand-displacement amplification (SDA) combined with hybridization chain reaction (HCR) for quadratic amplification. The SDA-HCR method utilizes a stem-loop capture probe for target specificity. After the target opens the capture probe, a SDA primer is then able to bind and is elongated during the SDA process which causes the release of *let*-7a. The released target is then able to open an additional capture probe resulting in the target recycling producing several SDA products for each target molecule yielding linear amplification. To enhance the amplification, the SDA primer acts as an initiator for HCR, this causes the opening and hybridization of one hairpin primer and in turn opens and hybridizes with a second hairpin primer. The second hairpin is then able to open and hybridize the first hairpin primer. This efficient technique produces long double stranded DNA scaffolds from only the initiator and two supplied DNA hairpins. Direct detection after SDA-HCR using SYBR Gold DNA dye yields a detection limit of 1.31 fmol (S/N=5).

Tagging of the HCR product is possible through 5' biotin modifications of the DNA hairpin primers. In this study we employed a streptavidin conjugated horseradish peroxidase (HRP) for the tagging of the product and the production of an amplified luminescent signal. This SDA-HCR method coupled with the HRP signal amplification gave a detection limit of 2.02 amol (S/N=5) and 264 zmol (S/N=3.3) which is which is 2-3 orders of magnitude lower then that achieved in our RCA-CXAmp method.

Still future work is necessary for further optimization of the method and integration into a microarray format. Despite the low detection limits, the process gives relatively high background which should be reduced. Additionally the specificity for the *let*-7a target against single, double, or triple base mismatches needs to be investigated. Current optimization and testing is being conducted to improve and investigate these points. Also the use of CXAmp[4–6] may provide an additional 1-2 order of magnitude improvement in the limit of detection which would produce a detection method competitive with quantitative PCR. Once the method is optimized, the last steps are; production of additional capture probes for analysis of another target, integration onto a microarray format within a simple PDMS-glass device, and analysis of miRNA extracted from real samples such as serum for illustration of clinical applications.

Lastly in Chapter 5, I present the work completed in the optimization of methods for solid-phase extraction of miRNA. First the optimization of silica-based miRNA extraction is discussed, and the parameters affecting the extraction efficiency and difficulties in miRNA extraction from complex media with miRNA bound to carrier species is explored. High recoveries were obtained from simple sample matrices, water

use as an example, yielding recoveries between 70-80% with the optimized protocol. The efficiency using this protocol dropped drastically when extracting native miRNA quantities in whole human serum. This is due to the complex nature of sera and the miRNA association with various carriers such as proteins, lipoprotein complexes, and encapsulation in exosome vesicles. The effect of various chaotropic reagents, salts, surfactants, and alcohols as well as the addition of heat were investigated in the denaturation and release of the miRNAs as seen in the RT-qPCR quantification of the extracted miRNAs. In the same chapter, we also investigated the use of an additional material in novel methods for extraction of DNA and miRNA. The material utilized in titanium dioxide (titania) which contains many characteristics in common with silica and the potential for strong nucleic acid binding through similar routes. In this work we produced titania nanofibers under 150 nm in diameter using simple electro-spinning methods. In the optimization of miRNA extraction using titania, we compared our extraction of standard miRNA from water to the recovery using commercial silica based columns and a variety of extraction reagent compositions. From our results we found that our extraction is able to slightly outperform the commercial columns in the recovery with our method yielding a relative recovery of 34.2% versus 30.4% for the commercial column in our incompletely optimized technique. Further optimization is necessary to improve our miRNA extraction efficiency further to produce higher recoveries then that previously optimized with silica materials. Current work is being completed by my coworkers and promising results for DNA extractions have already been completed and the optimization of RNA extractions seems to be following a similar course.

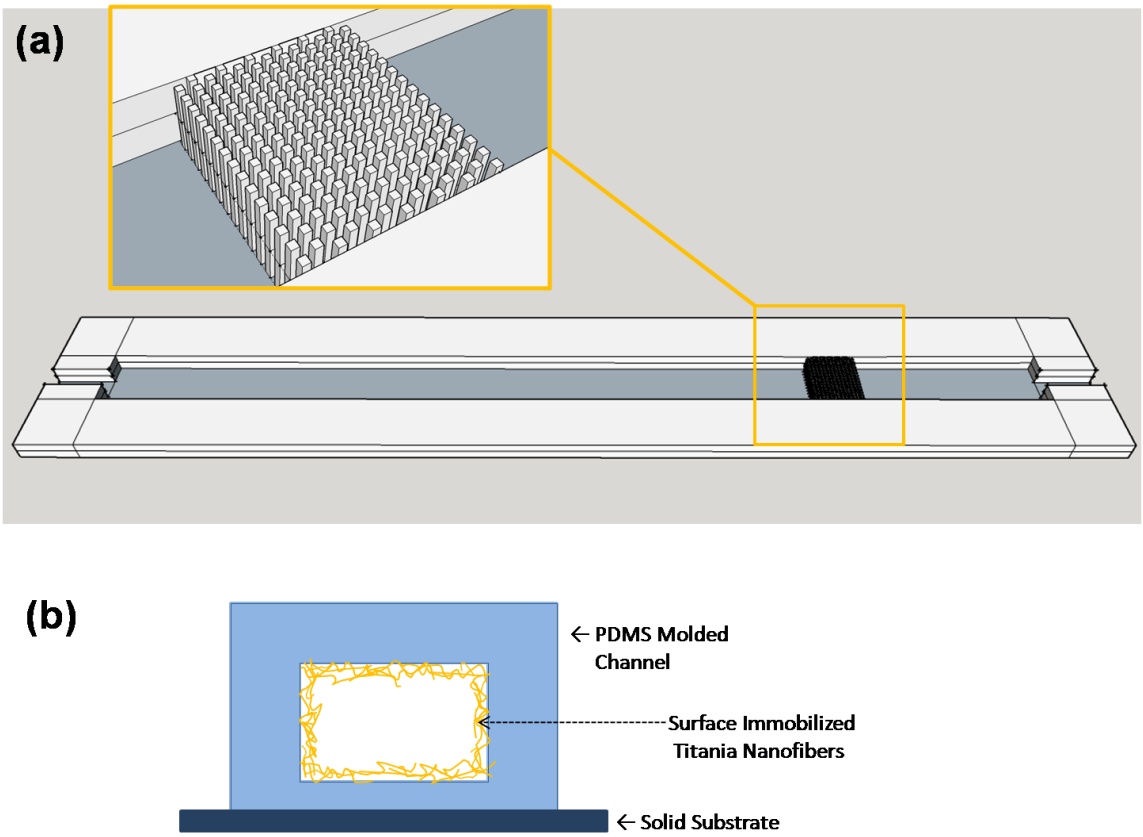

Figure 6.01. Microfluidic devices for titania nanofibers based extraction. (a) A 3D printed microchannel with a carefully designed frit composed of dense packing of micro pillars. (b) A separate device with a PDMS microchannel with immobilized titania nanofibers. Titanium dioxide can be immobilized on PDMS, similar to silica, via condensation of Si-OH and Ti-OH groups.

Future work on the titania extractions and the integration on a microfluidic device[7] are being investigated in our group using 3D printing for the fabrication of prototype extraction devices.[8] Two methods for the integration of the titania fibers within a microfluidic channel should be explored; physical barriers for production of a packed fiber column on-chip[9] and the covalent immobilization of titania fibers to PDMS surfaces within a PDMS molded channel.[10] In the former the extraction would be more efficient due to the increased surfaces for the miRNA to bind to, yet the device would be limited to the back-pressure experienced in such packed channels. In the latter the incubation times required for extraction would be longer to achieve adequate recovery of miRNA, however the conditions in the open channel are gentler and do not create the back-pressure situations found in a packed channel. With proper design, the packed channel may be more applicable to total miRNA extractions and potential direct coupling with the AF4 separation method, discussed in Chapter 2. A potential 3D prototype design is illustrated in Figure 6.01a. In Figure 6.01b, an illustration of the device channel for the open channel extraction of miRNA is shown. The open-channel microfluidic device with fibers immobilized on the PDMS surface creates a forest of fibers which contains a relatively high surface area for the miRNA to bind with. Through careful design of the extraction column dimensions with a relatively thin height, we can reduce the problem of diffusion within the center of the open channel to the fibers on the walls. The potential application of this open-channel extraction device could be in the production of a flow-driven miRNA extraction device utilizing the same optimized method as that presented in Chapter 3 for serum miRNA profiling. With the addition of a selective and sensitive

isothermal miRNA detection microarray, the device would be capable of simple analysis of a large number of miRNA targets.[11,12] Such a microfluidic technique can be employed for high-throughput biomarker analysis of many samples in a simultaneous multi-channel format for novel biomarker discovery or in a single sample format for diagnostic value in analysis of clinical samples.

References:

(1) Choi, K.; Ng, A. H. C.; Fobel, R.; Chang-Yen, D. A.; Yarnell, L. E.; Pearson, E. L.; Oleksak, C. M.; Fischer, A. T.; Luoma, R. P.; Robinson, J. M.; Audet, J.; Wheeler, A. R. Automated Digital Microfluidic Platform for Magnetic-Particle-Based Immunoassays with Optimization by Design of Experiments. *Anal. Chem.* **2013**, *85* (20), 9638–9646.

(2) Rossier, J. S.; Baranek, S.; Morier, P.; Vollet, C.; Vulliet, F.; Chastonay, Y. D.; Reymond, F. GRAVI: Robotized Microfluidics for Fast and Automated Immunoassays in Low Volume. *J. Assoc. Lab. Autom.* **2008**, *13* (6), 322–329.

(3) Wang, J.; Jiao, N.; Tung, S.; Liu, L. Magnetic Microrobot and Its Application in a Microfluidic System. *Robot. Biomim.* **2014**, *1* (1), 1–8.

(4) Li, J.; Zhang, T.; Ge, J.; Yin, Y.; Zhong, W. Fluorescence Signal Amplification by Cation Exchange in Ionic Nanocrystals. *Angew. Chem. Int. Ed.* **2009**, *48* (9), 1588–1591.

(5) Yao, J.; Han, X.; Zeng, S.; Zhong, W. Detection of Femtomolar Proteins by Nonfluorescent ZnS Nanocrystal Clusters. *Anal. Chem.* **2012**, *84* (3), 1645–1652.

(6) Yao, J.; Schachermeyer, S.; Yin, Y.; Zhong, W. Cation Exchange in ZnSe Nanocrystals for Signal Amplification in Bioassays. *Anal. Chem.* **2011**, *83* (1), 402–408.

(7) Price, C. W.; Leslie, D. C.; Landers, J. P. Nucleic Acid Extraction Techniques and Application to the Microchip. *Lab. Chip* **2009**, *9* (17), 2484–2494.

(8) Au, A. K.; Bhattacharjee, N.; Horowitz, L. F.; Chang, T. C.; Folch, A. 3D-Printed Microfluidic Automation. *Lab. Chip* **2015**, *15* (8), 1934–1941.

(9) Oleschuk, R. D.; Shultz-Lockyear, L. L.; Ning, Y.; Harrison, D. J. Trapping of Bead-Based Reagents within Microfluidic Systems: On-Chip Solid-Phase Extraction and Electrochromatography. *Anal. Chem.* **2000**, *72* (3), 585–590.

(10) Dimov, I. K.; Garcia-Cordero, J. L.; O'Grady, J.; Poulsen, C. R.; Viguier, C.; Kent, L.; Daly, P.; Lincoln, B.; Maher, M.; O'Kennedy, R.; Smith, T. J.; Ricco, A. J.; Lee, L. P. Integrated Microfluidic tmRNA Purification and Real-Time NASBA Device for Molecular Diagnostics. *Lab. Chip* **2008**, *8* (12), 2071.

(11) Roy, S.; Soh, J. H.; Gao, Z. A Microfluidic-Assisted Microarray for Ultrasensitive Detection of miRNA under an Optical Microscope. *Lab. Chip* **2011**, *11* (11), 1886–1894.

(12) Konry, T.; Hayman, R. B.; Walt, D. R. Microsphere-Based Rolling Circle Amplification Microarray for the Detection of DNA and Proteins in a Single Assay. *Anal. Chem.* **2009**, *81* (14), 5777–5782.